High Performance Concrete in Washington State SR 18/SR 516 Overcrossing: Interim Report on Girder Monitoring

PUBLICATION NO. FHWA-RD-00-070

APRIL 2000

U.S. Department of Transportation
Federal Highway Administration

Research, Development, and Technology
Turner-Fairbank Highway Research Center
6300 Georgetown Pike
McLean, VA 22101-2296

FOREWORD

In the mid 1990's the FHWA established a High Performance Concrete (HPC) program aimed at demonstrating the positive effects of utilizing HPC in bridges. This, first of a two part interim report, presents results of the effectiveness of using HPC in prestressed precast concrete girders on a bridge in the state of Washington.

This report will be of interest to bridge design engineers and structural research engineers.

Copies may be obtained from the National Technical Information Service, 5285 Port Royal Road, Springfield, Virginia 22161.

John O'Fallon PE

for T. Paul Teng, P.E.
Director, Office of Infrastructure R&D

Technical Report Documentation Page

1. Report No.	2. Government Accession No.	3. Recipient's Catalog No.	
4. Title and Subtitle High Performance Concrete in Washington State SR 18/SR 516 Overcrossing: Interim Report on Girder Monitoring		5. Report Date 6. Performing Organization Code	
7. Author(s) P. Barr, E. Fekete, M. Eberhard, J. Stanton, B. Khaleghi, J.C.Hsieh		8. Performing Organization Report No.	
9. Performing Organization Name and Address Washington State Departmetn of Transportation, Olympia, WA 98504-7340 & University of Washington, 1107 N.E. 45th St., Suite 535 Seattle, Washington 98105-4631		10. Work Unit No. (TRAIS) 11. Contract or Grant No. DTFH71-96-TE036-WA-28	
12. Sponsoring Agency Name and Address Federal Highway Administration 6300 Georgetown Pike McLean, VA 22101-2296		13. Type of Report and Period Covered Interim Report January 1996 - November 1998 14. Sponsoring Agency Code	

15. Supplementary Notes

FHWA contacts: Sheila Rimal Duwadi, Office of Infrastructure, R&D
Terry Halkyard, Office of Infrastructure
Barry Brecto, Washington State Division Office

16. Abstract

In the mid 1990's the FHWA established a High Performance Concrete (HPC) program aimed at demonstrating the positive effects of utilizing HPC in bridges. Research on the benefits of using high performance concrete for bridges has shown a number of benefits. These include increased span capacities, or wider girder spacings (and hence a fewer number of girders); increased concrete compressive and flexural capacities; and improved concrete durability. However, inspite all of these positive research results, relatively little has been done regarding the implementation of high performance concrete in bridges in the United States. The general goals of the FHWA program are: to encourage the States to implement HPC in bridges; to develop appropriate mix designs and establish quality control procedures; to encourage the use of larger diameter (15mm (0.6")) prestressing strands in the girders; to evaluate the performance of the structure; and to provide for technology transfer through development of a workshop (showcase).

This report presents interim results of the effectiveness of using HPC in prestressed precast concrete girders on a bridge in the state of Washington. State Route 516 utilizes WSDOT 74G pretensioned I-girders with a 190 mm cast-in-place composite deck. The girders were fabricated with 15mm diameter prestressing strands at 50 mm spacing, and designed for a concrete compressive strength of 69 MPa at 56 days. This report documents fabrication of a test girder and the bridge girders; provides a description of the instrumentation program; presents the measured data including strain, camber, temperature time histories, and prestress losses; and evaluates the accuracy of the prestress loss equations in predicting observed prestress losses.

This is the first of a two part interim report. The second report is titled, 'High Performance Concrete in Washington State SR18/SR516 Overcrossing: **Interim Report on Materials Tests'**.

17. Key Word	18. Distribution Statement		
High Performance Concrete, bridges, field monitoring			
19. Security Classif. (of this report) Unclassified	20. Security Classif. (of this page) Unclassified	21. No. of Pages 137	22. Price

TABLE OF CONTENTS

SUMMARY

The Federal Highway Administration has recently developed a program to encourage the use of High Performance Concrete (HPC) in bridges. As part of that program, the University of Washington and the Washington State Department of Transportation (WSDOT) undertook this project to investigate the long-term behavior of an HPC pretensioned concrete girder bridge. This interim report provides preliminary results from the first year of the girder design, monitoring, and evaluation program. A companion interim report provides preliminary results of the materials testing program.

WSDOT builds many precast, pretensioned concrete girders, largely because this form of construction is very economical, thanks to the excellent aggregates that are available locally and the competitive nature of the precast industry. Pretensioned girders can be made stronger by using more prestressing steel, but this in turn necessitates that the concrete be stronger. The stronger girders offer several potential benefits, such as more shallow girders for a given span, longer spans with a given girder size, or fewer girder lines in a bridge of given size. In the latter case, the cost per girder may increase slightly, but the total initial cost of the bridge is expected to decrease compared with bridges made of conventional concrete.

The prestressing force in a girder under service conditions is significantly lower than the initial jacking stress, because losses occur due to elastic shortening, creep, shrinkage, and relaxation. Accurate prediction of the losses, and thus the final prestressing force, is an important step in the design of any prestressed concrete girder; this prediction assumes even greater importance in a highly stressed HPC girder.

The bridge used for the study is located near Kent, WA, and carries the eastbound lanes of SR 18 over SR 516. The bridge has three spans, of 24, 42, and 24 m (80, 137, and 80 ft), five lines of girders, and a skew of 40°. The girders are WSDOT 74G pretensioned I-girders, and the deck is 190-mm- (7.5-in-) thick, cast-in-place composite. The prestressing force was supplied by forty 15-mm (0.6-in.) diameter strands in the longer girders and by 14 strands in the shorter ones. The girders were designed as simply

supported, but significant continuity steel was still supplied at the interior pier supports. The girders were designed for zero bottom tension under full service load.

Using seven girders, WSDOT could have satisfied all of the design requirements with conventional concrete. To meet the design requirements for the long span using only five girders, it was necessary for WSDOT to specify a nominal concrete compressive strength of 51 MPa (7400 psi) at release of prestress and 69 MPa (10,000 psi) at 56 days. A suitable mix was developed by the precast fabricator, Central Premix Prestress Co. of Spokane, WA.

A 6-m- (20-ft-) long test girder was cast in December 1996 in order to provide the fabricator with experience in handling the HPC. The test girder casting also provided the researchers with an opportunity to evaluate various specimen preparation procedures and to install instrumentation under field conditions. The girder was designed so that the stress conditions at midspan would be the same as those at midspan of a long bridge girder. The bridge girders were cast during March and April of 1997. They were transported and erected in May 1997, and the deck was cast in September 1997. The time between the girder erection and deck casting was longer than had been scheduled, but it provided an opportunity to take relatively long-term strain and deflection readings on the bare girders.

The primary instrumentation was designed to record temperatures, strains, and deflections in the girders. During casting, additional instrumentation was used to measure strand slip-back from which the transfer length of the strands could be estimated. Two stress gauges were installed in the test girder on an experimental basis, but their subsequent use was rejected because they were too sensitive to temperature variations.

Embedded Vibrating Wire Strain Gauges (VWSGs) were used to measure concrete strains. They were chosen on the basis of their long-term stability and durability, and the fact that they contain an integral thermistor for measuring temperature as well as strains. They were installed in a standard pattern at 10 locations on the bridge: the midspan and at 1.5 m (5 ft) from one end of each of three long girders and two short ones. The standard pattern consisted of six gauges over the height of the girder and two

more in the slab above the girder. Several gauges were also installed at other selected locations.

Midspan cambers were recorded using two methods. An automatic recording system, based on a wire stretched between the girder ends and a midspan displacement sensor (an LVDT) was developed and installed on three long girders and three short ones. Supplementary readings were taken with a surveyor's level, in the yard and, when possible, at the bridge site. The automatic system was plagued by damage in the fabricator's yard and by vandalism on site. Thus the records from that system are far from complete. However, a modified, more robust system appears to be working well. The surveyor's level readings provided an independent measure of camber, but these measurements were inevitably intermittent. Both methods provide approximately ± 1 mm (0.04 in) accuracy on site, and somewhat worse accuracy in the yard.

Initial results suggest that the general pattern of behavior is similar to that expected based on performance of comparable bridges made from conventional concrete, but that several numerical values differ.

The slip-back of the strands showed considerable scatter but implied a transfer length between 50 and 100 strand diameters, compared with the 60 predicted by the American Association of State and Highway Transportation Officials (AASHTO) equations. Only 5 of the 24 measurements lay within the prediction. The readings could only be taken over a period of about 1 hour during destressing, so they do not include the effects of "creep slipback," which has been reported by others. Thus, the true transfer length probably exceeds that reported here.

The thermistors in the VWSGs showed that the concrete temperature during curing varied by approximately 25 °C over the girder height. The concrete was coldest and, therefore, presumably weakest at the bottom. The reason for this variation is believed to be that the girders were cast out of doors during the winter when the freezing ground acted as a heat sink. The fabricator installed, at mid-height of the girder, a thermocouple connected to a "sure-cure" cylinder curing system. This observation is significant, because the prestressing release time was based on the strength of concrete at

mid-height, rather than at the bottom flange of the girder, where the stress is highest and concrete is weakest.

In general, strains recorded in the field are frequently susceptible to errors and to large scatter. However, those recorded here are believed to be reliable because they satisfy several consistency criteria. They are similar in similar girders, and they vary consistently over the height of the girders. Moreover, the relative magnitudes of the strains among the girders are consistent with the relative magnitudes among the measured cambers.

The losses computed from the measured strains are, in general, similar to those implied by the AASHTO equations for prestress losses. However, this overall agreement is perhaps fortuitous, because the elastic shortening and creep strains are larger than expected, whereas the shrinkage strains are smaller. In addition, the initial cambers are larger than expected. It appears that the elastic modulus of the concrete is lower than the value suggested by AASHTO for concrete of this strength.

Several methods for estimating prestress losses have been proposed in the literature. They may be supplemented by recently proposed methods for estimating creep and shrinkage in concrete. Initial trial calculations showed that no single method provided the best fit to all the field data. The prestress losses were estimated during design using the Modified Rate of Creep method, but that method underpredicted the values computed from the measured strains.

At the time of writing, the deck has been cast, and measurements at the bridge continue to be taken every 3 hours. A few of the strain gauges have ceased to function, but most are operational. The stretched-wire camber system is still installed on three of the girders and is working well.

CHAPTER 1

INTRODUCTION

1.1 CONTEXT

The American Concrete Institute defines High-Performance Concrete (HPC) as "concrete that meets special performance and uniformity requirements that cannot always be obtained using conventional ingredients, normal mixing procedures, and typical curing practices" (Goodspeed et. al., 1996). These requirements may include the following enhancements: (1) easier placement and consolidation, (2) high early strength, (3) better long-term mechanical properties, (4) increased toughness, (5) better volume stability, and (6) longer life in severe environments.

The use of HPC can be a step toward further improving the durability of our nation's bridges. There are 596,047 bridges in the National Bridge Inventory, of which 107,543 (18 percent) have been identified as structurally deficient. It has been estimated that more than $400 billion would be needed by the year 2000 just to replace the existing deteriorated bridges and highway system in the United States (NBI, 1997). Well-designed conventional concrete has proved to be very durable and requires little maintenance. The use of HPC for the deck and columns of bridges would further increase durability, resulting in longer life and decreased long-term maintenance costs.

In precast, prestressed girders the availability of high-strength concrete would enable engineers to design longer span lengths, increased girder spacings, and more shallow sections. The longer spans would permit the use of fewer supports. Increased girder spacing would decrease fabrication, transportation, and erection costs. If girders were shallower, it would be possible to increase underpass clearances or lower embankment heights.

Despite the benefits of using HPC, there are reasons why it has not yet been widely used in prestressed members. Current methods for calculating prestress losses, such as those advocated by the American Association of State Highway and Transportation officials (AASHTO) (AASHTO, 1994) and the Precast Prestressed

Concrete Institute (PCI) (PCI, 1975), were based on the behavior of conventional concrete, with strengths usually below 41.4 MPa (6000 psi). In particular, several equations for calculating prestress losses are empirically related to concrete strength. Because incorrect calculations of prestress losses can lead to unacceptable service conditions, these losses need to be predicted correctly. The appropriateness of applying current design codes to HPC needs to be evaluated.

Elastic shortening and creep are two major components of the total prestress loss. Because an HPC girder will almost certainly be more highly stressed than one made from conventional concrete, those components will probably be higher. It is unknown whether the change is adequately predicted by present methods of analysis.

The use of larger diameter strand with HPC has also been an area of concern for designers. In comparison with lower strength concrete, the use of HPC permits additional prestressing force to be used. To obtain this force without inducing excess congestion, larger diameter strand must often be used. However, in 1988 the Federal Highway Administration (FHWA) placed a moratorium on the use of 15-mm (0.6-in) diameter strands for pretensioned applications because of uncertainties in its bond properties. In May 1996, based on preliminary studies at the University of Texas (Russell and Burns, 1997) on the transfer and development length of the 15-mm (0.6-in) strand, the FHWA permitted the use of 15-mm (0.6-in) diameter strands at 51-mm (2-in) spacings. The current design equations for transfer and development length were based on smaller, 13-mm (0.5-in) diameter strands. Whether they are universally applicable for the 15-mm (0.6-in) diameter strands remains an open question.

Precast fabricators have also hesitated to use HPC. They prefer to produce girders on a 24-hour cycle in order to make the most efficient use of the casting beds. The higher the prestressing force in the girder, the larger the concrete compressive strength needs to be at release of the prestressing strands. To achieve this higher strength, the precast plants must use a combination of different materials, longer curing times, and increased curing rates. Each of these options is likely to increase costs. Many plants already steam

cure conventional concrete to increase the curing rate and remain on a 24 hour-cycle. A better understanding of the effects of this heating on HPC is also needed.

1.2 SR 516 OVERCROSSING

The FHWA has been encouraging States to use HPC in bridge applications. Since Washington State Department of Transportation (WSDOT) was also interested in expanding the use of HPC to structural applications, WSDOT (with sponsorship from the FHWA) designed a new bridge to carry the eastbound lanes of State Route 18 (SR 18) over SR 516. This HPC bridge has three spans with lengths of 24.4 m, 41.7 m, and 24.4 m (80 ft, 137 ft, and 80 ft), respectively. The girders were designed to have a release strength of 51 MPa (7,400 psi) and a 56-day compressive strength of 68.9 MPa (10,000 psi). As a result of specifying HPC, WSDOT was able to reduce the number of lines of girders from seven to five.

The roadway deck has a width of 11.6 m (38 ft). The design compressive strength of the deck concrete is only 27.6 MPa (4000 psi), but it has enhanced durability properties due to the use of fly ash and the requirement of a 14-day water cure. The HPC bridge is described further in Chapter 3.

This report documents a part of the study undertaken to evaluate the benefits of HPC.

1.3 RESEARCH OBJECTIVES

In general, the use of HPC in bridge applications is considered an innovative concept. Therefore, the bridges built under the FHWA HPC programs are being monitored and evaluated for satisfactory performance. The research phase of the study focuses on evaluating the effectiveness of using HPC in prestressed, precast concrete girders. Specific objectives include:

- Documenting the prestress losses of a test girder and five bridge girders made with HPC.
- Documenting the camber growth for five bridge girders made with HPC.

- Comparing measured field behavior with that expected according to current design methods.
- Estimating the transfer length for 15-mm (0.6-in.) diameter strands based on measured slip-back displacements.
- Evaluating the material properties of the HPC.

Bullet items 1 to 4 above are reported on in this report, while bullet item 5 is reported in a separate report by Fekete et al. (1998) titled "High Performance Concrete in Washington State SR 516 Overcrossing, Eastbound Bridge No. 18/25S: Interim Report on Materials Tests."

1.4 SCOPE AND ORGANIZATION OF REPORT

This report describes how these research objectives were achieved. The report is organized as follows:

- Chapter 2 describes the AASHTO, PCI, and Modified Rate of Creep methods for calculating prestress losses.
- Chapter 3 outlines the fabrication of the test girder and bridge girders.
- Chapter 4 describes the instrumentation program that was used to monitor a 6.1-m- (20-ft-) long HPC test girder and the five HPC bridge girders. The monitoring program for the instrumentation is also presented in this chapter.
- Chapter 5 presents the measured data for the bridge girders. The measurements include strain, camber, and temperature time histories. Also presented are the estimates of transfer length and a chronology of important events during fabrication of the test girder and bridge. Differences in concrete maturity as a result of the temperature history during curing are also discussed.
- Chapter 6 focuses on estimating prestress losses from the measured response of the girders. Creep, shrinkage, and elastic shortening losses were calculated from measured strain data at the prestressing centroid. Relaxation values were

taken from the manufacturer's tests. Possible prestress losses due to the effects of temperature changes during casting of the girders are also estimated.

- Chapter 7 evaluates the accuracy of prestress loss equations in predicting the observed prestress losses. Specific methods discussed include the AASHTO and PCI recommended methods.
- Chapter 8 summarizes the report. Conclusions are drawn, and comments on the application of conventional design methods to HPC are presented.

CHAPTER 2
METHODS FOR ESTIMATING PRESTRESS LOSSES

2.1 INTRODUCTION

The final prestressing force in a girder is less than the value at initial stressing because losses occur. The primary causes are relaxation of the steel, elastic shortening of the concrete when the prestress is applied, and creep and shrinkage of the concrete during the life of the girder. Stress is regained with the addition of load, caused, for example, by casting of the deck or traffic barriers. The stress losses in the tendon must be estimated when the girder is designed so that the value of the initial prestress needed to provide the desired final prestress can be calculated. The initial prestress is needed for fabrication of the girders.

Several methods of estimating prestress losses have been proposed, but many of them were developed in the 1970s. Two of the more recent methods are the three AASHTO LRFD methods (AASHTO, 1994) and the Modified Rate of Creep method (Lwin and Kaleghi, 1997), which is derived from the AASHTO ones. In this chapter five methods are described. They are used subsequently in Chapter 3, Design and Construction of HPC Girders, and in Chapter 6, Observed Prestress Losses. The methods described here are the PCI General method, the three AASHTO LRFD methods, and the Modified Rate of Creep method.

Methods of predicting prestress losses can be classified into four groups according to their complexity (Fekete, 1997). True Lump Sum methods are the crudest, and require no knowledge of material properties. Single Equation methods use a single equation to predict the ultimate loss, but the coefficients in the equation differ for different materials. Component methods predict the ultimate loss by calculating explicitly the components of loss due to different causes, such as elastic shortening or creep, based on a knowledge of the material properties. Time Step methods use a similar methodology to Component methods, but compute the loss at user-selected time intervals. They require as input the

time-dependence of the material properties, for which approximations are available in the absence of material-specific data.

According to this classification system, the AASHTO Lump Sum method is a Single Equation method. (AASHTO's description of it as a Lump Sum method is unfortunate and confusing, since previous editions of the AASHTO Specifications contained a method that is a true Lump Sum method). The AASHTO Refined method contains a more detailed estimate of the time-dependent components of loss, but does so only for the ultimate condition, and is therefore a Component Method. The equations in the AASHTO Refined method can be made time-dependent by dividing up the life of the girder into several intervals and applying each calculation in that time interval. This approach is not explicitly contained in the AASHTO Specifications, but is feasible nonetheless. It is referred to here as the AASHTO Time Step method. The Modified Rate of Creep method is based on the AASHTO Time Step method and is nearly identical to it, except that it accounts for casting of the slab and the transition to composite action. The PCI General method is not related to the AASHTO methods and is also a Time Step method.

None of these methods was developed specifically for HPC. One of the goals of this project has been to evaluate the real prestress losses and to determine if any one of the existing prediction methods is able to predict them accurately. The methods are described here, but specific loss values are computed in Chapters 3 and 6.

2.2 AASHTO LUMP SUM METHOD

The total stress loss is given by

$$\Delta f_{pTOT} = + \Delta f_{pES} + \Delta f_{pTD} \qquad (2.1)$$

where

Δf_{pT} = total prestress loss
Δf_{pES} = prestress loss due to elastic shortening
Δf_{pTD} = total time-dependent prestress loss.

The elastic shortening loss is given by

$$\Delta f_{pES} = (E_p/E_{ci}) / f_{cgp} \tag{2.2}$$

where

f_{cgp} = concrete stress at the center of gravity of the prestressing strand (cgp) directly after transfer.
E_P = modulus of elasticity of prestressing strand
E_{ci} = initial modulus of elasticity of concrete

Unfortunately, f_{cgp} depends on Δf_{pES} , so an iterative calculation is necessary. However, it can be avoided by calculating the stress directly after transfer as

$$f_{Pi} = \frac{f_{Pj} + \frac{neM_{sw}}{I_{ut}}}{\left(1 + n\rho_n\alpha_n\right)} \tag{2.3}$$

where

f_{Pi} = stress in steel directly after transfer [MPa]
f_{Pj} = stress in steel directly before transfer [MPa]
M_{sw} = girder self-weight moment [kN-m]
e = eccentricity of center of gravity of prestressing strand (c.g.p.) [m]
I_{ut} = moment of inertia of cross-section [m^4]

and

$$n = \frac{E_p}{E_{ci}} \tag{2.4}$$

$$\rho_n = \frac{A_{ps}}{A_{nc}} \tag{2.5}$$

A_{ps} = total area of prestressing steel [mm^2]
A_{nc} = net cross-sectional area of concrete [mm^2]

$$\alpha_n = 1 + \frac{e^2}{r_n^2} \tag{2.6}$$

r_n = radius of gyration [m]

Here the subscript ‘n’ refers to properties of the net concrete section, calculated assuming voids at the prestressing locations but including the transformed effect of any bonded reinforcing bars. The subscript ‘ut’ refers to the uncracked transformed properties, calculated by including the effects of both the prestressing steel and bonded

reinforcing bars. In the interest of simplicity, the gross concrete section is often used for both net and uncracked transformed properties.

For I-shaped girders that are prestressed with 1860 MPa (270 ksi) grade low-relaxation strands, which contain no mild reinforcement and have a concrete strength above 41 MPa (6 ksi), the time-dependent losses are approximated by:

$$\Delta f_{pTOT} = 230 \, [1 - 0.15 \, (f'_c - 41) / 41] \tag{2.7}$$

2.3 AASHTO REFINED METHOD

The total stress loss is given by

$$\Delta f_{pTOT} = + \Delta f_{pES} + \Delta f_{pRE} + \Delta f_{pSH} + \Delta f_{pCR} \tag{2.8}$$

where the time-dependent components of the loss are

Δf_{pRE} = prestress loss due to relaxation
Δf_{pSH} = prestress loss due to shrinkage
Δf_{pCR} = prestress loss due to creep

The relaxation loss is divided into two components. The one that occurs before transfer is given by

$$\Delta f_{P,RE} = \log(24*t)/40.0 \, [f_{Pj}/f_{Py}-0.55]f_{Pj} \tag{2.9}$$

where

t = time in days from stressing to transfer.

After transfer, it is given by

$$\Delta f_{pRE} = 0.30 \, [\, 138 - 0.4 \, \Delta f_{pES} - 0.2(\Delta f_{pSH} + \Delta f_{pCR})] \qquad \text{[MPa]} \tag{2.10}$$

Equation 2.10 is intended to account for the fact that the strand is subjected to continuously decreasing strain, due to creep and shrinkage in the concrete, rather than the constant strain that exists before transfer.

Prestress loss due to shrinkage is given by:

$$\Delta f_{pSH} = (117.0 - 1.035\ H) \qquad \text{[MPa]} \qquad (2.11)$$

where

H = relative humidity
Δf_{pSH} = shrinkage loss in MPa

The prestress loss due to creep is given by:

$$\Delta f_{pCR} = 12.0\ f_{cgp} - 7.0\ \Delta f_{cdp} \quad > 0.0 \qquad (2.12)$$

where

f_{cgp} = sum of the concrete stresses due to prestressing and the self-weight of the girder at the center of gravity of the prestressing strands at mid-span.
Δf_{cdp} = change in the concrete stress at the level of the prestressing strands due to the weight of the concrete deck slab and diaphragms.

The term $7.0\ \Delta f_{cdp}$ in the above equation is the approximate estimate of prestress gain due to dead load of slab and diaphragm.

2.4 AASHTO TIME STEP METHOD

In this modification of the AASHTO Refined method, the life of the girder is divided into convenient time steps. The stresses are known at the start of each step and are used as the initial conditions for the equations of the AASHTO Refined method. The prestress loss during the time step is calculated and the concrete stresses at the end of the step are computed, based on the new value of total prestress force. These are then used as the initial conditions for the next time step.

2.5 MODIFIED RATE OF CREEP METHOD

The Modified Rate of Creep method is similar to the AASHTO Time Step method, but it takes into account the instantaneous and time-dependent effect of slab casting, and the transition from non-composite to composite section properties. It also includes provision for the effects of differential shrinkage between the slab and girders,

and allows for different creep rates before and after slab casting. The rate after slab casting is a weighted average of the slab and girder concrete properties. The elastic shortening loss is computed using equation 2.2 or 2.3.

Time-dependent prestress losses using the Modified Rate of Creep are given by:

$$\Delta f_{pTD} = \Delta f_{pSH} + \Delta f_{pCR1} + \Delta f_{pCR2} + \Delta f_{pRE} - \Delta f_{pEG} - \Delta f_{pCRG} - \Delta f_{pDSH} \quad (2.13)$$

For non-composite girders, the time-dependent prestress losses may be taken as:

$$\Delta f_{pTD} = \Delta f_{pSH} + \Delta f_{pCR1} + \Delta f_{pRE} \quad (2.14)$$

The prestress loss due to girder shrinkage is computed using Equation 2.11. The prestress loss due to creep is calculated in two stages:

Stage 1 is the creep loss between time of transfer and slab casting, and is given by:

$$\Delta f_{pCR1} = n\, f_{cgp}\, \Psi_{t,tisc}\, (1-\Delta F_{SC}/2F_o) \quad (2.15)$$

Stage 2 is the creep loss for any time after slab casting, which may be expressed as:

$$\Delta f_{pCR2} = n\, f_{cgp}\, (\Psi_{t,ti}-\Psi_{t,tisc})\, (1-(\Delta F_{SC}+\Delta F_t)/2F_o)\, I_g/I_c \quad (2.16)$$

where

$\Psi_{t,ti}$ = creep coefficient of girder at any time
$\Psi_{t,tisc}$ = creep coefficient of girder at the time of slab casting
ΔF_{SC} = total loss at the time of slab casting minus initial elastic shortening loss
F_o = prestressing force at transfer after elastic losses
ΔF_t = total prestressing loss at any time minus initial elastic shortening loss
I_g/I_c = ratio of moment of inertia of prestressed girder to composite girder

In the above equations, the terms $\Psi_{t,tisc}(1-\Delta F_{SC}/2F_o)$ and $(\Psi_{t,ti}-\Psi_{t,tisc})(1-\Delta F_{SC}+\Delta F_t)/2F_o)$ represent the effect of variable stress history from the time of transfer to

the time of slab casting and from slab casting to final conditions, respectively. The term I_g/I_c represents the effect of composite section properties after slab casting.

The AASHTO LRFD Specifications recognize the prestress gain due to the deck weight by the term 7.0 Δf_{cdp} in Equation 2.12. In the Modified Rate of Creep method, the creep response to slab and diaphragm dead load may be treated as a prestress gain. Part of the initial compressive strain induced in the concrete immediately after transfer is reduced by the tensile strain resulting from permanent loads. The prestress gain due to slab dead load consists of two parts. The first part is due to instantaneous elastic prestress gain. The second part is a time-dependent creep effect. Prestress gain due to elastic and creep effect of slab casting is given as:

$$\Delta f_{pEG} = n_{SC}\, f_{S+D} \tag{2.17}$$

$$\Delta f_{pCRG} = n_{SC}\, f_{S+D}\, (\Psi_{t,ti} - \Psi_{t,tisc})\, I_g/I_c \tag{2.18}$$

where

Δf_{pEG} = gain in prestress from elastic response to superimposed dead load
Δf_{pCRG} = gain in prestress from to creep response to superimposed dead load
n_{SC} = modular ratio at the time of slab casting
f_{S+D} = stress in concrete at the level of prestressing strands due to dead load of slab and diaphragms

In composite prestressed girder bridges, the concrete in the girder is steam-cured while the concrete in slab is usually cast-in-place and moist-cured. Slab concrete is also cast at a later time when the girders are in place. Due to differences in the concrete properties, curing processes, and times of casting, a prestress gain due to differential shrinkage occurs and is given by:

$$\Delta f_{pDS} = n_{SC}\, f_{CD} \qquad (2.19)$$

where

f_{CD} = concrete stress at the level of prestressing strands $= [\Delta\varepsilon_{S\text{-}G}\, A_{cSLAB}\, E_{cSLAB} / (1 + \Psi_{t,ti})]\, (y_{CS}\, e_c / I_c)$

$\Delta\varepsilon_{S\text{-}G}$ = differential shrinkage strain

A_{cSLAB} = area of concrete deck slab

E_{cSLAB} = modulus of elasticity of slab

y_{CS} = distance between the c.g. of composite section to the c.g. of slab

e_c = eccentricity of prestressing strands in composite section

I_c = moment of inertia of composite section

The denominator $(1 + \Psi_{t,ti})$ approximates the long-term creep effect.

2.6 PCI GENERAL METHOD

The Precast Concrete Institute (PCI) Committee on Prestress Losses (PCI, 1977) recommends two methods for calculating the change in prestress. The General Method is a Time Step method that computes the total loss in stress in the prestressing strand as the sum of the separate components, over discrete time steps. Elastic shortening, creep, and shrinkage of the concrete, and relaxation of the steel are the pertinent elements of the total prestress loss, which is given by:

$$\Delta f_p = \Delta f_{pANC} + \Delta f_{pDEF} + \Delta f_{pES} + \sum_t (\delta f_{pSH} + \delta f_{pCR} + \delta f_{pRE}) \qquad (2.20)$$

where

Δf_{pANC} = change in prestress due to anchorage

Δf_{pDEF} = change in prestress due to deflection points

Δf_{pES} = change in prestress due to elastic shortening

δf_{pCR} = incremental change due to creep of concrete

δf_{pSH} = incremental change due to shrinkage of concrete

δf_{pRE} = incremental change due to relaxation of prestressing steel

Δf_{pANC}, Δf_{pDEF}, and Δf_{pES} are one-time changes. δf_{pCR}, δf_{pSH}, and δf_{pRE} are time-dependent and are calculated at each time step. In pretensioned construction Δf_{pANC} is not applicable. Equation 2.20 is reduced to:

$$\Delta f_{pTOT} = \Delta f_{pES} + \sum_{t}(\delta f_{pSH} + \delta f_{pCR} + \delta f_{pRE}) \quad (2.21)$$

Instantaneous elastic shortening is calculated using Equation 2.2 or 2.3.

The incremental change of prestress due to shrinkage over any time interval is described by:

$$\delta_{pf,SH} = (USH)(SSF)(PSH) \quad (2.22)$$

where

USH = ultimate change in stress due to shrinkage
SSF = size and shape factor
PSH = portion of ultimate shrinkage during a given time step

The ultimate change in stress due to shrinkage is:

$$USH = 186 - 0.003E_c \leq 83\,MPa \quad (2.23)$$

E_c is the 28-day elastic modulus of the concrete in MPa.

Equation 2.23 is illustrated in Figure 2.1. The equation suggests a link between the shrinkage strain and the elastic modulus rather than the concrete strength. A possible explanation is the fact that both shrinkage and elastic modulus depend on the paste content of the concrete.

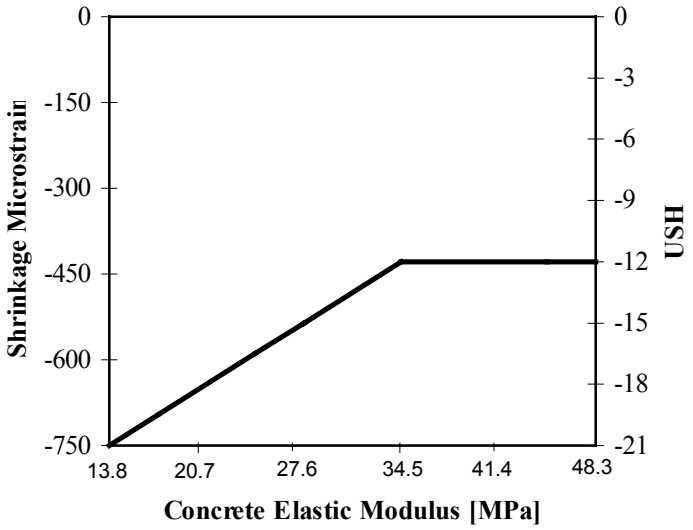

Figure 2.1 Ultimate Shrinkage Strain

The size and shape factor are determined using Table 2.1. The use of the factor SSF implies that the V/S ratio influences the total shrinkage at infinite time, rather than the rate of shrinkage. The concept of shrinkage caused by diffusion and evaporation of moisture from the sample suggests the opposite. The reasons for the apparently anomalous choice in the PCI Method are unknown.

Table 2.1. Shrinkage Size and Shape Factor

V/S (mm)	SSF
25	1.04
50	0.96
75	0.86
100	0.77
125	0.69
150	0.60

The portion of ultimate shrinkage during a given time step is:

$$PSH = (AUS)_t - (AUS)_{t_1} \tag{2.24}$$

AUS is the variation of shrinkage with time provided in Table 2.2. Linear interpolation should be used for values between those listed. Times t_1 and t are the beginning and end of the interval, respectively, in days. The fact that AUS is based on the time since the end of curing suggests that it addresses only drying shrinkage and ignores basic shrinkage.

Table 2.2. Shrinkage Coefficients

Time After Curing (Days)	AUS
1	0.08
3	0.15
5	0.20
7	0.22
10	0.27
20	0.36
30	0.42
60	0.55
90	0.62
180	0.68
365	0.86
End of Service Life	1.00

Tabular values are inconvenient for automation of the procedure. A good fit to the data is given by:

$$AUS = \frac{t^{0.65}}{12 + t^{0.65}} \tag{2.25}$$

The incremental change in prestress due to creep over a time interval, δf_{pCR}, is directly related to the stress in the concrete at the end of the previous time interval.

$$\delta f_{p,CR} = (UCR)(SCF)(MCF) \times (PCR)(f_c) \quad (2.26)$$

where

UCR = ultimate change in prestress due to creep
SCF = size and shape factor
MCF = factor for age of moist cured concrete at transfer
PCR = portion of ultimate creep during a given time interval
f_c = net concrete compressive stress at the c.g.p. at the end of the previous time interval [MPa]

The ultimate change in prestress due to creep for accelerated-cured concrete is given by:

$$UCR = 434 - 0.002E_c \geq 76 \qquad \text{[MPa]} \quad (2.27)$$

The size and shape factor is provided in Table 2.3 as a function of the volume-to-surface ratio of the member in inches. The values are different from those given for shrinkage by a maximum of 0.01. That such a difference is considered justifiable is surprising in light of the scatter and sensitivity commonly found in creep and shrinkage tests.

Table 2.3. Size and Shape Factor for Creep

V/S (mm)	SCF
25	1.05
50	0.96
75	0.87
100	0.77
125	0.68

The portion of ultimate creep during a given time step is:

$$PCR = (AUC)_t - (AUC)_{t_1} \quad (2.28)$$

AUC is the variation of creep with time after application of the prestress force, given in Table 2.4. Linear interpolation is used to determine the value for times between those listed. Times t_1 and t are as described above.

Table 2.4. Variation of Creep With Time

Time After Prestress (Days)	AUC
1	0.08
2	0.15
5	0.18
7	0.23
10	0.24
20	0.30
30	0.35
60	0.45
90	0.51
180	0.61
365	0.74
End of Service Life	1.00

Again, an equation to express the data in Table 2.4 is desirable for automation purposes. Equation 2.29 provides an acceptable curve fit.

$$AUC = \frac{t^{0.70}}{20 + t^{0.70}} \tag{2.29}$$

The relaxation contribution to the total change in prestress for low-relaxation steel is:

$$\delta f_{pRE} = f_p \left\{ \left[\frac{\log 24t - \log 24t_1}{45} \right] \times \left[\frac{f_p}{f_{py}} - 0.55 \right] \right\} \qquad \text{[MPa]} \tag{2.30}$$

where

$$\frac{f_p}{f_{py}} \geq 0.60$$

f_p = stress in the prestressing steel at the end of the previous interval, taking into account all previous changes in stress [MPa]

f_{py} = 0.90 f_{pu} (the tensile strength of the prestressing steel) [MPa]

f_{pu} = the ultimate strength of the prestressing steel [MPa]

If the ratio of applied stress to yield strength of the prestressing strand is less than 0.60 it is assumed that no relaxation will take place and the incremental change in prestress for that time interval is equal to zero. For the first interval, the time of anchorage, t_1, is assumed to be 1/24 day (1 hour). It should also be noted that different ultimate values of change in stress due to relaxation are found using time steps rather than a single calculation over the lifetime of the girder. However, the total change due to relaxation is typically so small in low-relaxation strands that the difference has little practical importance.

2.7 DEFLECTIONS OF PRESTRESSED GIRDERS

Deflections of prestressed girders are computed as the sum of individual deflection contributions. Each contribution consists of an elastic and a creep component. Prestressing causes the girder to camber upward, but girder self-weight, slab and diaphragm weight, and live load all cause the girder to deflect downwards. Differential shrinkage between the deck and girder concretes also causes downward deflection. The final deflection of a prestressed girder according to the Modified Rate of Creep method is given as:

$$\Delta_{TOT} = \Delta_{DLg}+\Delta_{DLgbsCR}+\Delta_{P/S}+\Delta_{P/SbsCR}+\Delta_{P/SasCR}+\Delta_{DLs}+\Delta_{DLgasCR}+\Delta_{DLsCR}+\Delta_{SH} \qquad (2.31)$$

where

Δ_{DLg} is the elastic deflection due to girder dead load and is given by:

$$\Delta_{DLg} = 5w_gL^4/384E_gI_g \qquad (2.32)$$

$\Delta_{DLgbsCR}$ is the creep deflection due to of girder dead load and is given by:

$$\Delta_{DLgbsCR} = \Psi_{t,ti}\ \Delta_{DLg} \qquad (2.33)$$

$\Delta_{DLgasCR}$ is the creep deflection of the composite girder due to slab load and is given by:

$$\Delta_{DlgasCR} = \Delta_{DLg}\ (\Psi_{t,ti} - \Psi_{t,tisc})\ I_g/I_c \qquad (2.34)$$

Δ_{DLs} is the deflection due to slab plus diaphragm dead load and may be taken as:

$$\Delta_{DLs} = 5w_sL^4/384E_gI_g + 19PL^3/384E_gI_g \quad (2.35)$$

Δ_{DLsCR} is the creep effect deflection of composite girder after slab casting and, assuming that the girder may be treated as simply supported, may be taken as:

$$\Delta_{DLsCR} = \Psi_{t,ti}\, \Delta_{DLs}\, I_g/I_c \quad (2.36)$$

$\Delta_{P/S}$ is the deflection due to prestressing and may be taken as:

$$\Delta_{P/S} = P_s\, e_s\, L^2/(8E_gI_g) + P_h\, /E_gI_g\, (L^2/8 - a^2/6)\, (e_s - e_h) \quad (2.37)$$

$\Delta_{P/SbsCR}$ is the creep deflection before slab casting due to prestressing and may be taken as:

$$\Delta_{P/SbsCR} = [(1-\Delta F_{SC}/2F_o)\, \Psi_{t,ti} - \Delta F_{SC}/F_o]\, \Delta_{P/S} \quad (2.38)$$

$\Delta_{P/SasCR}$ is the creep deflection of the composite girder after slab casting due to prestressing and may be taken as:

$$\Delta_{P/SasCR} = [(1-(\Delta F_{SC}+\Delta F_t)/2F_o)\, (\Psi_{t,ti}-\Psi_{t,tisc}) - (\Delta F_t-\Delta F_{SC})/F_o]\, \Delta_{P/S}\, I_g/I_c \quad (2.39)$$

Δ_{SH} is the deflection due to differential shrinkage and may be taken as:

$$\Delta_{SH} = [\Delta\varepsilon_{S\text{-}G}\, A_S\, E_S / (1 + \Psi_{t,ti})]\, (y_{CS}\, L^2 / 8E_gI_c) \quad (2.40)$$

where

w_g = unit weight of girder
E_g = modulus of elasticity of girder
w_s = unit weight of slab and pad
P = weight of diaphragm
P_s = prestressing force in straight strands
P_h = prestressing force in harped strands
a = distance from the centerline of bearing to the harping point
e_s = eccentricity of straight strands from neutral axis
e_h = eccentricity of harped strands from neutral axis

The denominator $(1 + \Psi_{t,ti})$ approximates the long-term creep effect.

In the above equations, the terms $\Psi_{t,ti}(1-\Delta F_{SC}/2F_o)$ and $(\Psi_{t,ti}-\Psi_{t,tisc})(1-(\Delta F_{SC}+\Delta F_t)/2F_o)$ represent the effect of variable stress history from the time of transfer to

the time of slab casting and from slab casting to final conditions, respectively. The term I_g/I_c represents the effect of composite section properties after slab casting.

CHAPTER 3
DESIGN AND CONSTRUCTION OF THE HPC GIRDERS

3.1 TEST GIRDER

A 6.1-m-long test girder was fabricated for the precaster to gain experience with using the concrete mix and for the researchers to gain experience installing the instrumentation under field conditions. The Washington W74G girder cross-section was selected for the test girder to match the bridge girders. Its cross-section is shown in Figure 3.1. Table 3.1 lists the cross-sectional properties of the W74G test girder.

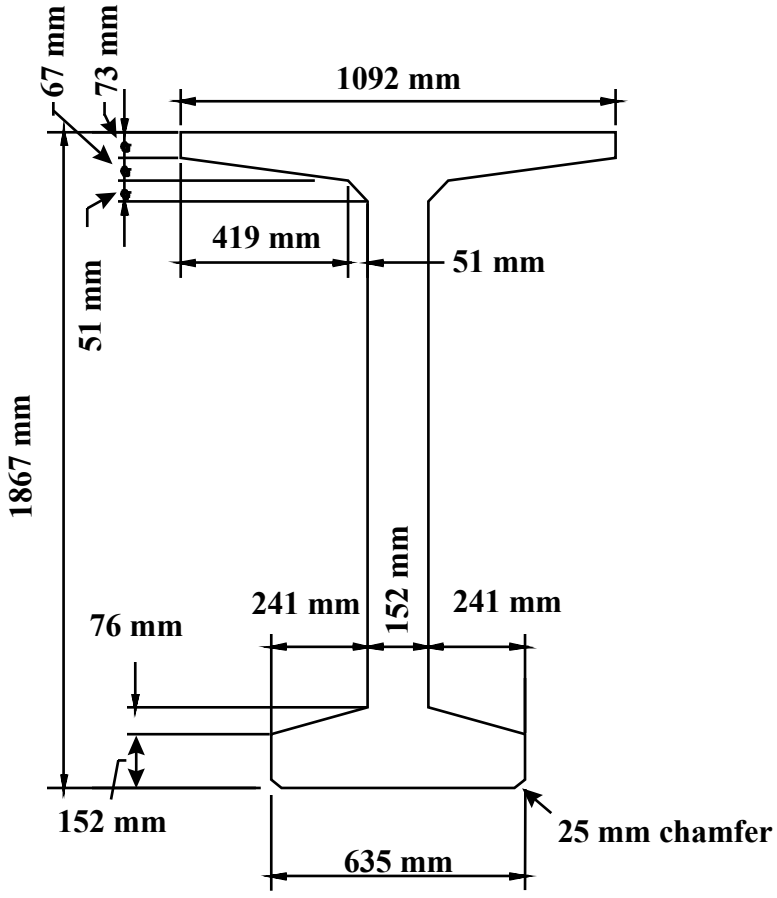

Figure 3.1. W74G Girder Dimensions

Table 3.1. W74G Cross-Section Properties

Property	I (mm^4)	A (mm^2)	Y_t (mm.)	Y_b (mm)	S_{top} (mm^3)	S_{bot} (mm^3)
Value	227.8 (10^9)	482400	901.2	965.7	252.8 (10^6)	235.9 (10^6)

The test girder was prestressed with 15-mm (0.6-in) diameter, 1860 MPa (270 ksi) strands. The tendon profile was designed so that the stress profiles of the test girder and the long bridge girders would be the same at release. The strands were straight because the self-weight moment was less than 1 percent of the prestressing moment. Table 3.2 lists the design details for the test girder. The distances from the bottom of the girder to the center of gravity of the web strands and the bottom flange strands are labeled $W_{C.G.}$ and $B_{C.G.,}$ respectively.

Table 3.2. HPC Test Girder Design Details

Property	Skew	Length (m)	56-day f'c (MPa)	Release f'c (Mpa)	No. of Web Strands	Jacking Force (KN)	No. of Bot. Strands	Jacking Force (KN)	$W_{C.G.}$ (mm)	$B_{C.G.}$ (mm)
Value	0°	6.10	68.9	51.0	14	2710	26	5030	851	76.2

An elevation view of the test girder, showing the centroids of the prestressing strands, is shown in Figure 3.2.

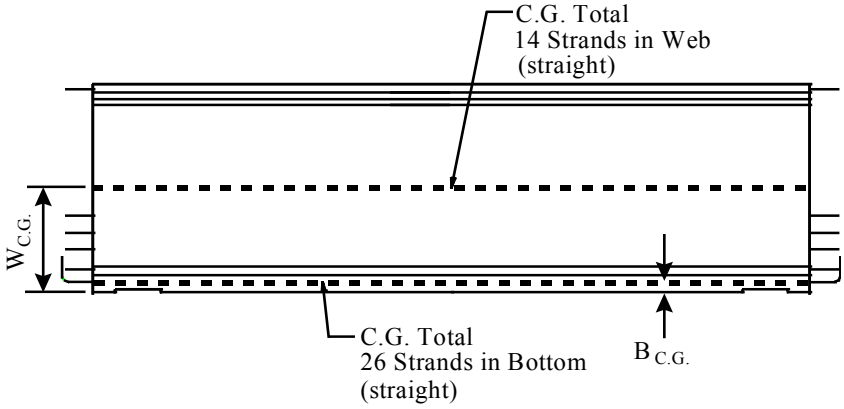

Figure 3.2. Elevation of Test Girder

The grade 60 (420 MPa) mild reinforcing steel in the test girder was placed in the same locations as in the bridge girders. This placement provided the researchers with the opportunity to practice installing the instrumentation with the reinforcing steel before the bridge girders were cast. Figure 3.3 shows the mild steel reinforcement for the test girder.

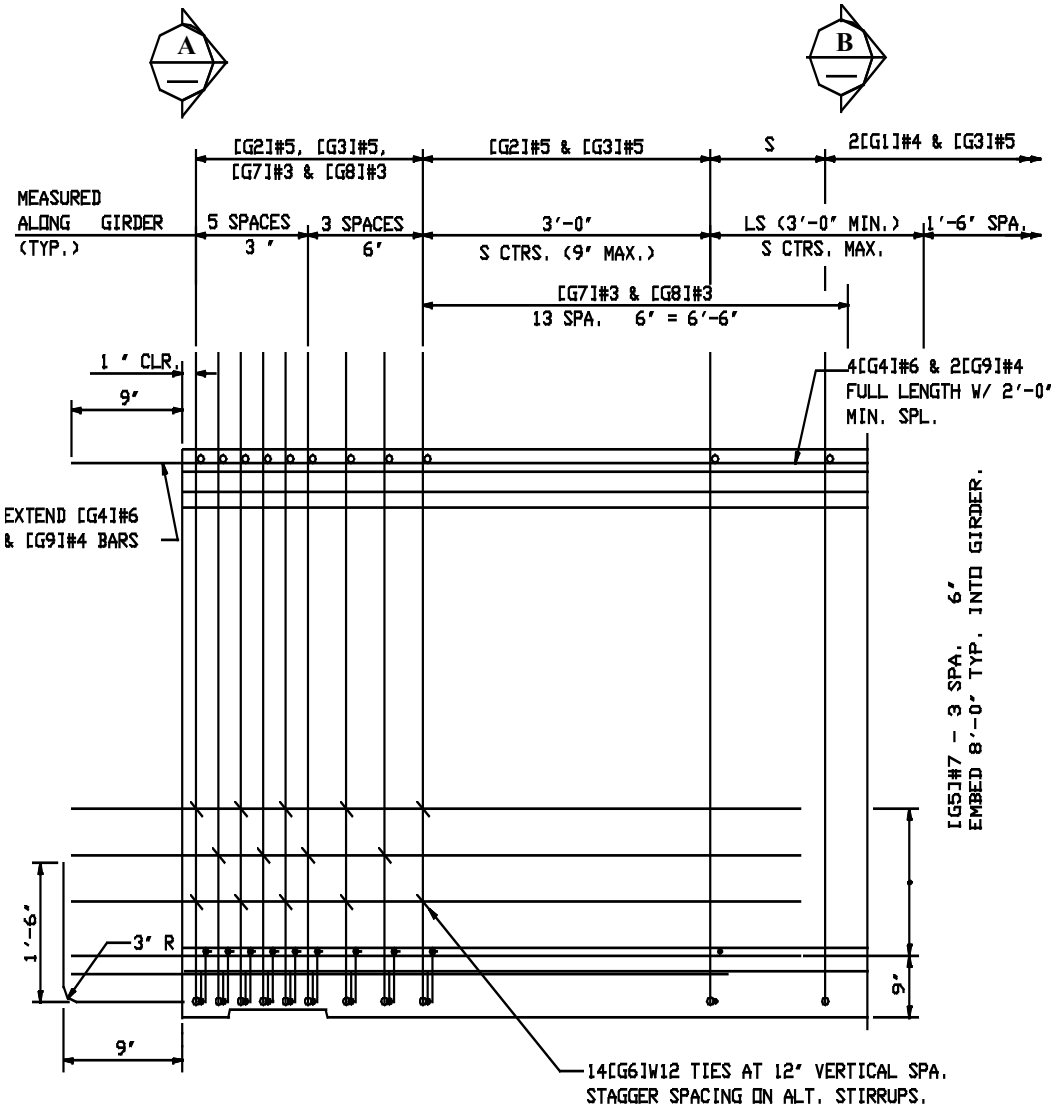

Figure 3.3. Test Girder Mild Reinforcing Steel

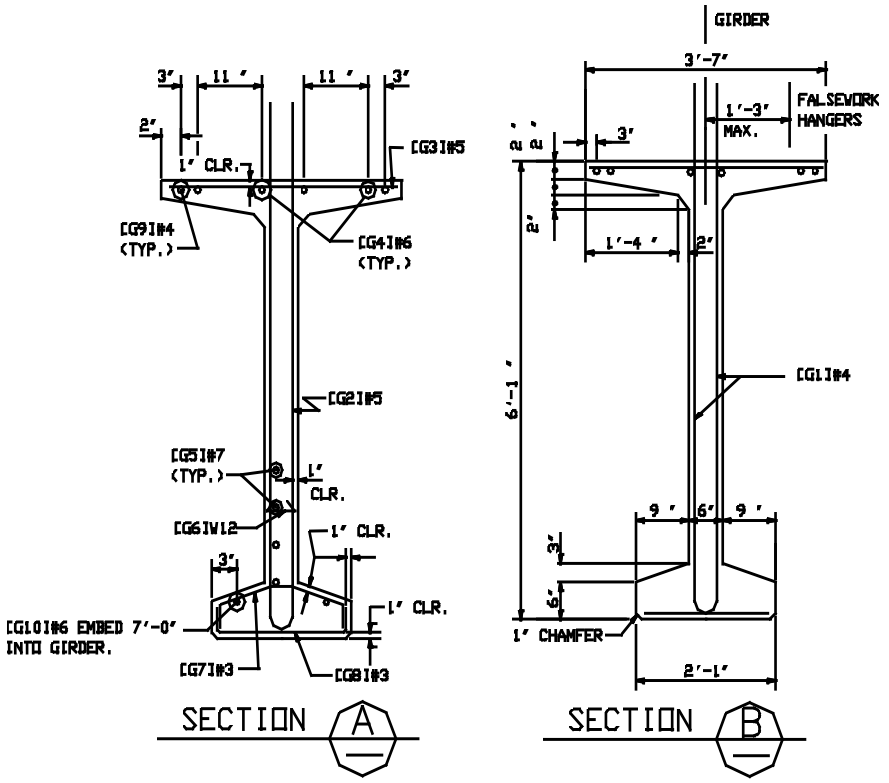

BENDING DIAGRAM

ALL DIMENSIONS ARE OUT TO OUT

MARK	LOCATION	SIZE	
G1	GIRDER STIRRUPS	4	
G2	GIRDER END STIRRUPS	5	
G3	GIRDER TOP FLANGE	5	STR.
G4	GIRDER LONGIT. FULL LENGTH	6	STR.
G5	GIRDER END LONGIT.	7	STR.
G6	GIRDER END TIES	W12	
G7	GIRDER END TIES	3	
G8	GIRDER END TIES	3	
G9	GIRDER LONGIT. FULL LENGTH	4	STR.
G10	GIRDER LONGIT.	6	STR.

** = VARIES FOR SKEWED SPANS

#3 OR #4 MAY BE SUBSTITUTED FOR W12, FIELD BENDING IS OPTIONAL.

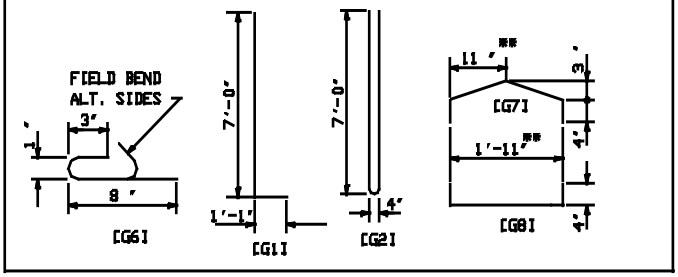

Figure 3.3. Test Girder Mild Reinforcement Steel (cont.)

The test girder was cast at Central Premix Prestress Co., Spokane, WA. The casting yard is out of doors. The ambient temperature lay in the range of -5°C to +5°C during the stressing and casting.

The strand for the test girder was stressed during the afternoon of Dec 11, 1996. The instrumentation was installed that evening and the concrete was cast on the morning of December 12, 1996. After casting the concrete, an insulating blanket was placed over the girder form to contain the heat generated by hydration and added steam. A thermocouple was embedded 1.52 m (5 ft) from one end at approximately mid-height of the girder in order to regulate the application of steam to the girder. The concrete was allowed to cure for 29 h, after which the forms were removed and the strands were destressed.

After destressing, the test girder was placed on timber blocks until it was approved for shipment. The test girder was shipped to the University of Washington campus on January 4, 1997. It was stored outside the Structural Research Laboratory on the north side of the building, in order to replicate, as closely as possible, the environmental conditions of the bridge girders.

3.2 BRIDGE GIRDERS

Figure 3.5 shows a layout of the bridge and the girder numbering system. Each girder line is denoted by a letter, and each span, by a number. Figure 3.6 shows a section through the bridge at pier 2.

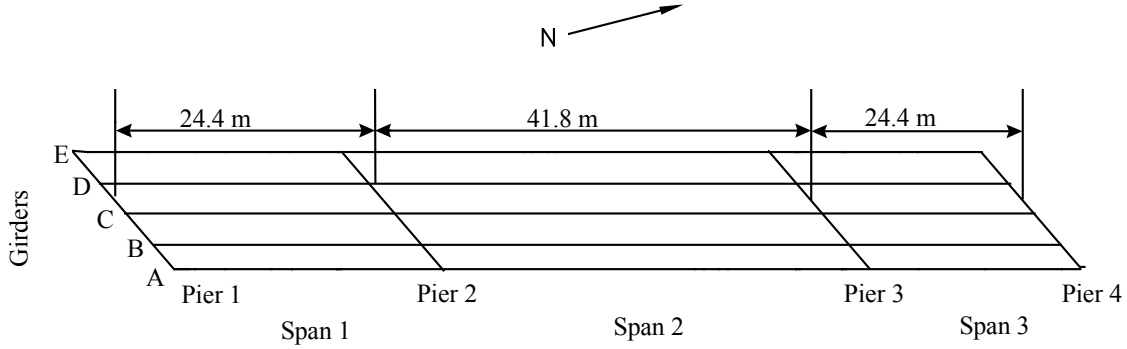

Figure 3.4. Bridge Layout

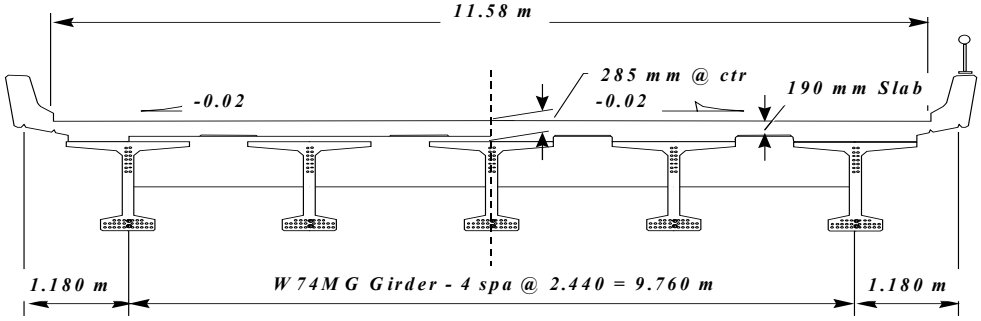

Figure 3.5. Bridge Cross-Section at Pier 2 (looking north)

Fifteen bridge girders were fabricated for the three-span bridge. Ten had spans of 24.4 m (80 ft), and 5 had spans of 41.8 m (137 ft). The Washington W74G cross-section, shown in Figure 3.1, was used for all girders. In the field, the girders were made composite with the 190-mm (7.5-in.) deck slab, which includes a 10-mm (0.4-in.) integral wearing surface. Table 3.3 lists section properties.

Table 3.3. Section Properties

	Girder	Composite
Depth, mm	1 865	2 045
Area, mm^2	485 300	765 100
I, mm^4	227.5×10^9	400.4×10^9
y_b, mm	970	1 330
S_b, mm^3	234.4×10^6	301.0×10^6
y_t girder, mm	895	535
S_t girder, mm^3	254.3×10^6	748.8×10^6
y_t slab, mm	-	715
S_t slab, mm^3	-	560.2×10^6

The arrangement of mild reinforcing steel for the bridge girders was similar to that of the test girder, shown in Figure 3.3.

Each bridge girder contained both harped web strands and straight bottom flange strands. The web strands were harped at a distance of 0.4 times the length from each end. Figure 3.6 shows an elevation of one half of one of the bridge girders with the tendon strand profile. The web strands are splayed from the harping point, where they are bundled, and are spaced vertically at 51 mm (2 in) at the girder end.

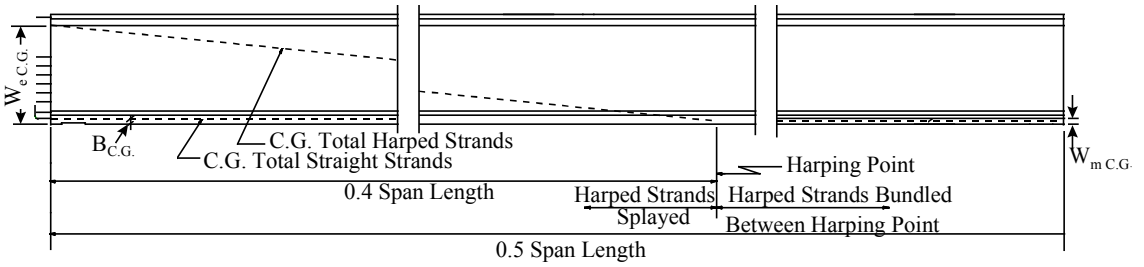

Figure 3.6. Elevation of Bridge Girders

Table 3.4 lists the design details for the bridge girders. The distances from the bottom of the girder to the center of gravity of the harped web strands at the end and at mid-span are labeled $W_{e\,C.G.}$ and $W_{m\,C.G.}$, respectively. The location of the center of gravity of the bottom strands is labeled $B_{C.G.}$. For the long girders, 14 harped and 26

straight strands were used.

Table 3.4. HPC Bridge Girder Design Details

Girder	Skew	Length (m)	56-day f'c (MPa)	Release f'c (MPa)	No. of Harped Strands	No. of Straight Strands	Jacking Stress (MPa)	$W_{m\ C.G.}$ (mm)	$W_{e\ C.G.}$ (mm)	$B_{C.G.}$ (mm)
Span 1	40°	23.3	68.9	34.5	6	8	1400	76.2	1360	47.6
Span 2	40°	40.6	68.9	51.0	16	26	1400	85.7	1130	92.1
Span 3	40°	23.3	68.9	34.5	6	8	1400	76.2	1360	47.6

Table 3.5 summarizes time-dependent prestress losses for the interior long girders obtained from different methods discussed in Chapter 2. Losses from the AASHTO Time Step method are lower than the ones obtained from the AASHTO LRFD Refined method, because the Time Step method is based on effective prestress force rather than the initial force at transfer. Prestress losses computed from the Modified Rate of Creep method are lower than those obtained from other methods. The WSDOT selected the Modified Rate of Creep method as the basis for the design.

Table 3.5. Predicted Time-Dependent Prestress Losses (MPa)

	AASHTO Lump Sum	AASHTO Refined	AASHTO Time Step	Modified Rate of Creep
Transfer	159.2	159.2	159.2	159.2
Before Slab Cast.	-	238.5	227.3	197.3
After Slab Cast.	-	232.5	214.2	175.8
Final	348.2	376.1	327.5	283.5

The final service stresses at the mid-span and the harping point, predicted using the Modified Rate of Creep method, are summarized in Table 3.6. The concrete stresses at transfer are not shown, but they also satisfy the requirements of the AASHTO Specifications.

Table 3.6. Summary of Concrete Stresses at Service

	At Mid-Span			At Harping Point		
Stress (MPa)	f_b	f_t(girder)	f_t(slab)	f_b	f_t(girder)	f_t(slab)
Girder	10.15	-9.35	-	9.74	-8.98	-
Slab + haunch	12.26	-11.30	-	11.77	-10.85	-
Diaphragm	1.41	-1.30	-	1.27	-1.17	-
Traffic barrier	1.85	-0.74	-0.99	1.77	-0.71	-0.95
ΣDL	25.67	-22.69	-0.99	24.55	-21.71	-0.95
LL - Service I	-	-4.73	-6.33	-	-4.58	-6.12
LL - Service III	9.42	-	-	9.11	-	-
Prestressing	-35.98	8.66	-	-35.98	8.66	-
Stresses under permanent load	-	-14.03	-0.99	-	-13.04	-0.95
Allowable	-	-31.05	-12.60	-	-31.05	-12.60
Stresses under all loads	-0.89	-18.76	-7.32	-2.32	-17.62	-7.07
Allowable	0.00	-41.40	-16.80	0.00	-41.40	-16.80

Note: Tension (+)

Girder deflections predicted by the Modified Rate of Creep method are presented in Table 3.7.

Table 3.7. Girder Deflection

	Total Deflection in mm
At Transfer	-80
Before Slab Casting	-107
After Slab Casting	-56
Final	-44

The long girders were cast individually on a 61.0-m- (200- ft-) long casting bed. After they were complete, the bed was reconfigured and the short girders were cast in it, end-to-end in pairs. The steam curing arrangements were the same as in the Test Girder except that, in girder 2B, the thermocouple was located approximately 508 mm (20 in) above the bottom. The curing time differed for each instrumented girder. Table 3.8 lists the critical events and times for each of the instrumented bridge girders.

Table 3.8. Fabrication Information for Bridge Girders

Girder	Instrumentation Installation Day	Casting Day	Destressing Day	Time to Destress (Hours)
2A	3/5/97	3/6/97	3/7/97	28.25
2B	3/9/97	3/10/97	3/11/97	25
2C	3/11/97	3/12/97	3/13/97	24
1A	4/1/97	4/2/97	4/3/97	24.25
1C	4/1/97	4/2/97	4/3/97	24.25

After destressing, the girders were placed on timber supports in the yard, where they remained until the shipping date. During this time, finishing work was performed on the girders. Strain and camber readings were taken automatically and without interruption until April 29 when the instrumentation was removed for shipping. The girders for spans 1 and 2 were shipped on May 7, and the girders for span 3 were shipped on May 8.

The girders were erected during the night following the day they were shipped. During the next 5 months, work was done on the bridge at the contractor's convenience. During this time, the forms for the intermediate diaphragms, pier caps, and soffit were erected. The intermediate diaphragms were cast over a 10-day period between July 14 and July 23, and the deck was cast on September 23, 1997.

CHAPTER 4
INSTRUMENTATION PROGRAM

Instrumentation was installed in both the Test Girder (Section 4.1) and in bridge girders 1A, 1C, 2A, 2B, and 2C (Section 4.2). The instrumentation measured strains, temperature, strand slip-back, camber, and strand stress.

4.1 TEST GIRDER

The Test Girder was constructed and tested to gain experience installing the instrumentation. Results from the Test Girder's instrumentation helped finalize the locations and types of instrumentation that would be used for the bridge girders. Figure 4.1 shows the cross-section of the Test Girder with individual strand locations.

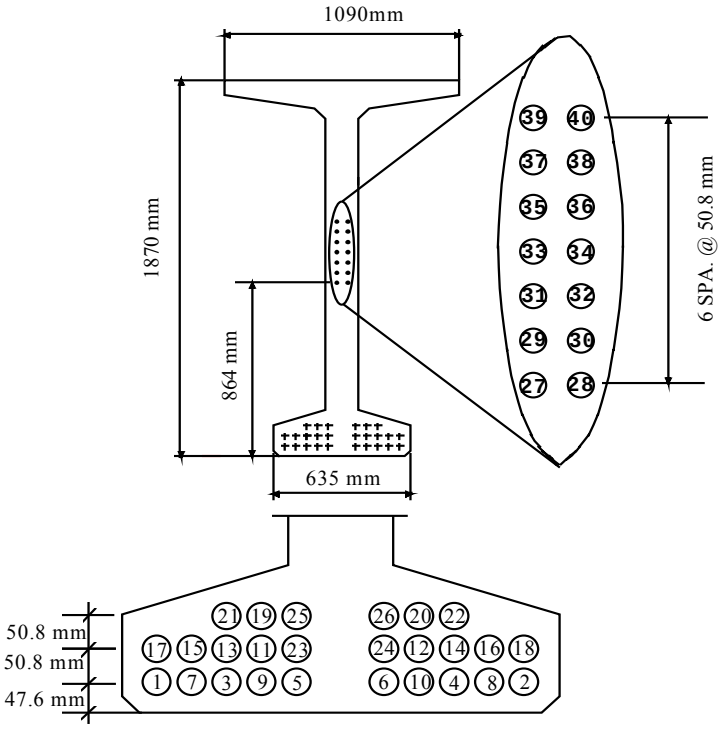

Figure 4.1. Strand Pattern in W74G Test Girder

4.1.1 Concrete Strains and Temperatures

Vibrating wire strain gauges were embedded in the Test Girder to monitor both temperatures and longitudinal strains. They were selected because of their history of long-term reliability. These gauges (Geokon model VCE-4200, 152-mm (6-in) gauge length) were embedded at mid-span and 1.52 m (5 ft) from one end. The layout of the midspan gauges is shown in Figure 4.2; the instrumentation layout at the 1.52-m (5-ft) cross-section was identical to the one at mid-span except the LW and UW gauges were omitted. In addition, a single vibrating wire strain gauge was embedded in each of two 152 x 305 mm (6 x 12 in) cylinders to monitor curing temperatures and for gauge calibration.

Two vibrating wire strain gauges (BL and BR) were embedded in the bottom flange of the girder. To secure the gauges in place, they were attached with a nylon cable tie to a 9.53-mm (3/8-in) diameter U-shaped section of reinforcement. Before casting, the U-shaped reinforcement was tied to the existing prestressed strands within the girder.

At mid-span, three gauges (LW, MW, and UW) were placed at the quarter points over the height of the girder. The gauge at mid-height of the girder (MW) was attached to a U-shaped piece of reinforcement and then tied to the prestressing strand in the web of the girder. The remaining two gauges (LW and UW) were attached to a welded grid of four pieces of #3 reinforcing bar. Figure 3.3 shows the dimensions of the welded rebar grid. The grids were tied to the vertical stirrups in the girder. The gauge at mid-height of the 1.52-m (5-ft) instrumentation location (MW) was attached in the same manner as the mid-height gauge at the mid-span location.

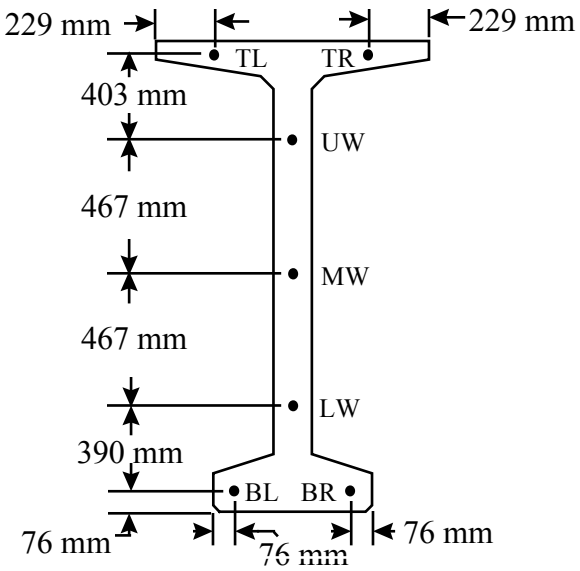

Figure 4.2. Vibrating Wire Strain Gauge Nominal Locations

Two vibrating wire strain gauges (TL and TR) were placed in the top flange of the girder at both instrumentation sites. These gauges were attached to grids similar to those used in the web (Figure 4.3). The steel grids and gauges were placed in the girder by tying them to the girder's horizontal top reinforcement.

After installing the gauges, all gauge locations were measured to the nearest 3 mm (1/8 in). The lead wires were then gathered into a bundle, inserted into a section of garden hose for protection, and brought out the top of the girder.

A blockout was formed in the top flange with a section of a 76-mm (3-in) diameter PVC tube. After the forms were removed, the lead wires from the gauges were run down through the tube and connected to a multiplexer.

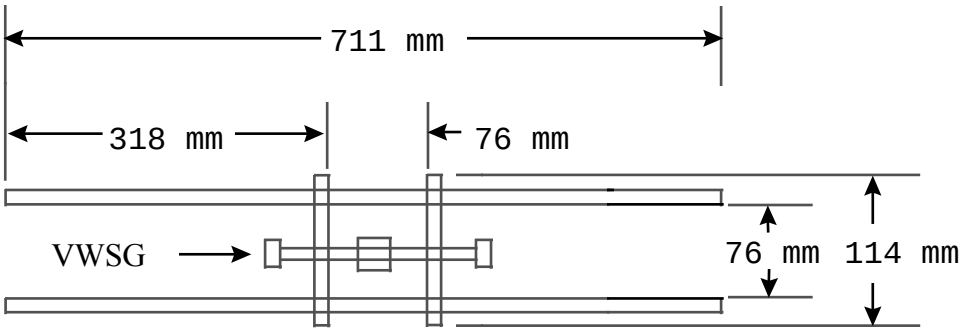

Figure 4.3. Welded Grid Rebar Cage

4.1.2 Strand Slip-Back

Potentiometers were used to measure the strand slip-back as the strand force was transferred to the Test Girder. The goal was to compute the transfer length from the slip-back. Strand slip measurements were made only at the jacking end, where the strand was released gradually. The slip-back could not be measured on the dead end, where the strand was flame cut, without damaging the instruments. After the girder end forms were removed, potentiometers were attached to 10 strands, namely strands 1, 2, 13, 14, 25, 26, 27, 32, 35, and 40 (Figure 4.1).

Each potentiometer was pre-attached to a wooden block that had a 15-mm (0.6-in) diameter hole drilled longitudinally though the block as shown in Figure 4.4. The block was cut in half, which allowed it to be placed over the prestressing strand, and then the two halves were bolted together. To provide a flat and smooth bearing surface for the potentiometers, a 25.4-mm (1-in) square piece of sheet metal was attached with epoxy to the face of the Test Girder next to the instrumented strand. The potentiometer, which was attached to the top of the block, read the relative displacement between the strand and the sheet metal. Each potentiometer was wired to a central patch board. Voltage readings were taken after each destressing stage using a digital voltage meter. The voltage readings were then converted into slip-back measurements.

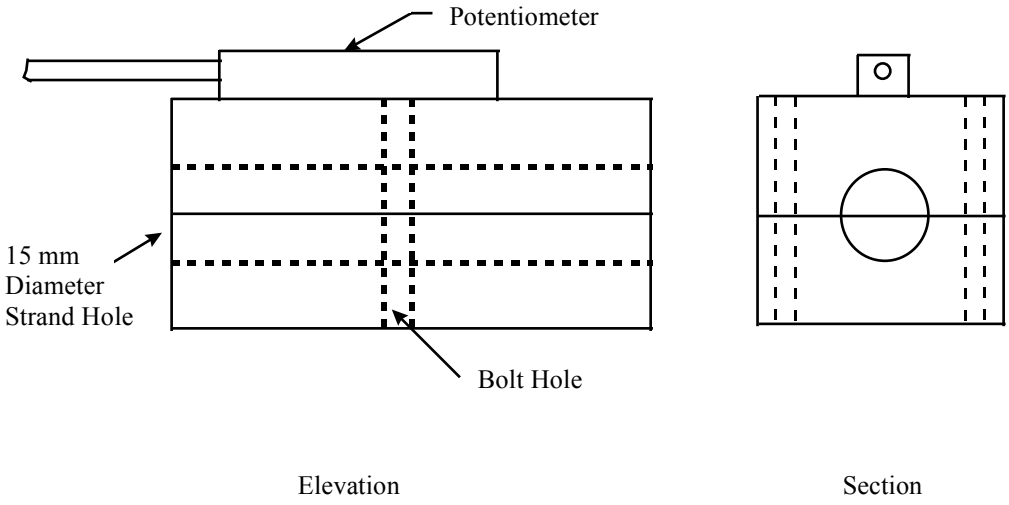

Figure 4.4. Potentiometer and Wooden Block

4.1.3 Girder Camber

A stretched-wire system was used to measure the camber in the Test Girder (Figure 4.5). A bearing pulley was fitted over a bolt through the web at one end of the girder. At the opposite end, a high-strength wire was fixed to another bolt through the girder web. The wire was then placed over the pulley and stressed by hanging a 0.155-KN (35-lb) weight on the wire. At mid-span a light trolley ran on two pulley wheels on the stretched wire. The trolley was prevented from falling by a third pulley wheel below the wire and by the fact that its center of gravity lay below the wire. An LVDT attached to a board on the girder web measured the relative vertical displacement between the trolley and the girder web. The trolley was constrained to move only vertically with respect to the girder by installing a drawer-glide vertically on the board and connecting the trolley to the gliding end.

The drawer glide was not really necessary on the Test Girder, but it was installed in order to verify that it would work on the bridge girders, where it would be needed to prevent horizontal movement of the wire away from the web. Such motion could damage the LVDT plunger, which might subsequently bind.

During design of the stretched-wire system, it was found that pulley friction controlled the accuracy of the system. Only if the pulley were perfectly frictionless would the tension, and thus the mid-span sag in the wire, remain constant. High-quality pulleys with sealed roller bearings were thus used in all cases. Figure 4.5 shows an elevation of the Test Girder with the stretched-wire system.

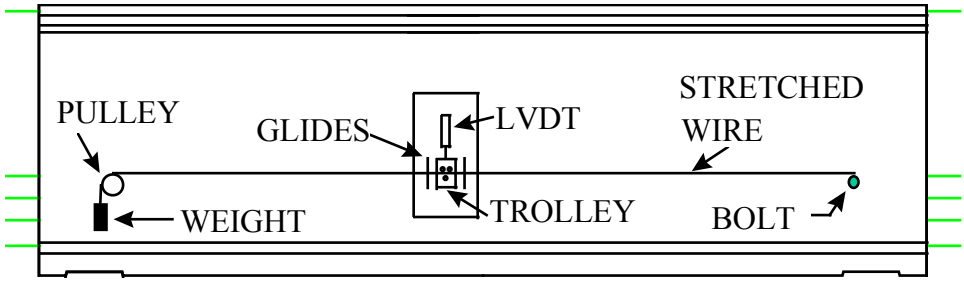

Figure 4.5. Test Girder Stretched-Wire System

4.1.4 Concrete Stress

Vibrating wire stress gauges, also supplied by Geokon, were installed to measure the concrete stress. Two stress gauges were placed at mid-span, one in the top of the girder and one in the bottom (Figure 4.6). Each stress gauge was attached to the vertical stirrups using tie wire. Unfortunately, the gauge readings were so strongly influenced by the large change in concrete temperature during curing that they were useless. As a result, such gauges were not installed in the bridge girders.

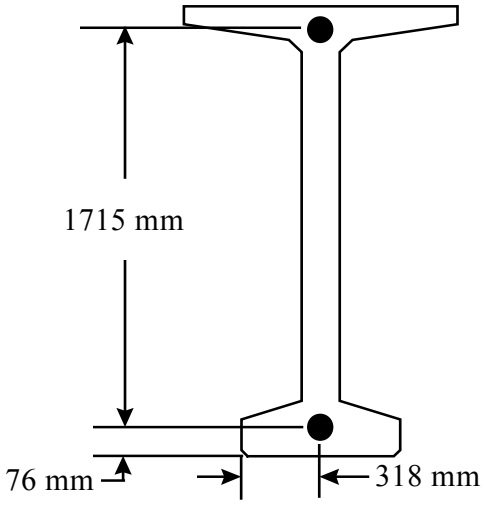

Figure 4.6. Locations of Vibrating Wire Stress Gauges

4.1.5 Strand Stress

A load cell was installed by the precaster on strand number 29 (Figure 4.1) to measure the strand stress during fabrication. The load cell was located at the dead end anchorage. Unfortunately, the readings proved unreliable and so were not used in the subsequent analysis.

4.2 BRIDGE GIRDERS

Experience gained during the instrumentation of the Test Girder was used to design the instrumentation in the bridge girders. The system used was similar, but not identical, to that used in the Test Girder.

4.2.1 Concrete Strains and Temperatures

VWSGs were embedded in five of the W74G bridge girders. In these instrumented girders, gauges were embedded both at 1.52 m (5 ft) from the end nearest pier 2 and 457 mm (18 in) from mid-span toward pier 2. The gauges could not be placed exactly at mid-span due to dowel-ducts at mid-span. Figure 4.7 shows a plan and elevation view of the bridge, with the instrumentation sites marked. Each

instrumentation site can be identified by span (1 or 2), girder (A, B, or C) and span location (E or M).

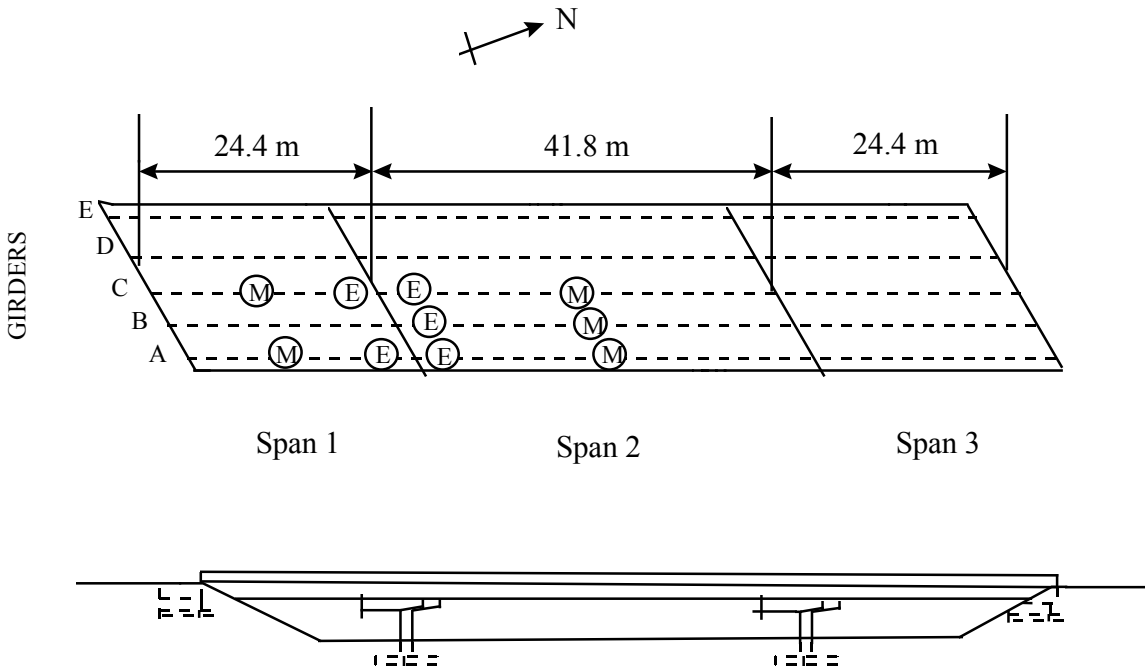

Figure 4.7. Instrumentation Sites in HPC Bridge

Each instrumentation site was instrumented in the same manner. Figure 4.7 shows the VWSG locations at a typical instrumentation site. To speed installation, the gauges were pre-attached to welded rebar grids. In the last girders cast, gauges LW, MW, UW, and TG were all attached to a single grid. This led to fast, accurate gauge placement. All lead wires were gathered, protected in a short section of garden hose, and run out of the top of the girder. At each instrumentation site, a section of PVC pipe was placed through the top flange to accommodate the running of lead wires after the girder forms had been stripped.

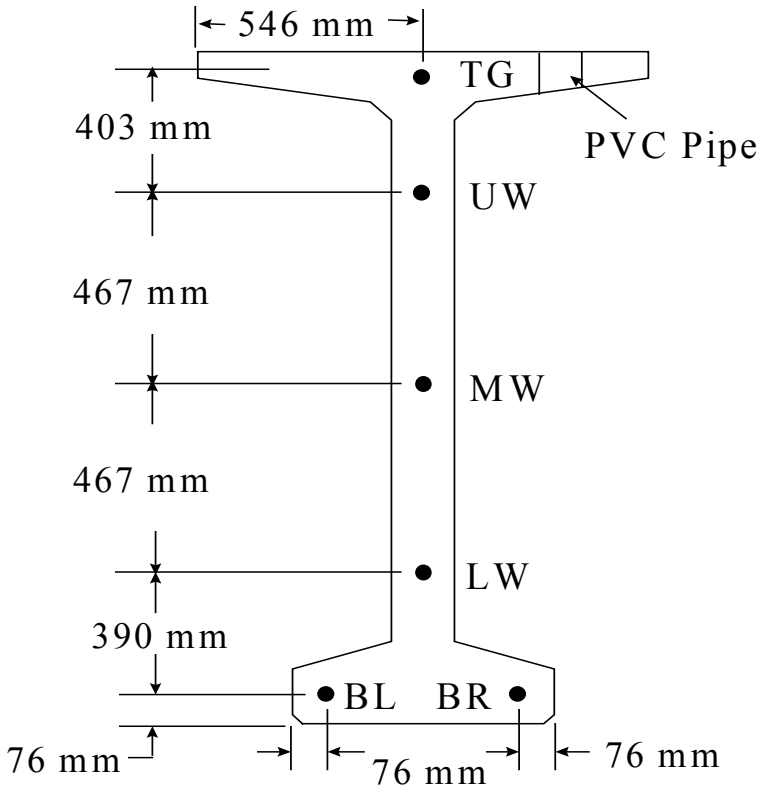

Figure 4.8. Cross-Section of Typical Instrumentation Site

After the forms were removed, a multiplexer was attached to the web of each girder at sites 1A-E, 1C-E, 2A-E, 2B-E, and 2C-E. Here, the symbol 1A-E indicates the end instrumentation site in girder A of span 1. The cables from the gauges at these sites ran down through the flange blockouts and were connected to the multiplexers. Cables from the mid-span gauge sites (1A-M, 1C-M, 2A-M, 2B-M, and 2C-M) were fed through their respective PVC pipes and ran along the length of the girder to the multiplexers at sites 1A-E, 1C-E, 2A-E, 2B-E, and 2C-E, respectively. Each multiplexer was connected to a datalogger located near pier 2 on Girder B in span 1 (1B). To support the cables, cable trays made from 50.8-mm (2-ih) diameter plastic pipe, split longitudinally, were bolted to the web of each of the five instrumented girders. The trays were bolted every 1.52 m (5 ft) between mid-span and the instrumentation site near pier 2.

4.2.2 Strand Slip-Back

Strand slip-back was measured on girders 1-A, 2-A, and 2-B (Figure 4.7). The method for installing the potentiometers and measuring the strand slip-back in the bridge girders was the same as in the Test Girder, except that a wooden block, cut to the same skew as the bridge, was used to provide a flat, perpendicular reference surface. The strand pattern at the end of the long bridge girders (span 2) was the same as the strand pattern in the Test Girder (Figure 4.1).

On the first girder to be instrumented, the wooden blocks were attached with epoxy but dropped off the girder, which led to delays. This was unfortunate, because the precaster was anxious to stress the concrete quickly before it cooled and cracked. Installation time was particularly critical because the blocks could not be attached before the end forms were removed. The problem was caused by the fact that the epoxy would not adhere to the hot, moist concrete. In subsequent girders hot glue was used instead and gave good results.

Table 4.1 lists the locations at which strand slip-back measurements were taken. The strand locations for the short girders (spans 1 and 3) are shown in Figure 3.9.

Table 4.1. Instrumented Slip-Back Strands

Girder	Strands Measured
1A	1,4,5,8,9,10,13,14
2A	5,6,13,14,25,26,27,32,35,40
2B	6,13,14,25,26,27,32,35,40

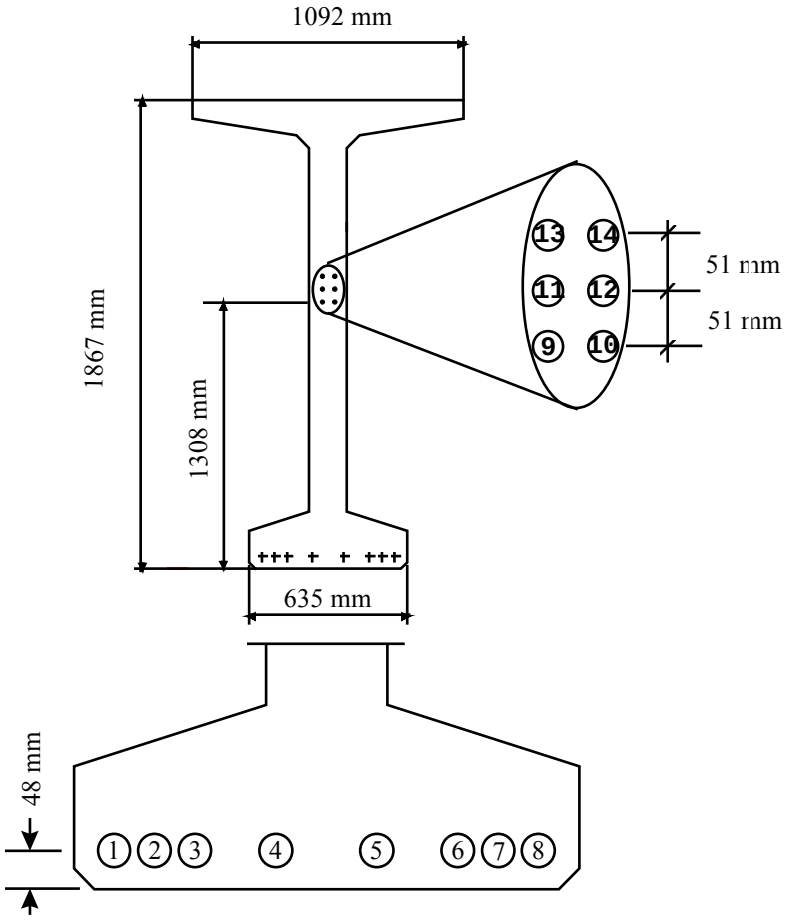

Figure 4.9. Strand Pattern for Spans 1 and 3

4.2.3 Girder Camber

A stretched-wire system was used to measure the camber of the bridge girders. The stretched-wire setup was identical to the setup for the Test Girder (Figure 4.4), except that the magnitude of the weights at mid-span were increased to force the wire to pass below the intermediate diaphragms. The LVDTs were connected to a multiplexer and displacements were recorded using a datalogger.

The drawer glides on the stretched-wire-system had suffered damage in the precast yard because their bearings had been contaminated with cement powder during the finishing. Cleaning them sufficiently proved impossible. They were replaced by a pair of oil-impregnated plastic blocks with vertical slots that allowed the stretched wire to

move freely vertically, but prevented horizontal motion (Figure 4.10). That system worked well and led to an accuracy of approximately ± 1.5 mm (± 0.06 in). The weight of the trolley was effective in minimizing vibrations. Additional protection against accidental damage at the bridge site was provided by enclosing the trolley and LVDT in a plywood box.

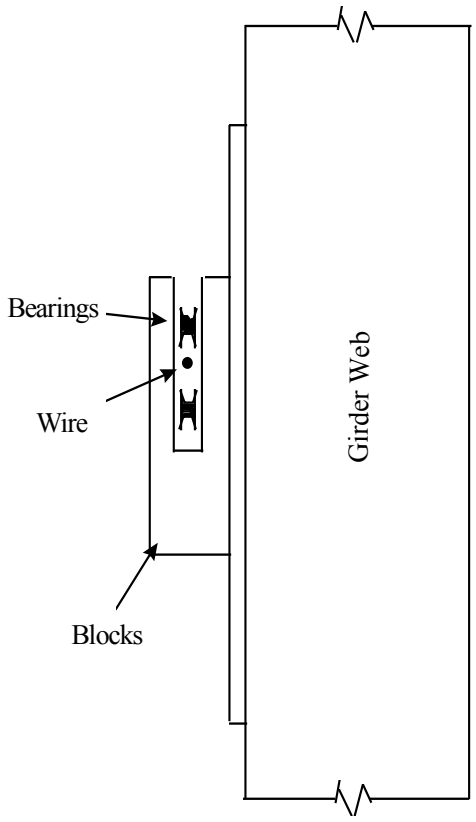

Figure 4.10. Bridge Stretched-Wire System

To complement the stretched-wire system, level readings were obtained in the production yard by reading rulers that were attached to the webs of the girders at mid-span and 0.914 m (3 ft) from each end. At the bridge site, level readings were taken by placing a titanium rod vertically at marked locations along the bottom of the girders. A ruler, which was attached to the rod, was then read with the level. The calculated values of camber were adjusted using the girder's deflection curve to compensate for the fact

that the readings were not taken exactly at the end of the girders. Readings at the bridge site were always taken between 6 A.M. and 8 A.M. in order to minimize the effects of temperature.

At the bridge site, the level produced readings that were repeatable to ±1 mm (±0.04 in). In the casting yard, access to the girders was more difficult and, particularly for the readings taken at destressing, the accuracy was almost certainly not as good.

4.2.4 Strand Stress

A load cell was used by the fabricator to measure the strand stress during fabrication. One load cell was attached to strand number 29 (Figure 4.1) in each of the long-span girders (span 2) and to strand number 9 (Figure 4.8) in the two short girders (span 1). In each case the load cell was placed directly behind the strand chuck at the dead end anchor. Unfortunately, the readings proved too unreliable to be used.

4.3 GAUGE PREPARATION

Prior to casting, calibration tests were performed on the VWSGs, stress gauges, potentiometers, and LVDTs. All calibration tests were performed in air only, except for the VWSGs, which were calibrated in both air and concrete. The air calibration numbers for each gauge closely matched the calibration number given by the manufacturers. The calibration test for the VWSG embedded in a 152 x 304 mm (6 x 12 in) cylinder proved inaccurate due to the end effects on the cylinder.

Each gauge was tagged with an individual label and color to help facilitate field instrumentation and monitoring. Field manuals were made for each type of instrumentation location. These manuals had matching tags, which were marked next to a figure identifying gauge locations within the girders. The instrumentation team practiced using these manuals and gauges on a 1.83-m (6-ft) mock-up of the girder. Steel was placed in every location that would be encountered in the field in an effort to discover any problems prior to field installation. Photographs were taken of the installed gauges in the mock-up and then placed in the manuals to help provide a visual picture of

how the gauge would be installed in the girder. This was necessary because the same installation team members were not available for all girders.

4.4 MONITORING PROGRAM

During fabrication, the jacking stress, release stress, and strand slip-back were measured for the Test Girder and five bridge girders. Temperature, strain distributions at mid-span and 1.52-m (5-ft) locations, and mid-span camber were monitored during fabrication. Monitoring will continue at the bridge site for 3 years from the time of girder fabrication.

4.4.1 Concrete Strains and Temperatures

Concrete strain and temperature are being monitored using VWSGs. Table 4.2 shows the frequency of strain and temperature readings in the Test Girder and production girders.

Table 4.2. Frequency of Strain and Temperature Readings

Girder	Time	Reading Interval
Test Girder	Until Destress	15 minutes
	During Destress	1 minute
	Until Approximately 6 Months After Casting	1 hour
	As Long As Possible	6 hours
Production Girders	Until Destress	15 minutes
	During Destress	1 minute
	Until 6 Months After Casting of Deck	1 hour
	At 6 Months After Casting of Deck	intense 36-hour monitoring
	Until End Of Project	6 hours

4.4.2 Strand Slip-Back

Strand slip-back was measured in the Test Girder, two of the long bridge girders (span 2), and one short bridge girder (span 1)(Sections 4.1.2 and 4.2.2). Transfer of the stress from the prestressing strands occurred in stages, the number of which depended on the girder. Readings from the potentiometers were taken before transfer and again after each destressing stage. Table 4.3 lists the number of destressing stages in each girder and the strands that were monitored (Figures 4.1 and 4.8).

Table 4.3. Strand and Number of Stages

Girder	Destressing Stages	Strands Monitored
Test Girder	18	1,2,13,14,25,26,27,32,35,40
2A	10	5,6,13,14,25,26,27,32,35,40
2B	10	6,13,14,25,26,27,32,35,40
1A	14	1,4,5,8,9,10,13,14

4.4.3 Girder Camber

Camber for girders A, B, and C in span 1, and all five girders in span 2 will be measured periodically using a surveyor's level. Level readings will continue for 3 years after casting. Table 4.4 shows the schedule for camber measurements with the level.

Table 4.4. Schedule of Level Readings

Time of Reading	Test Girder	Production Girders
Before Transfer	•	•
During Transfer (after each transfer stage)	•	•
As Permitted in Yard		•
Before Shipment		•
Bi-Weekly Until Slab Casting		•
Slab Casting		•
Approximately 1,3,6 Months		•
Approximately 1,2,3 Years	•	•

During construction an automated stretched-wire system was installed on the instrumented girders (1A, 1B, 1C, 2A, 2B, and 2C) as often as construction permitted. After construction is completed, the automated stretched-wire system will be permanently attached to the instrumented girders. Camber readings from each of these girders will be taken at the same frequency as the concrete strains and temperatures.

4.4.4 Strand Stress

A load cell was attached to one 15-mm (0.6-in) prestressing strand on both the Test Girder and all five of the production girders. Strand force was measured after jacking and again before transfer.

CHAPTER 5
OBSERVED BEHAVIOR

The discussion of observed behavior is organized into two sections. Section 5.1 discusses the behavior of the girders from the time of casting to the time of destressing. Section 5.2 discusses the service behavior of the girders after destressing.

5.1 CASTING THROUGH DESTRESSING

Table 5.1 lists the casting dates, average slump, hours of curing until destressing, and the average compressive strengths measured by Central Premix Prestress Co. at the time of destressing for the instrumented girders. Destressing was usually completed approximately 2 h after the cylinders were broken, so at the end of destressing the concrete strength adjacent to the thermocouple was somewhat higher than the value in Table 5.1.

Table 5.1. Girder Fabrication Data

Girder	Casting Date	Average Slump (mm)	Time to Destress (hours)	Average Strength at Destress (MPa)
Test	12/11/96	108	28	56.2
2-A	3/6/97	111	28.25	55.2
2-B	3/10/97	105	25	52.2
2-C	3/12/97	127	24	51.7
1-A	4/2/97	121	24.25	53.7
1-C	4/2/97	121	24.25	53.7

5.1.1 Temperature

Figure 5.1 shows the temperature history for the mid-span of girder 2B, measured from casting through destressing. The temperature histories during casting for the remaining instrumented girders are provided by Barr (Barr, 1997). The time shown as the abscissa in each of the plots starts at the time when the first girder was cast (March 6, 1997, for the production girders).

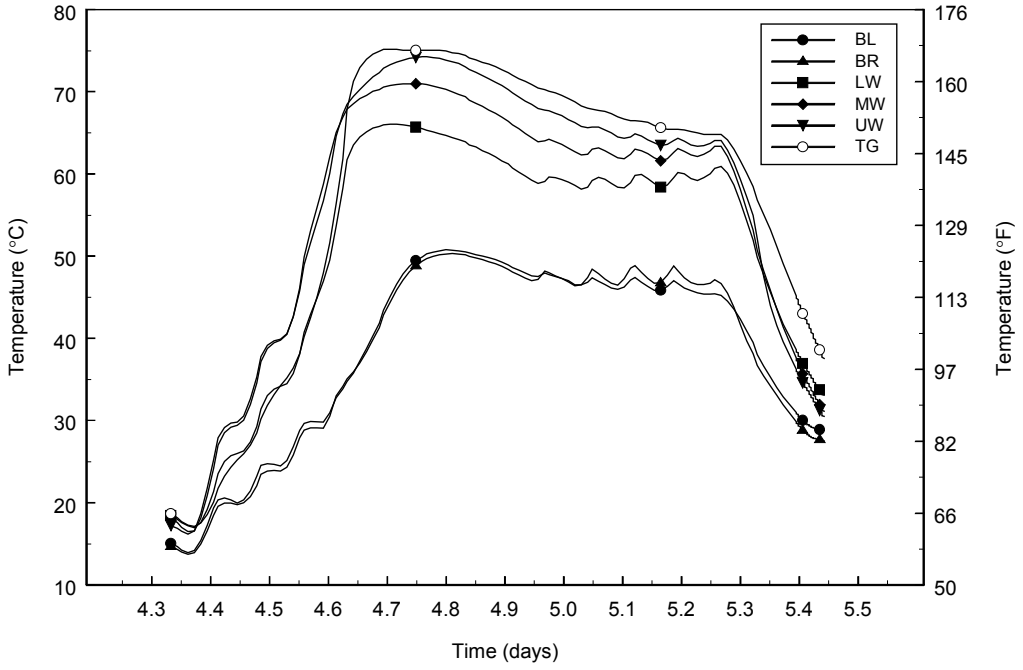

Figure 5.1. Casting Temperatures at Mid-Span of Girder 2B

Figure 5.1 shows that the concrete temperature varied with time; it was coldest when the concrete was first cast but it heated up as the curing process continued. The ripples represent activation of the automatic steam system. Directly after casting, hydration had not started so steam heat was needed to reach the target temperature. Thereafter, the hydration reaction was sufficient to maintain the target temperature until

approximately 15 h after casting, when steam was again needed. At day 5.25 (25.5 h after casting), the steam was turned off and the forms removed, which resulted in a temperature decrease.

The temperature also varied substantially over the height of the girder. The concrete's temperature was lowest at the bottom and highest at the top. The peak temperature difference averaged nearly 25°C (45°F) in each girder. This variation can be attributed to the girder's being cast outside during winter, so the cold ground cooled the bottom of the girder, and because the steam heat rose to the top of the insulated blanket over the forms.

The temperature variation during curing may have significantly affected the concrete strength when the prestressing tendons were released. For the purpose of determining the release strength of the concrete in the girder, the contractor tested two 102 x 203 mm (4 x 8 in) cylinders, which had been connected to the sure-cure system (Table 5.1). Since the thermocouple for the sure-cure system was usually placed at the mid-height of the girder, the concrete in the 102 x 203 mm (4 x 8 in) cylinders was cured at higher temperatures than the concrete at the bottom of the girder. The lower curing temperatures in the bottom of the girder would be expected to produce concrete that was weaker than that of the 102 x 203 mm (4 x 8 in) cylinders. This effect can be significant, since the highest stress in the girder is at the bottom.

The effect of the temperature variation on concrete strength in the bottom of the girder can be estimated with maturity. Using the measured temperature histories during casting of girder 1A by the bottom (BL and BR) and LW gauges, the maturity of the concrete in the girder was calculated from the start of hydration using Equation 5.1 (Lew and Reichard, 1978). The temperature history of the 152 x 304 mm (6 x 12 in) cylinders taken from girder 1A was also monitored by the University of Washington (UW) researchers. Their maturity was also calculated using Equation 5.1.

$$maturity = \sum_{i=1}^{n} (T_i - (-12.2))(t_i) \qquad (5.1)$$

where

T_i = temperature (degrees Celsius)

t_i = time cured at T_i (hours)

Figure 5.2 shows the maturity values calculated using the LW temperature history, average temperature histories in the bottom gauges (BL and BR), and cylinder temperatures. Because the cylinders were taken back to the university, they were not cured with the sure-cure system. As a result of the thermocouple being placed near the LW gauge, the temperatures from the LW gauge can be used to calculate the maturity of the sure-cured cylinders, and the temperature of the bottom gauges represents the maturity of the concrete in the bottom of the girder. At the time of destressing, the cylinder concrete was the least mature, followed by the girder concrete at the bottom gauges, and then the LW gauge.

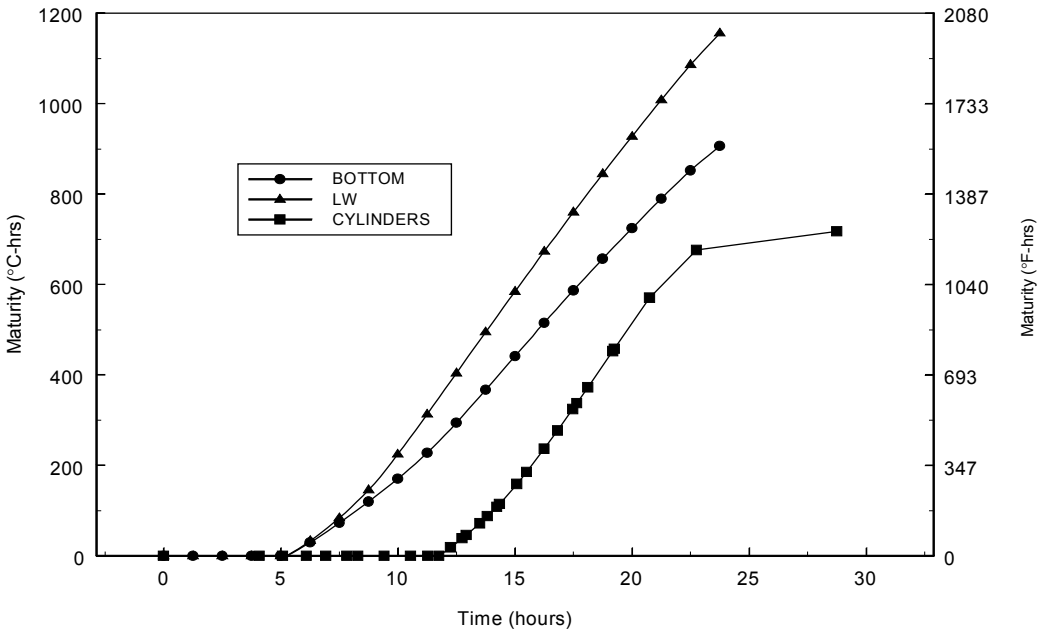

Figure 5.2. Maturity vs Time for Girder 1A Concrete

Two pairs of cylinders, which were cured in the same way as the temperature-monitored cylinders, were tested at 24.9 and 27.5 h after casting. The pairs had average compressive strengths of 43.9 MPa and 53.8 MPa (6,370 psi and 7,800 psi), respectively. Their strengths, at the time the sure-cure cylinders were broken (22.75 h), was estimated by fitting a straight line to the two known compressive strengths and calculating the strength at 22.75 h. The girder strength (Table 5.1) at the time the sure-cure cylinders were broken was then estimated by assuming a linear relation between strength and maturity. Based on these calculations, the strength of the concrete in the bottom flange and at the LW location of girder 1A, at the time the sure-cure cylinders were broken, was estimated to be 49.7 MPa and 54.2 MPa (7,210 psi and 7,860 psi), respectively. The estimated strength of the concrete at the LW location (54.2 MPa) is close to the sure-cure cylinder strength (53.8 MPa) measured by the fabricator, which indicates that the maturity is giving a good estimation of the concrete strength. As a result, the 49.7 MPa (7,210 psi) that was calculated for the strength of the concrete in the bottom flange is probably reasonable. Although a release strength of only 34.5 MPa (5,000 psi) was required for this girder, the effect of a similar temperature gradient on one of the girders that required a release strength of 51.0 MPa (7,400 psi) would be significant.

Figure 5.3 shows a comparison of the temperature histories for the BL gauges at mid-span in each of the girders that were instrumented. Because the thermocouple was placed lower in girder 2B than in the other girders, girder 2B experienced the highest maximum temperature. Except for the concrete in girder 2B, the concrete in the short girders (1A, 1C, and TG) was cured at higher temperatures than the concrete in the long girders.

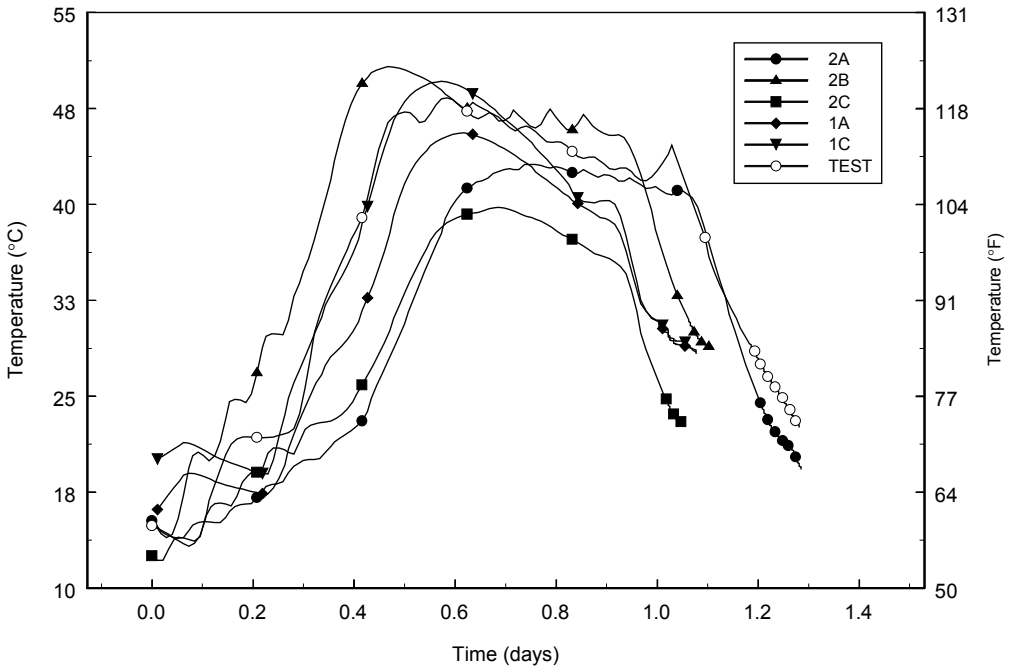

Figure 5.3. Mid-Span Temperatures in Instrumented Girders: Gauge BL

5.1.2 Strains

The strain histories during curing and destressing of the mid-span cross-section in girder 2B are shown in Figure 5.4. Compressive strains are negative.

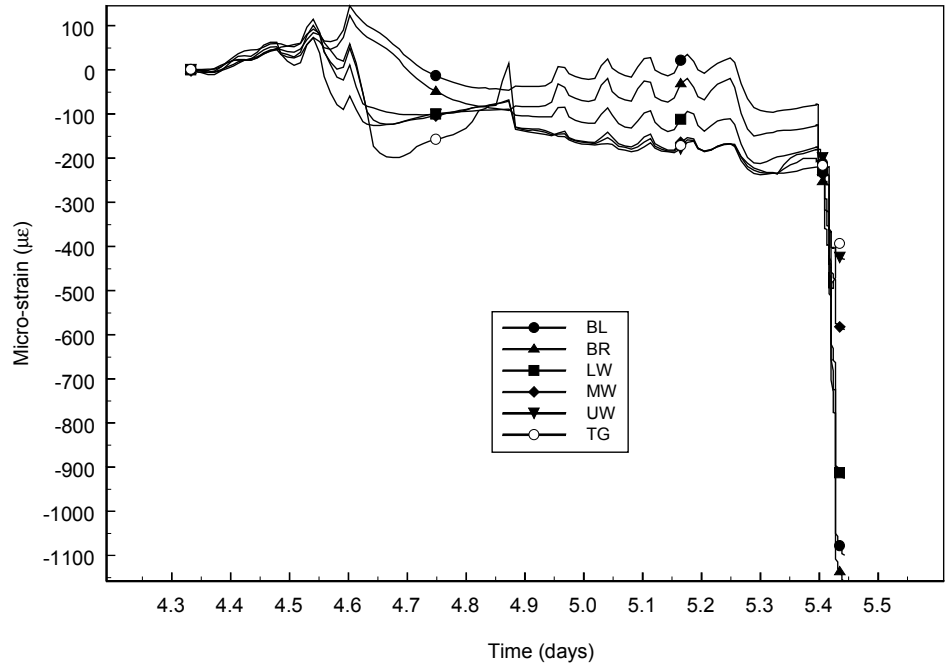

Figure 5.4. Casting Strains at Mid-Span of Girder 2B

The strains shown are the raw values recorded by the datalogger, and are approximately equal to the stress-induced component of the total strain. The internal configuration of the VWSG is such that a gauge suspended freely in air and heated will record no change in strain. Thus the total and non-thermal strains in concrete must be obtained from the raw values recorded by an embedded gauge. The total and non-thermal strains can be obtained by Equations 5.2 and 5.3, respectively. No corrections were made because the values of α_{conc} and α_{gauge} were not known with sufficient certainty. The gauges were made of stainless steel and the coefficients of thermal expansion of steel and concrete are often taken as being the same. If they are, Equation 5.2 shows that no correction is needed.

$$\varepsilon_{nonthermal} = \varepsilon_{raw} + \Delta T * (\alpha_{gauge} - \alpha_{conc}) \quad (5.2)$$

$$\varepsilon_{total} = \varepsilon_{raw} + \Delta T * \alpha_{gauge} \quad (5.3)$$

where

$\varepsilon_{nonthermal}$ = strain due to all non-thermal causes, including stress, creep, and shrinkage

ε_{raw} = raw strain values read from datalogger

ΔT = temperature change from time at which the concrete hardens

α_{gauge} = coefficient of thermal expansion of VWSG

α_{conc} = coefficient of thermal expansion of concrete

ε_{total} = strains due to all causes, including temperature

The strain histories for the other girders are similar (Barr, 1998), except for the UW and MW gauges at the mid-span of girder 1C, and the LW and MW at the mid-span of girder 2A. The UW and MW gauges at the mid-span of girder 1C experience large tensile strains during curing; however, they functioned correctly afterwards. The LW and MW gauges at the mid-span of girder 2A ceased to function when a hole was drilled through the web of the girder by Central Premix Prestress Co. and the gauge cables were severed.

Ripples in the strain measurements correspond to the ripples in Figure 5.1 and are casued by the activation of the steam. The abrupt change in strain at 5.45 days is a result of releasing the prestressing strands. The destressing process lasted about 2 h for girder

2A and about 1 h for each of the others.

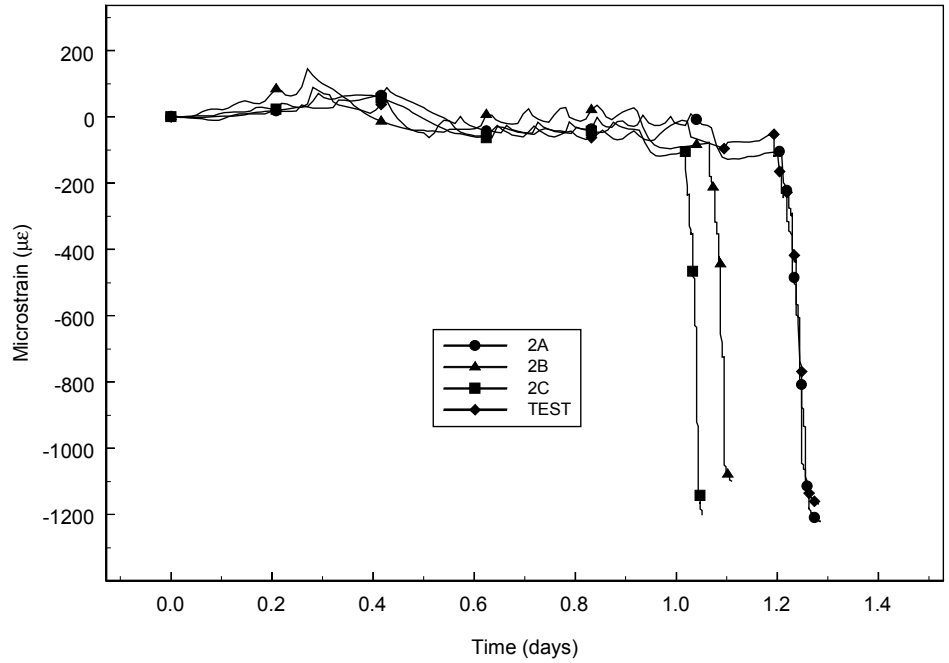

Figure 5.5. Mid-Span Strains in Most Highly Stressed Girders: Gauge BL

Figure 5.5 compares the BL gauge strain readings during curing and destressing of the four most highly stressed girders. The abrupt change in strain shows the effect of destressing. The differences in time at destressing reflect the different times to which the girders were cured. The difference between the bottom compressive strains at the end of destressing in girders 2A, 2C, and the Test Girder were within 4.5 percent of each other. The strain in girder 2B after destressing is less than that in the other girders as a result of being cured at a higher temperature. The strain in girder 2A is largest, because the destressing operation lasted the longest, so more creep occurred.

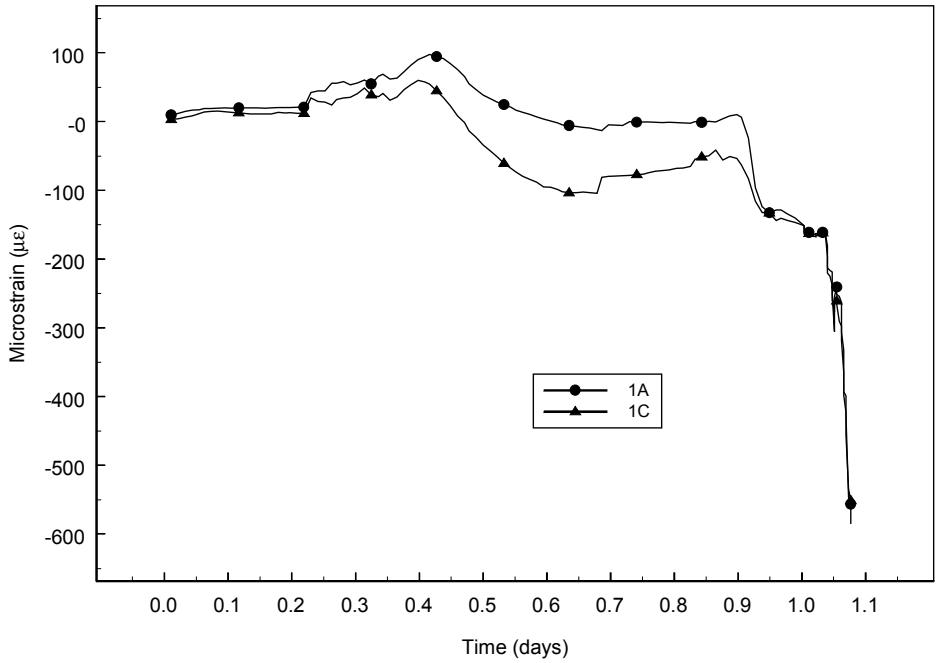

Figure 5.6. BL Gauge Strain Comparison of Span 1 Girders

Figure 5.6 shows the BL strains during curing and destressing for the instrumented girders in span 1. Girders 1A and 1C were cast and destressed in the same bed at the same time, therefore no time discrepancy at destressing exists. The difference between the strains in these two girders at the end of destressing was 4.2 percent. The magnitude of strain after destressing for the girders in span 1 was less than half that of the girders in span 2 because the girders contained fewer strands.

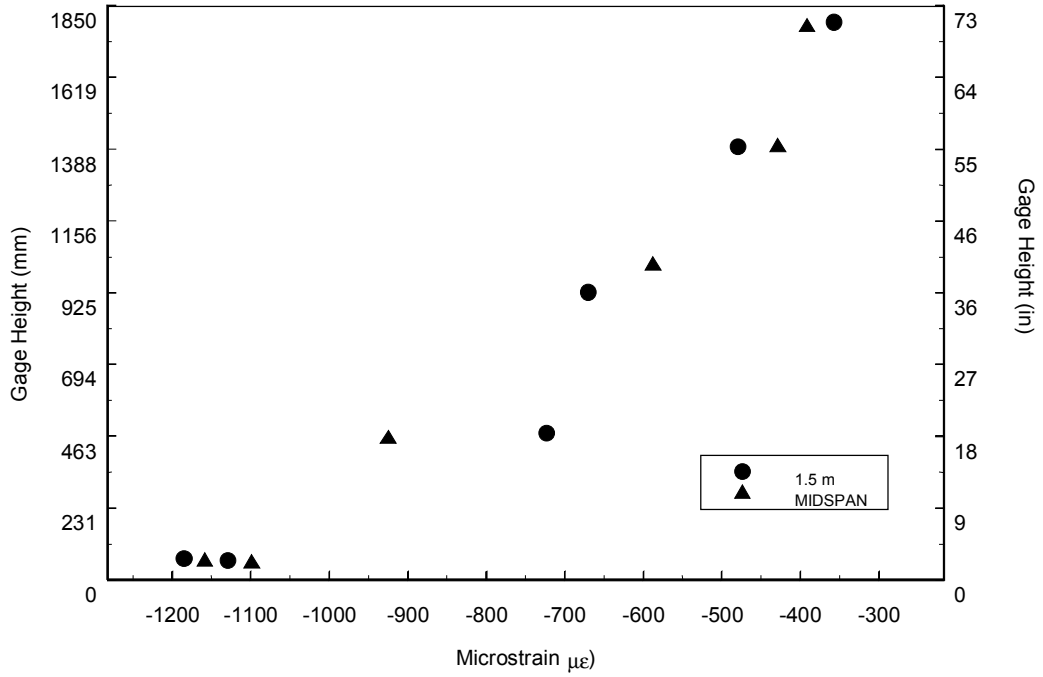

Figure 5.7. Cross-Sectional Strains in Girder 2B After Destressing

The VWSGs readings can be compared by checking whether plane sections remain plane after destressing. Figure 5.7 shows the strains in girder 2B immediately after destressing, at mid-span, and at the 1.5-m (5-ft) location.

At mid-span the strain distribution is nearly linear, except for the top gauge. At the 1.5-m (5-ft) cross-section, the strain distribution is also nearly linear, other than the gauge 18 in from the bottom (LW) and the top gauge. This discrepancy for gauge LW at the 1.5-m (5-ft) cross-section is typical of the other instrumented girders (Barr, 1998). During destressing, the end of the girder was lifted with lifting loops located near the 1.5-m (5-ft) cross-section. Stress concentrations caused by these lifting loops could account for the non-linear strain profile at the 1.5-m (5- ft) location.

5.1.3 Camber

Camber during destressing was measured with both a surveyor's level and a stretched-wire system for each of the girders, except the Test Girder and girder 2A, for which only the stretched-wire system was used. Because the level readings and the stretched-wire readings were taken from marks 0.91 m (3 ft) from the ends of the girders, adjustments were made to the level readings using the deflection equation for the girders to get a deflection relative to the end of the girder. Table 5.2 lists the cambers after destressing for each instrumented girder.

Table 5.2. Camber Measured by Surveyor's Level

Device	1A	1C	2A	2B	2C	Test Girder
Level (mm)	3.6	4.6	N/A	66.5	67.8	N/A
LVDT (mm)	1.5	6.4	63.5	65.3	66.0	2.29

The camber measurements for the span 2 girders are much larger than those for the girders in span 1 for both the level and stretched-wire system. The differences between the camber measurements for the level and stretched-wire system were within the accuracy of the instruments (3 mm).

Figure 5.8 shows the cambers measured during each stage of destressing for girder 2B. The strands in the web were cut in stages 1 to 4. Between stages 4 and 5, one end of the girder was lifted to prevent the concrete from crushing at the skewed corners, as the girder cambered upward. The change in camber readings between these two stages is thought to be a result of the lifting of the end. During stages 5 to 10, the bottom flanges were released. Similar trends were found with the other instrumented girders.

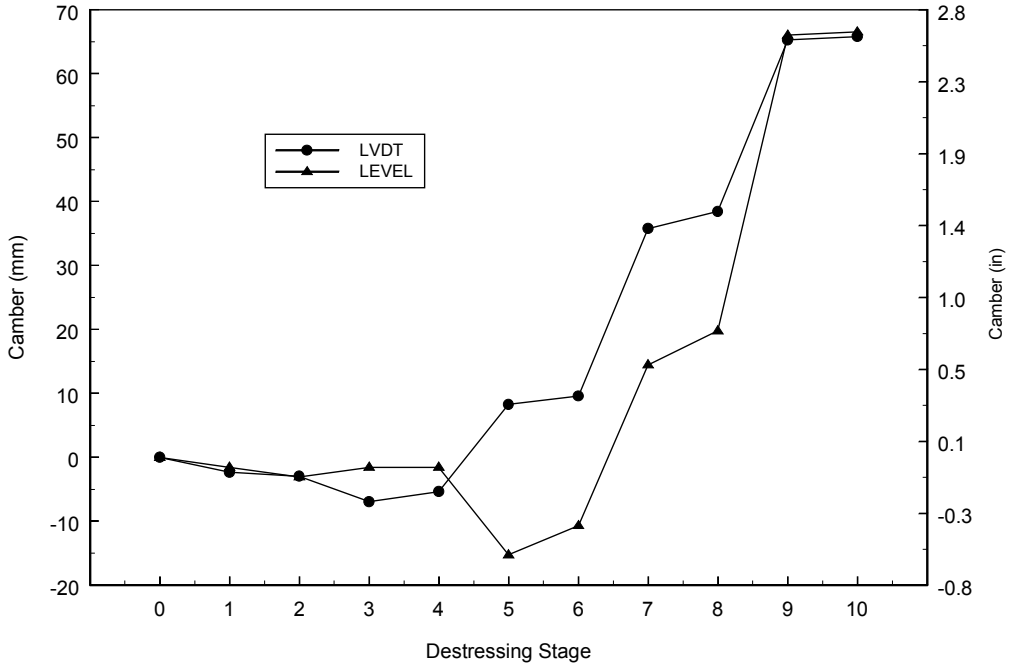

Figure 5.8. Camber During Destressing in Girder 2B

5.1.4 Transfer Length

Voltage readings were taken from potentiometers attached to prestressing strands in girders 1A, 2A, and 2B using a hand-held digital volt meter. The voltage readings were converted into end slip readings by multiplying them by the gauge factor. The end slip measurements for girder 2B are shown in Figure 5.9.

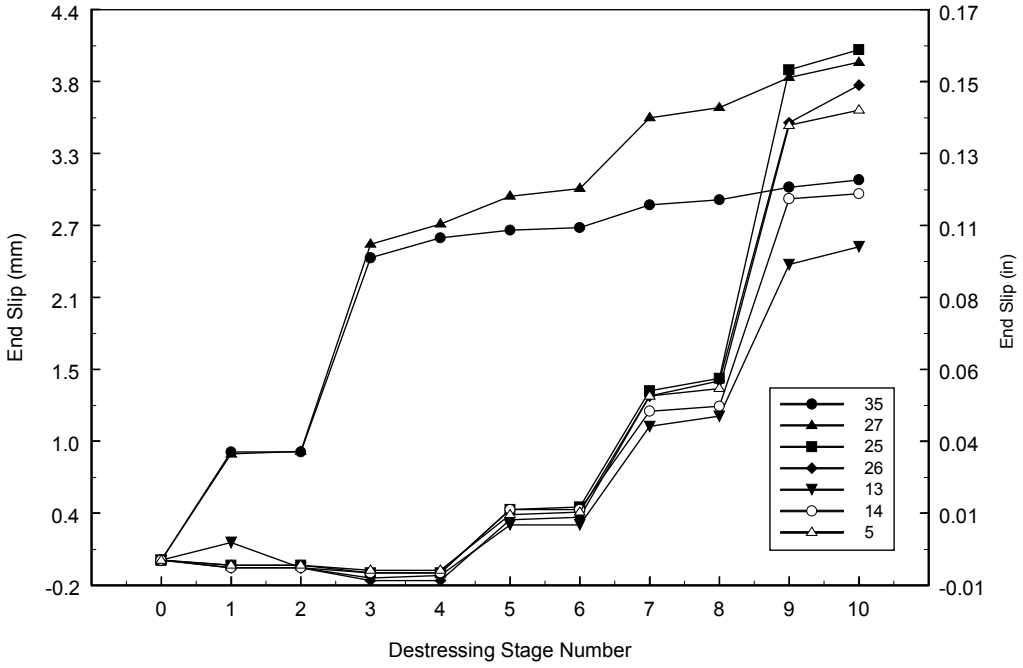

Figure 5.9. End Slip Measurements of Girder 2B

Transfer lengths were computed from strand slip measurements in girders 1A, 2A, and 2B. The two quantities are related by Equation 5.4 (Logan, 1997).

$$L_{tr} = (2 * \Delta * E_p) / f_{pi} \quad (5.4)$$

where

L_{tr} = transfer length

Δ = measured end slip

E_p = elastic modulus of strand =196.5 Gpa (28,500 ksi)

f_{pi} = initial prestress (GPa) directly after transfer (1.22 (2A and 2B), 1.32 (1A))

The transfer lengths calculated from measured end slips are shown in Figure 5.9. The strand locations are shown in Figure 4.2. During stages 1 to 4, the web strands were released, and the bottom strands were released in stages 5 to 10.

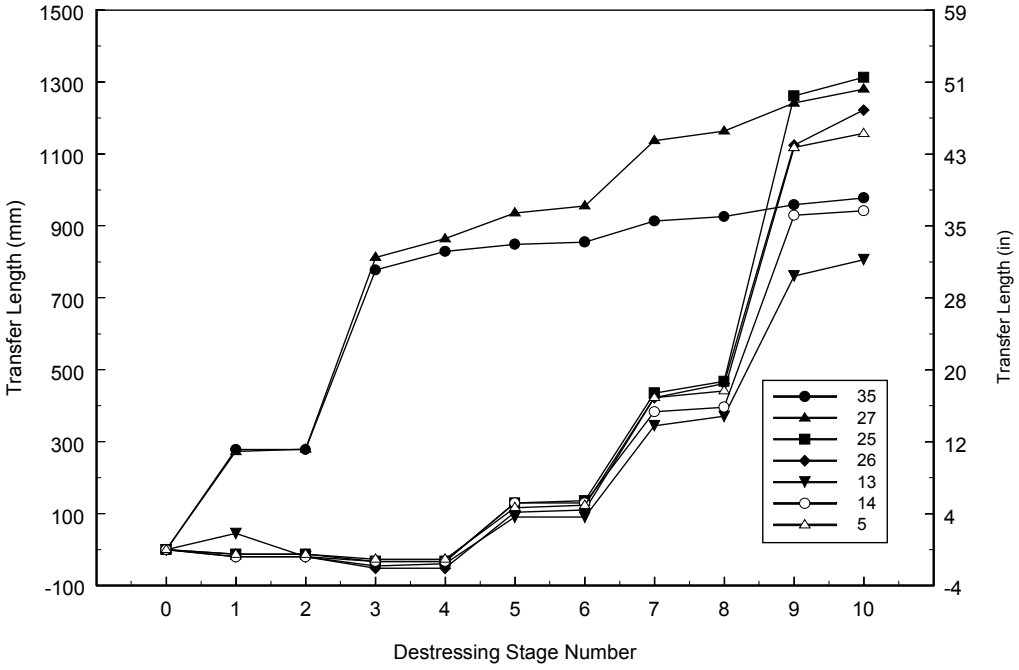

Figure 5.10. Calculated Transfer Lengths During Destressing of Girder 2B

End slip measurements ended after destressing was completed. Research has found that some additional end slip can occur after destressing is complete (Logan, 1997). Therefore, Figure 5.10 represents a minimum value for the actual transfer length. The transfer lengths for the other instrumented girders are presented by Barr (Barr, 1998). No correlation between maximum slip-back and location of strand was found.

Figure 5.11 summarizes all the transfer length data. All but five strands exceeded the transfer length value of 60 strand diameters that is provided by the AASHTO method (AASHTO, 1994). Because the vertical component of the prestressing force in the harped strands is used to help resist shear stresses, an increase in the transfer length near the supports can cause shear cracking problems. In addition, cracking near the supports is more likely to occur because the reduction of axial force due to the longer transfer length will increase the principal stresses. Cracking in the transfer zone has been shown (Russell and Rose, 1996) to cause anchorage failure in the strand. When bond failure occurs, the tension force in the strand is lost and the concrete's contribution to shear is reduced.

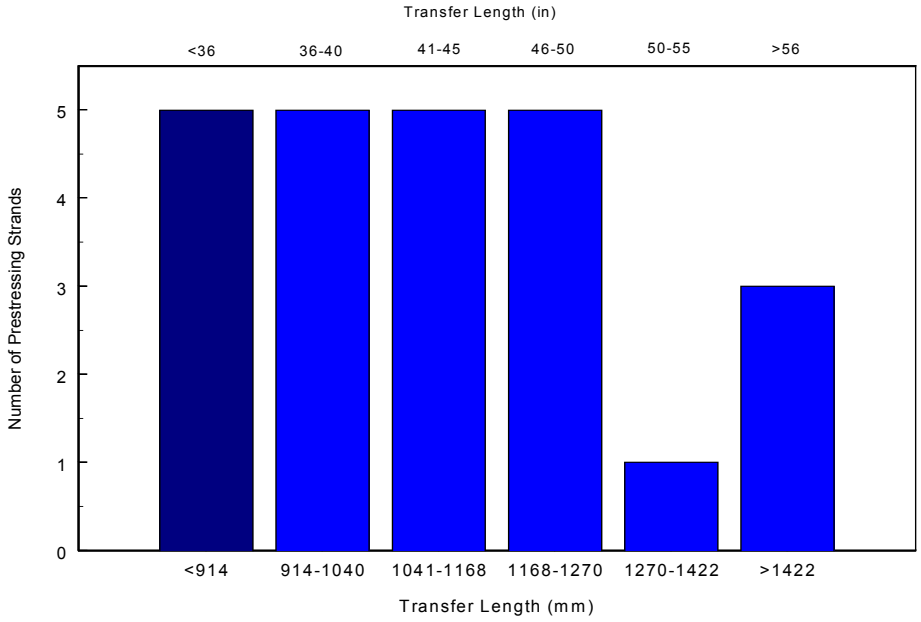

Figure 5.11. Summary of Calculated Transfer Lengths

5.2 SERVICE CONDITIONS

This section presents the behavior of the girder from the time the girders were taken from the casting bed until day 207, the last day for which data were available at the time of writing.

5.2.1 Temperature

Figure 5.12 shows the temperature histories of the mid-span gauges in girder 2B. The straight line between day 55 and 70 represents the time interval during which the equipment had to be removed while the girders were being transported.

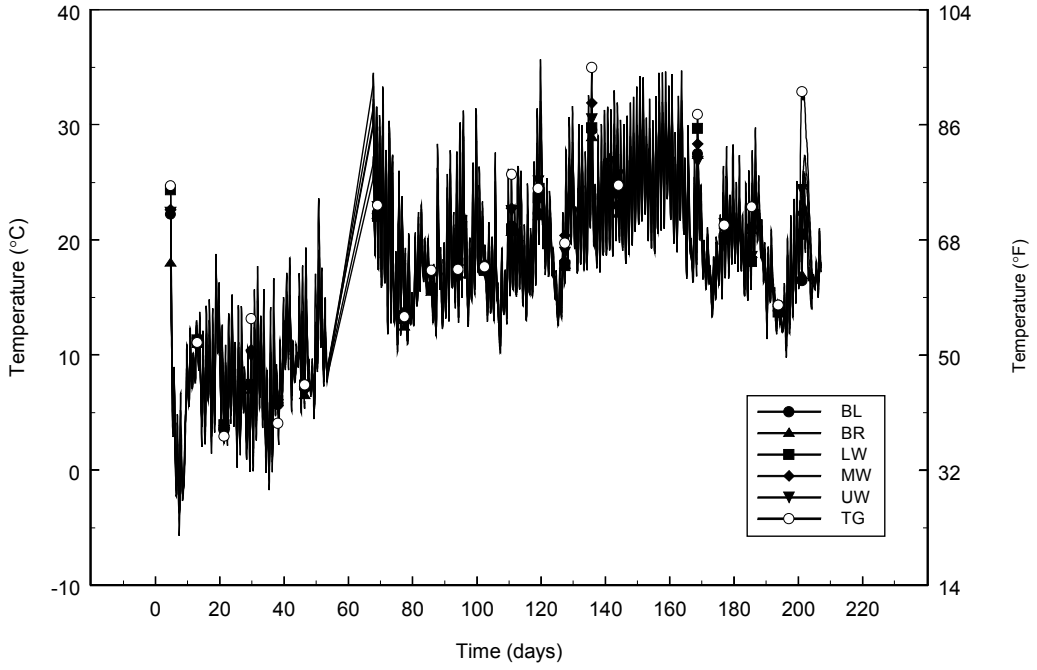

Figure 5.12. Service Temperatures at Mid-Span of Girder 2B

The thermistors in the VWSGs performed extremely well after casting. They provided readings without fail and those readings followed all expected trends. In general, the temperatures were colder during the winter and hotter during the summer months. They also read hotter during the day and colder at night. In all cases, the temperature during the day was highest at the top gauge (TG). The gauges in the exterior girders, both in the yard and after erection, registered higher temperatures than those gauges in the interior girders. This difference is attributed to the sun shining on the exterior face of the girders. The daily temperature cycles are represented by the sharp peaks in Figure 5.12. The daily temperature variations diminished starting at day 200,

which corresponded to the day the deck was cast. Similar findings for the other instrumented girders are shown in Appendix B.

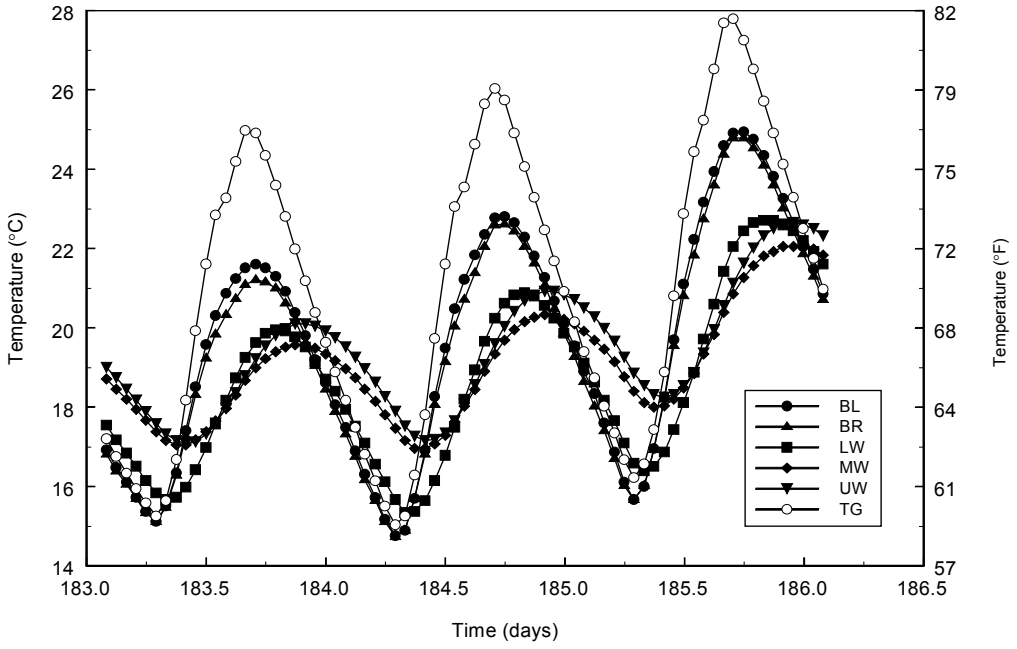

Figure 5.13. Typical Temperature Variation at Mid-Span in Girder 2B

Figure 5.13 shows a typical daily temperature history for the mid-span of girder 2B. The three peaks shown are for 4, 5, 6 September 1997. As expected, the top gauge (TG) measured the highest temperature during the day. As a result of the safety deck being above the bottom two gauges (BL and BR), but below the web gauges (LW, MW, and UW), the heat from the road below made the bottom gauges hotter than the web gauges. The extreme temperatures in the top gauge (TG) and bottom gauges (BL and BR) also occurred earlier than those in the web. The maximum temperatures occurred at 5:00 P.M., while the minimum temperatures usually occurred between 6:00 and 7:00

A.M. The daily temperature plots for the other instrumented girders are provided by Barr (Barr, 1998).

5.2.2 Strains

With the exception of transportation (days 55 to 70), strain readings were taken continuously after casting. Figure 5.14 shows the strain history for the mid-span of girder 2B.

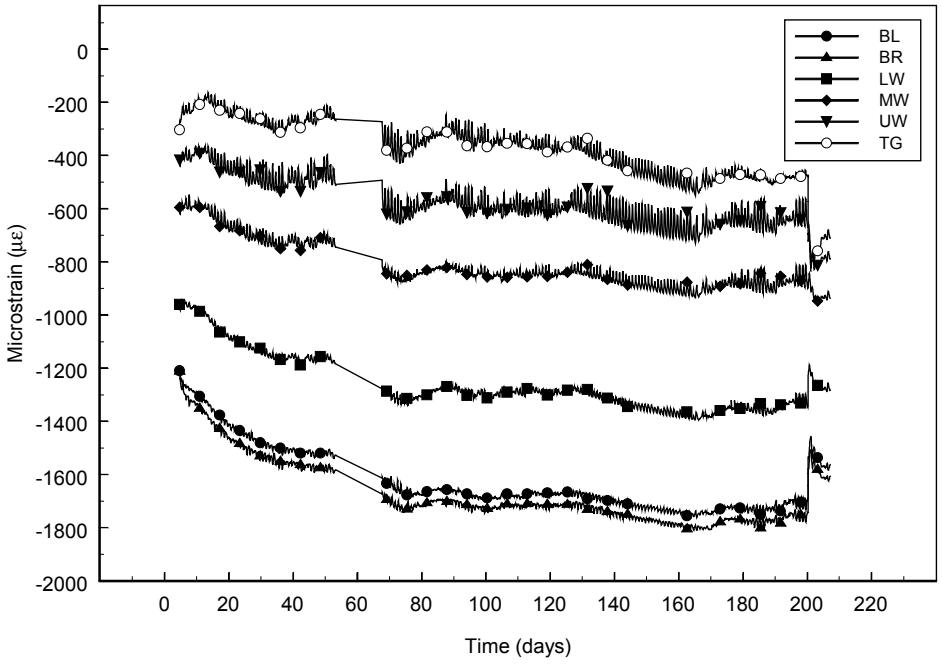

Figure 5.14. Service Strains at Mid-Span of Girder 2B

The changes in measured strains can be attributed to creep and shrinkage in the concrete and relaxation in the strand. The gauges toward the bottom of the girder experienced the largest change in strain, as a result of the high stresses there. The change in strain measurements for the top gauge was smaller, because the stresses were smaller.

A small increase in strain occurred after transportation. This increase may have been a result of the removal of wooden blocks, which supported the girder in the yard. They provided some frictional resistance at the supports, which in turn led to a positive end moment and reduced the camber. Once the girders were lifted off the supports, the girders were completely free to camber and the bottom strain increased.

The abrupt change in strain on day 200 corresponds to the deck casting. The BL, BR, and LW gauges experienced a decrease in strain, as the MW, UW, and TG gauges experienced increase in strain. The change in strain was largest in the top (TG) and bottom (BL and BR) gauges. The increase in strains was caused by creep and shrinkage in the concrete and relaxation in the strand. The recorded strains remained approximately linear during this time. Figure 5.14 also shows that during the first 100 days the bottom gauges experienced much more change in strain than in the second 100 days. This trend is consistent with the fact that the rates of creep and shrinkage decrease with time.

The cross-sectional strains at three different times during the service life of girder 2B are shown in Figure 5.15. The day-200 data was taken directly before casting of the deck. The measured data show a strain distribution that is nearly linear. This finding agrees with the assumptions of Euler-Bernoulli beam theory and thus provides confirmation that the gauges were working correctly.

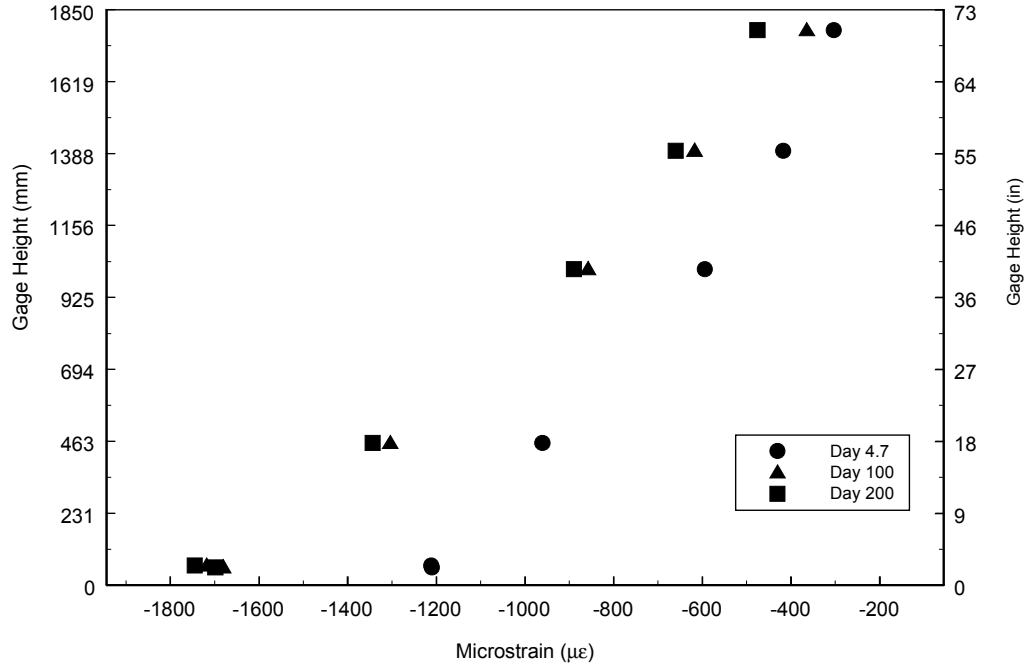

Figure 5.15. Cross-Sectional Strains at Mid-Span of Girder 2B

5.2.3 Camber

The camber histories for all five girders in span 2 are shown in Figure 5.16. Each reading was made using the surveyor's level. Each camber reading was corrected to account for the various end conditions using Euler-Bernoulli Beam theory. Before day 53, readings were taken at Central Premix Prestress Co. Because those level readings were taken as time permitted, a number of readings were taken during the day, when thermal effects were the largest. As a result, camber readings taken in the precast yard were affected by creep, shrinkage, the girder location, and the time of the day when the readings were taken. In particular, girder 2C was exposed to the most sun and therefore

temperature affected its camber more than that of girders 2A and 2B. The first reading after the girders were erected was taken on day 63.

All the girders displayed a downward deflection of 10 to 20 mm (0.4 to 0.8 in) between the last reading in the yard and after erection (day 53 and 62). The level readings on day 53 were taken on a sunny afternoon at 3:30 P.M., therefore experiencing thermal camber. The readings on day 62 were taken at 5:30 A.M., which led to minimal thermal camber. The difference in camber between days 53 and 62 is therefore thought to be a result of thermal camber, the magnitude of which is consistent with values after the girders were erected (Figure 5.20).

In addition to the instrumented girders, camber readings were also taken on girders 2D and 2E on the night that the girders were erected. After the girder erection, camber readings were taken approximately every 2 weeks. The slight dips in the curves between the readings on days 101 and 114 are related to the casting of the intermediate diaphragms. The cause for the decline in the camber readings between days 128 and 164 is unclear; however, the bottom foot of the pier diaphragms was cast around day 130. The girders had projecting end reinforcement and strand extensions, on some of which strand chucks were mounted to add anchorage, so pouring part of the pier diaphragm connected them in both tension and compression. The restraint to creep and shrinkage at the ends of the girders from this concrete could be an explanation for the observed decrease. The sudden drop in camber near day 200 corresponds to the deck casting. Each girder in span 2 deflected about 25.4 mm (1 in) during casting of the deck.

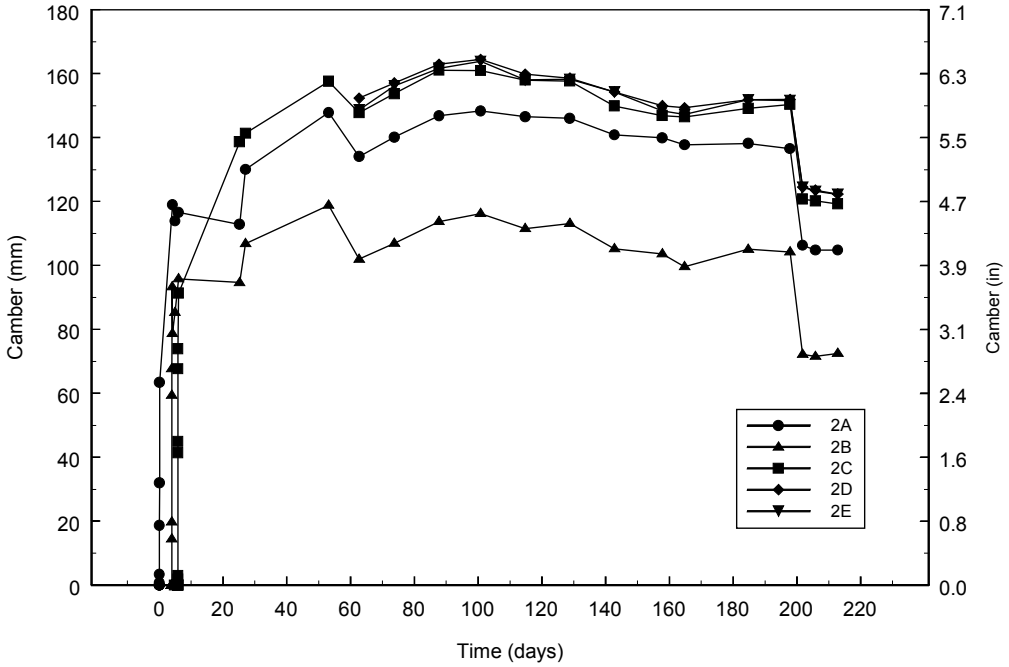

Figure 5.16. Camber Histories for Span 2 Girders (Surveyor's Level)

The camber histories for the instrumented girders in span 1 are shown in Figure 5.17. Each reading was taken with a surveyor's level. Transportation, erection, diaphragm casting, and deck casting occurred on the same days as for the girders in span 2. Camber on girder 1B was measured starting on day 73. Camber values could not be taken on the night of erection. The deck casting caused each girder to deflect 3 mm (1/8 in).

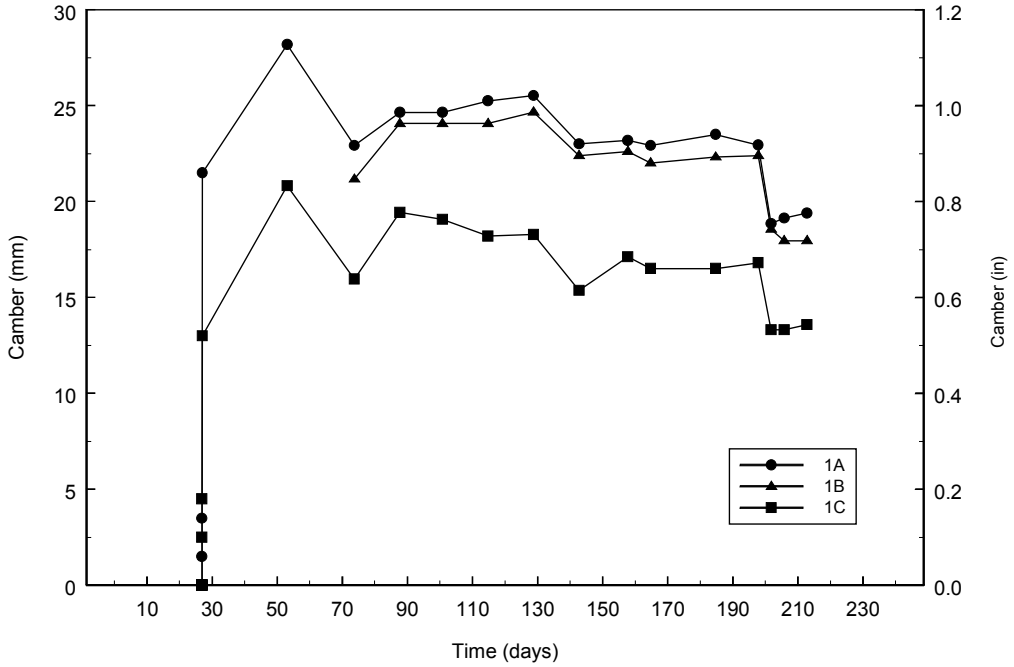

Figure 5.17. Camber Histories for Span 1 Instrumented Girders (Surveyor's Level)

Level readings were also taken approximately every 2 h on June 5 (day 89) in order to obtain a daily camber history. The first set of level readings was taken at 9:30 A.M., and the last readings were taken at 8:30 P.M. Figure 5.18 shows the difference in measured camber for each girder throughout the day for both spans. For girders 1A and 1C the maximum changes in camber were 2.5 and 3.0 mm (0.1 and 0.12 in), respectively. Girders 2A, 2B, and 2C had maximum changes in camber of 7.9, 6.9, and 8.4 mm (0.31, 0.27, and 0.33 inches), respectively. The change in camber during the day is believed to be a result of the temperature gradient in the girders.

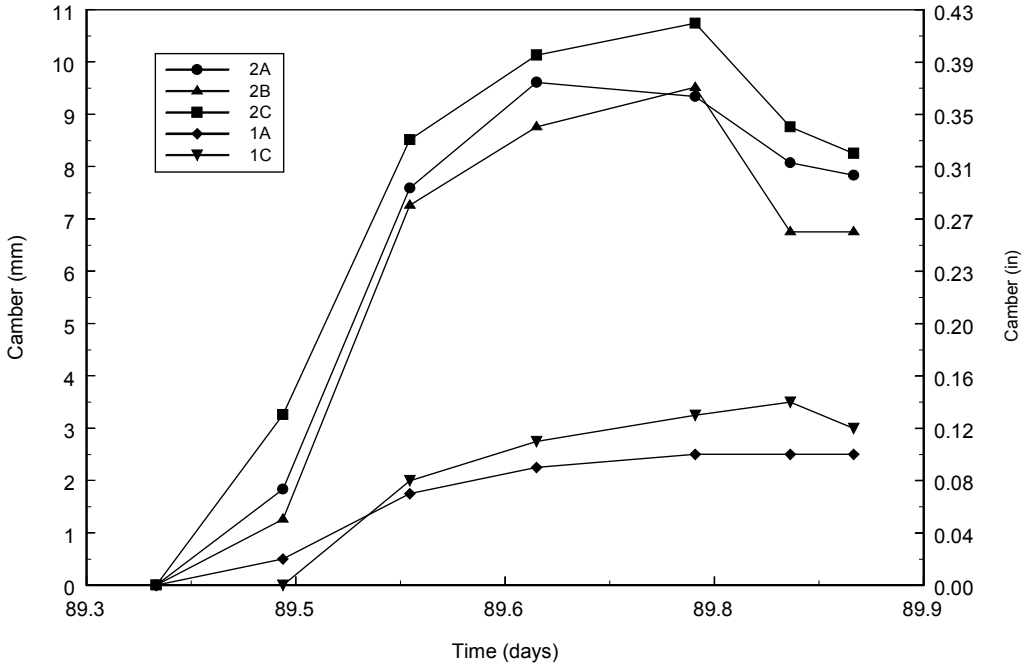

Figure 5.18. Camber vs Time on June 5 (Surveyor's Level)

Due to the likelihood of the stretched-wire system being damaged during construction of the bridge, it was only installed during a relatively short period of time before casting the deck. Figure 5.19 shows the camber readings taken during a 3-day period for girders 2B and 2C. On those days, the LVDT for girder 2A was being repaired, therefore that stretched-wire system was not installed. Daily camber variations range from 15 to 20 mm (0.6 to 0.8 in). The daily change in camber is a result of the variations in temperature gradient in the girders. The temperature variations for girders 2B and 2C during these 3 days can be seen in Figures 5.13 and B.34 (Barr, 1998), respectively. Each temperature plot shows a daily change in temperature, which corresponds to the change in camber. The temperatures for these two girders are similar, as are the changes in camber. The minimum camber occurs at 6:00 A.M., and the maximum camber occurs at 3:00

P.M. This contrasts with the finding in section 5.2.1 that the maximum temperature at the top occurs approximately at 5:00 P.M. The difference is attributed to the fact that the greatest temperature gradient, on which the camber depends, may not occur at the same time as the maximum top temperature. The relative smoothness of the camber curves and the fact that the values for the two girders are nearly identical, suggest that little frictional resistance existed in the system and that the new slides appear to work well. The reason for the slight roughness in girder 2B curve near its minimum is unknown.

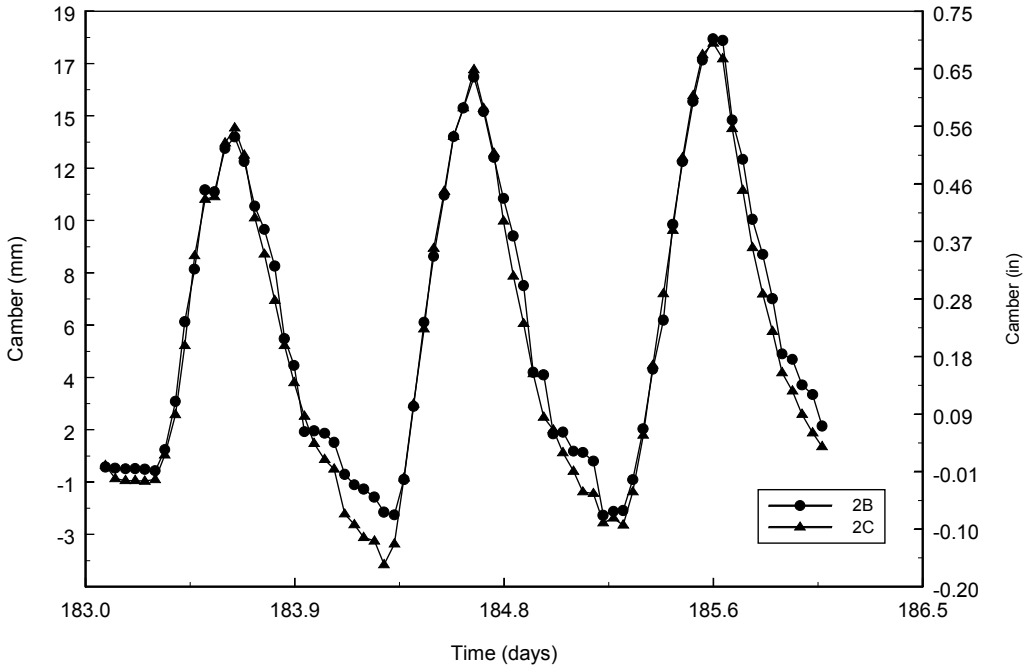

Figure 5.19. Daily Camber Readings for Span 2 (Stretched-Wire System)

Figure 5.20 shows the daily camber values for the instrumented girders in span 1. Temperature values during these same days are shown in Figures B.28 and B.30 (Barr, 1998). Girder 1B does not have any internal instrumentation and therefore the

temperature distribution is unknown. The highest camber values were recorded in girder 1C, and the smallest were recorded in girder 1A. The temperature plots show that the bottom of girder 1A was hotter than the bottom of girder 1C, and that a greater temperature gradient exists in girder 1C. This larger thermal gradient is the likely explanation for the difference between the cambers of these two girders. The bottom temperature in girder 1B could reasonably lie between these two girders and would therefore produce intermediate camber values.

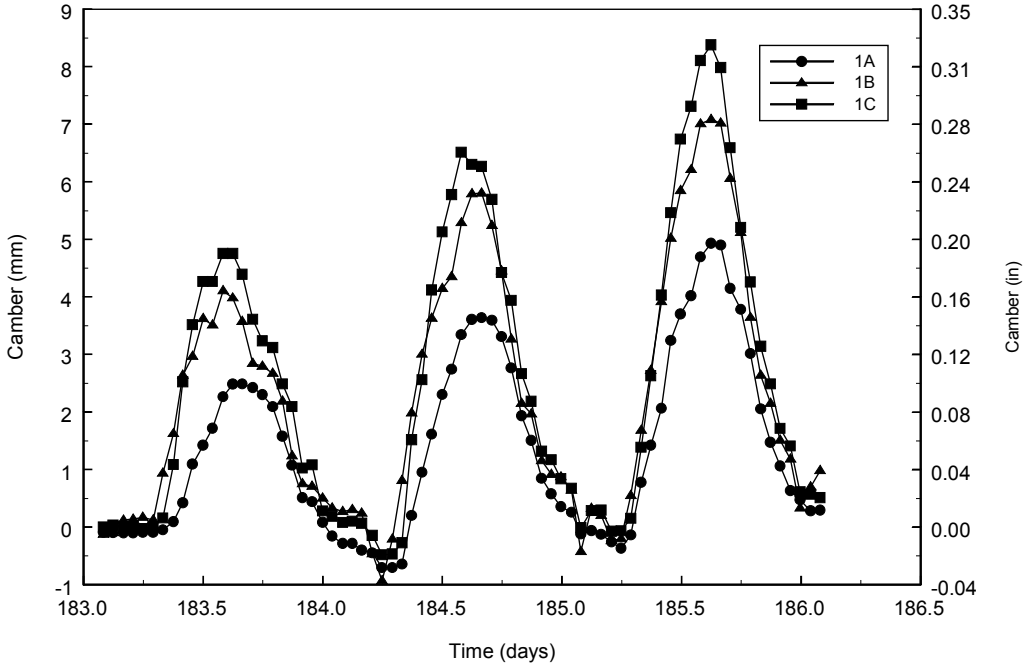

5.20. Daily Camber Readings for Span 1 (Stretched-Wire System)

CHAPTER 6

OBSERVED PRESTRESS LOSSES

This chapter discusses the observed prestress losses in the instrumented girders. Prestress losses occur due to relaxation of the prestressing strands (Section 6.1), elastic shortening of the concrete (Section 6.2), and shrinkage and creep of the concrete (Section 6.3). Additional losses may occur due to changes in temperature in the strand between the times of initial stressing and destressing (Section 6.4).

6.1 RELAXATION

Relaxation in a prestressing is the loss of strand stress while it is held at a constant length. This reduction in strand stress continues almost indefinitely, although the rate diminishes with time. Relaxation losses depend on the type and grade of prestressing steel along with time and magnitude of initial stress (Nilson, 1987). Low relaxation strand is used almost exclusively today, and was used in this study as well.

Prestress loss due to relaxation of the strand in the girders could not be measured independently from other losses, so relaxation test data performed at room temperature for typical 15-mm (0.6-in) prestressing strand were obtained from the manufacturer, Sumiden Wire Products Corporation. The relaxation loss is only a small part of the total loss, so any errors introduced by this approach have little influence on the predicted losses from other sources. Equation 6.1 provides an empirically based estimate, based on Sumiden test data, of the loss in stress due to relaxation with time for the 15-mm (0.6-in) strand used in the instrumented girders.

$$\Delta f_{p,\,RE} = \frac{\left[0.1466 * \ln(t*24) + 0.7959\right] * f_{pj}}{100} \qquad (6.1)$$

where

$\Delta f_{p,RE}$ = change in stress due to relaxation

ln = natural log

f_p = jacking stress

t = time (days)

Figure 6.1 shows a plot of stress loss due to relaxation (using equation 6.1) versus time for the prestressing strands used in the instrumented girders, which were jacked to 1396 MPa (202.5 ksi). The time shifts between curves represent differences in casting times. The relaxation loss within the first 24 hours [17.9 MPa (2.6 ksi)] corresponds to 63 percent of the ultimate relaxation loss during the first 207 days [28.3 MPa (4.1 ksi)]. The stress loss due to relaxation at day 207 is 2 percent of the total prestressing force.

Although the precaster installed a load cell behind the anchor chucks of one web strand, its readings were sufficiently unreliable that they could not be used to check the relaxation values. Stress changes due to thermal expansion would have made verification difficult, even if the load cell readings had been reliable.

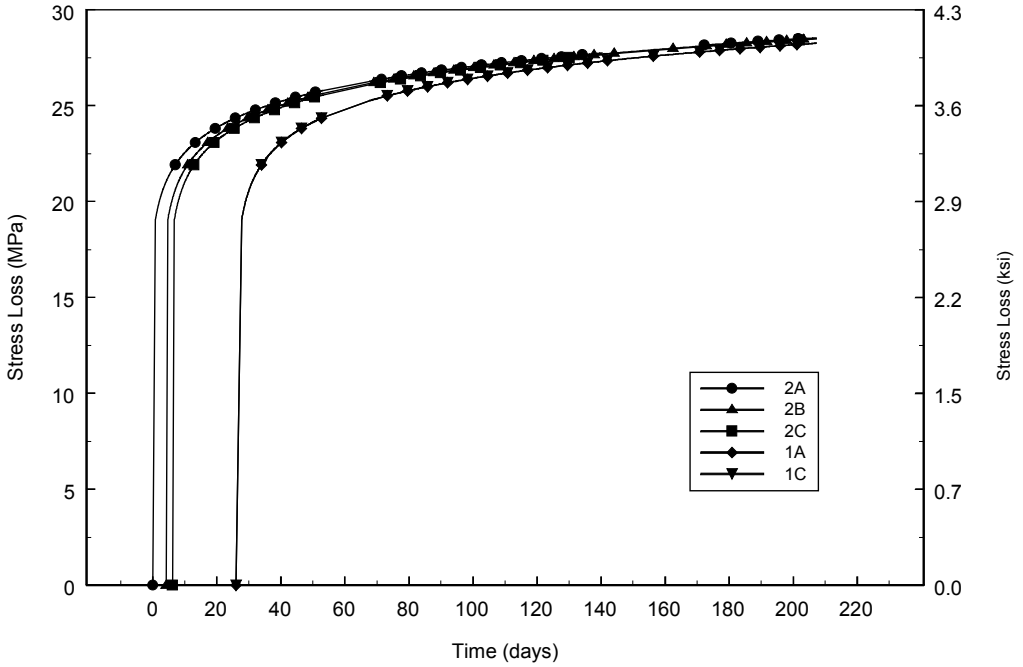

Figure 6.1. Stress Loss Due to Relaxation

6.2 ELASTIC SHORTENING AND EARLY CREEP

The compressive strain in the concrete at the centroid of the prestressing strand is composed of three parts: (1) axial due to prestressing force, (2) bending due to eccentricity of prestressing force, and (3) bending due to self-weight. Equation 6.2 calculates the change in concrete strain at mid-span due to the application of the prestressing force.

$$\Delta\varepsilon_c = \frac{P_i}{A_c * E_{ci}}\left(1 + \frac{e^2}{r^2}\right) + \frac{M_d * e}{I_c * E_{ci}} \tag{6.2}$$

where

$\Delta\varepsilon_c$ = change in concrete strain at steel centroid

P_i = initial prestress force (negative quantity) directly after transfer

A_c = cross-sectional area of girder

E_{ci} = modulus of elasticity of concrete at time of destress

e = distance from centroid of girder to prestressing steel centroid

r = radius of gyration of concrete girder = $\sqrt{I_c / A_c}$

M_d = moment due to self-weight of girder

I_c = moment of inertia of concrete girder

As the concrete shortens due to the applied force, the tendons that are bonded to the adjacent concrete also shorten. This shortening of the tendons causes a reduction in the prestressing force. Equation 6.3 relates the change in concrete stress to the change in prestressing force due to elastic shortening.

$$\Delta f_{p,ES} = E_p * \Delta\varepsilon_c \tag{6.3}$$

where

$\Delta f_{p,ES}$= change is steel stress due to elastic shortening

E_p = modulus of elasticity of prestressing steel (196.5 GPa (28,500 ksi) from manufacturer)

Elastic shortening losses in the prestressing strands were estimated by measuring the strain in the concrete near the centroid of the prestressing strands (gauges BL and BR) and multiplying this strain by the modulus of elasticity of the steel (Equation 6.3). Figure

6.2 shows a typical history near the prestressing centroid [76 mm (3 in) from the bottom] during destressing.

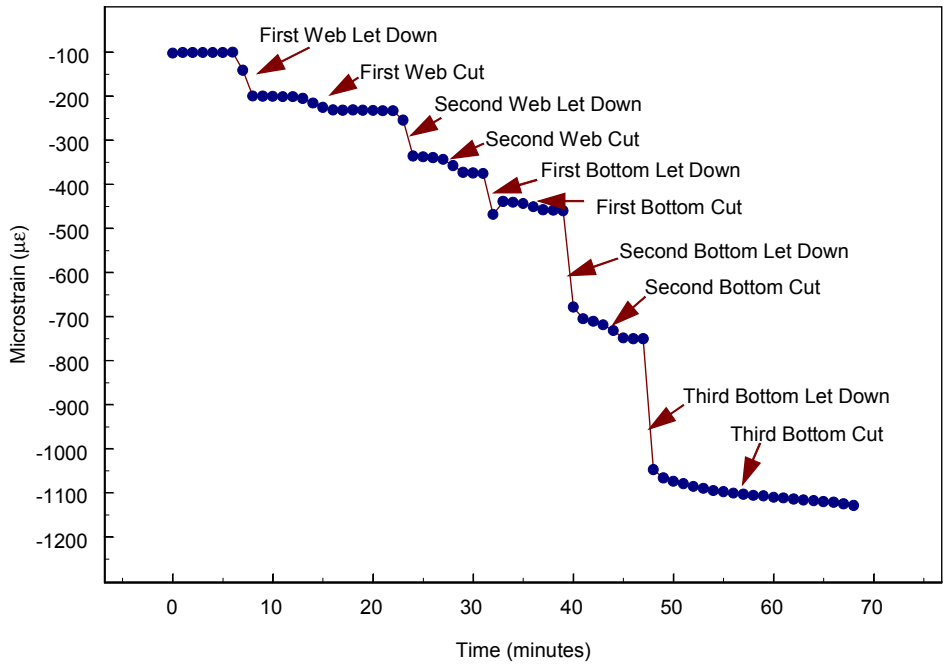

Figure 6.2. Strain History for Prestressing Centroid During Destressing at Mid-Span of Girder 2B

Figure 6.2 shows that the strains increased abruptly when the live end strands were let down. They increased further as the dead end strands were cut and between the destressing stages. This increase in strain between stages is attributed to creep in the concrete during the destressing operation, which typically lasted about 1 h. The change in strain due to early creep was estimated as the strain changes that occurred between destressing operations. Table 6.1 lists the stress losses attributable to creep during destressing for the instrumented girders. Girder 2A experienced the largest creep during destressing, which is reasonable because it also took the longest to destress. Girders 2B

and 2C experienced similar creep values. The creep values for girders 1A and 1C were also similar to each other.

Table 6.1. Early Creep Losses During Destressing

	1A	1B	2A	2B	2C
Change in Strain (με)	49	58	156	106	107
Stress Loss (MPa)	9.65	11.7	30.3	20.7	20.7
Destressing Time (minutes)	72	72	121	68	52

The values for creep strain (Table 6.1) were subtracted from the change in strain after destressing to estimate the strain due to elastic shortening only. Table 6.2 lists the elastic shortening losses computed in this way for each of the instrumented girders. For the short girders, the mean elastic shortening loss [71.7 MPa (10.4 ksi)] corresponds to 5.1 percent of the initial jacking stress. For the long girders, the mean loss [189 MPa (27.4 ksi)] corresponds to 13.5 percent of the initial jacking stress.

Table 6.2. Elastic Shortening Losses In Instrumented Girders

Girder	1A	1C	2A	2B	2C
Change in Strain (με)	374	353	982	920	985
Stress Loss (MPa)	73.1	69.6	193	181	194

6.3 SHRINKAGE AND CREEP

Shrinkage is defined as the change in volume of the concrete that is unrelated to load application or thermal effects. Concrete mixes contain more water than is needed for the hydration of the cementitious material, and this excess water evaporates in time. Drying of the concrete due to the evaporation of the excess water is accompanied by a

reduction in volume. The rate of volume reduction occurs initially at a high rate and later diminishes with time.

Shrinkage is affected by several time-dependent parameters, which include mix proportions, type of aggregate, type of cement, curing time, time between the end of external curing and the application of prestressing, and environmental conditions (Nawy, 1989). Shrinkage of the concrete shortens the prestressing strands, which causes a reduction in prestressing force.

Creep is the time-dependent flow of concrete caused by its being subjected to stress. This deformation, which occurs rapidly at first and then decreases with time, can be several times larger than the strains due to elastic shortening. Creep has been found to depend on the mix proportions, humidity, curing conditions, and maturity of the concrete when first loaded (Nilson, 1987). The deformation due to creep causes a shortening of the prestressing strands, which leads to a loss in stress in the strand.

The change in strain in the prestressing strands due to creep and shrinkage was computed by taking the average change in strain at the prestressing centroid and subtracting the strain due to elastic shortening (Table 6.1). Figure 6.3 shows the change in strain attributable to creep and shrinkage of the concrete at mid-span of each instrumented girder.

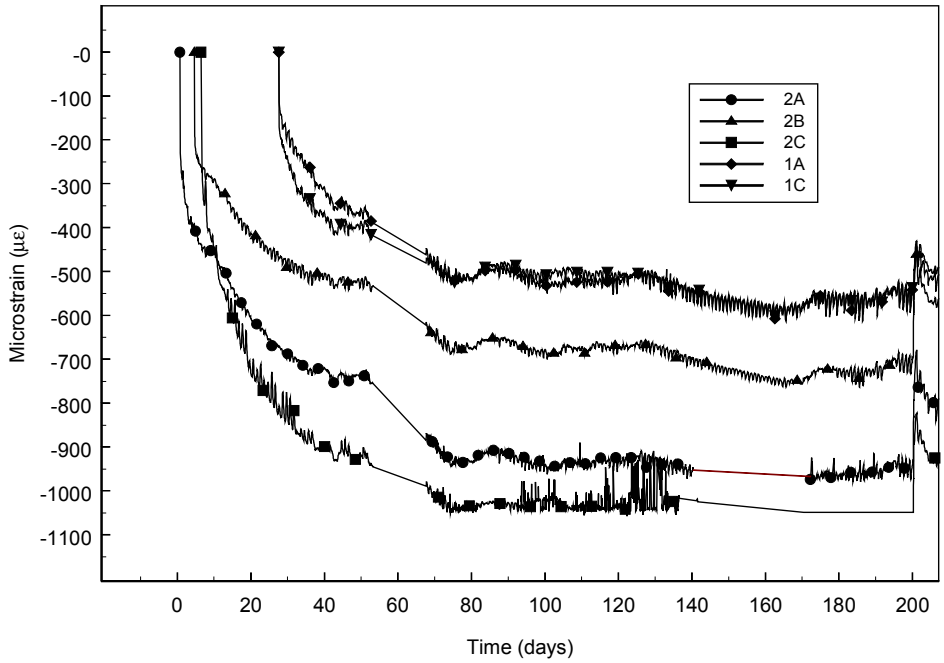

Figure 6.3. Change in Strain Due to Creep and Shrinkage

Figure 6.3 shows that the two instrumented girders in span 1 experienced similar changes in strain due to creep and shrinkage. The total creep strain at day 200 is provided in Table 6.3. The girders in span 2 experienced different values of creep and shrinkage strain. In particular, girder 2C experienced the largest change in strain, followed by girders 2A and 2B. The smooth line for girder 2C between days 140 and 200 is a result of removing erratic readings during this time.

The change in strain due to shrinkage of the concrete should be the same for all five girders because each girder has the same cross-sectional dimensions. Girders 1A and 2A may experience slightly more shrinkage because they were exposed to the sun; however, this increase in shrinkage is thought to be small. Therefore, the differences between the strain measurements in Figure 6.3 are likely due to differences in creep.

Since the mix proportions were the same for each girder, the differences between the girders in span 1 and 2 can be attributed to the different levels of prestress. However, the differences in loss among the span 2 girders are likely the result of differences in maturity at the time of destressing.

For each of the instrumented girders the maturity at the time of destressing at the centroid of the prestressing strand was calculated from Equation 5.1 during curing. As shown in Table 6.3, girders 1A and 1C had similar maturity values. Girder 2C had the lowest maturity value followed by girder 2A and then 2B. This trend is consistent with the findings that, the lower the maturity value, the more creep strain occurred.

Tables 6.3. Losses Due to Creep and Shrinkage (Day 200)

Girders	1A	1C	2A	2B	2C
Change in Strain (με)	541	536	940	700	1048
Stress Loss (MPa)	106	105	185	138	206
Maturity at Destress (°C-h)	914	948	932	1060	665

The change in stress at mid-span due to creep and shrinkage was calculated by multiplying the change in strain (Figure 6.3) due to creep and shrinkage by the modulus of elasticity of the prestressing strands. Figure 6.4 shows the prestress loss due to creep and shrinkage for each girder.

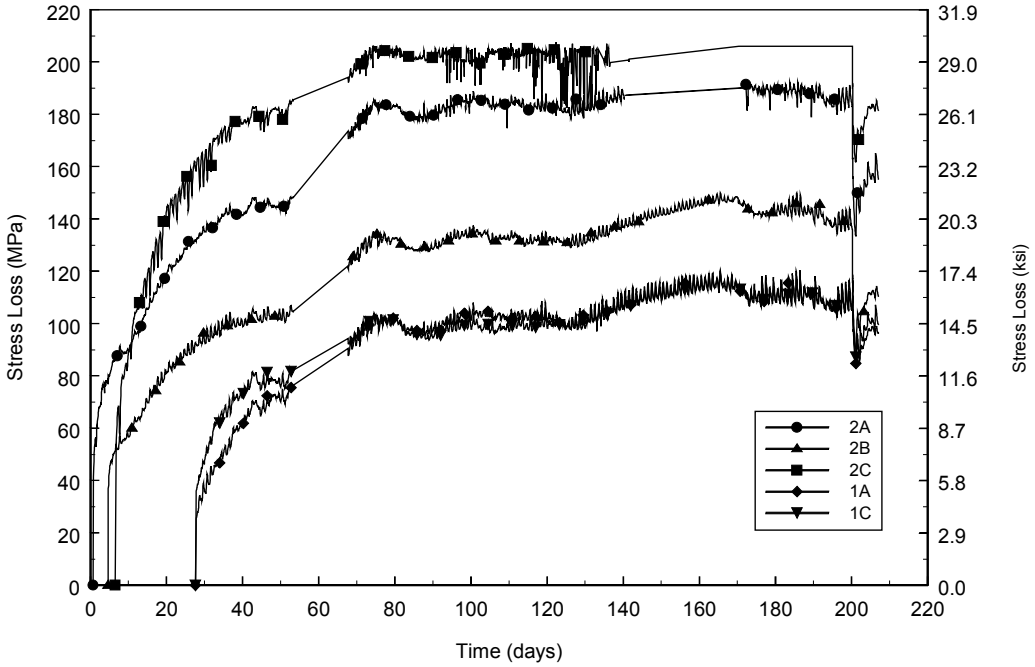

Figure 6.4. Prestress Losses Due to Creep and Shrinkage

The prestress loss due to creep and shrinkage of the concrete before casting the deck was observed to be 185 (2A), 138 (2B), and 206 (2C) MPa (26.8, 20.0, and 29.9 ksi respectively), which corresponds to 13.2, 9.8, and 14.7 percent of the total jacking stress, respectively. The loss due to creep and shrinkage in the short girders before casting the deck was 106 (1A) and 105 (1C) MPa (15.4 and 15.3 ksi, respectively), which corresponds to 7.6 percent of the total jacking stress.

6.4 CASTING OF BRIDGE DECK

The reduction of prestress losses at day 200 corresponds to the deck casting, at which time the prestressing strands experience an increase in strain due to the dead load of the slab. Casting of the deck caused a larger change in stress in the interior girders

(1C, 2B, and 2C) than in the outside girders (1A and 2A). Table 6.4 lists the gain in strand stress at mid-span due to the deck casting.

Table 6.4. Change in Strand Stress at Mid-Span Due to Deck Casting

Girder	1A	1C	2A	2B	2C
Stress Gain Due to Deck Casting (MPa)	21.4	17.9	49.7	46.2	44.1

6.5 PRESTRESS LOSS DUE TO TEMPERATURE CHANGES DURING CURING

Prestress loss may occur due to the large increase in girder temperature resulting from the steam curing and the heat of hydration of the concrete. Any change in temperature in the prestressing strands after jacking would cause a corresponding change in the stress in the strand.

Since part of the strand was embedded in the concrete or heated under the steam blanket, and the remaining strand was outside the blanket, the difference between these temperatures and the jacking temperature must be known in order to determine the change in stress of the strand due to temperature changes. If these temperatures in the strands, the length of strand under the blanket, and the total length of the casting bed are known, then the change in the strand stress due to the change in temperature during curing can be estimated with Equation 6.4.

$$\Delta f_{p,\,TEMP} = Ep * \alpha p * \left[\frac{(Tout - Tj) * Lout + (Tstrand - Tj) * Lg}{Lbed} \right] \qquad (6.4)$$

where

$\Delta f_{p,TEMP}$ = change in stress

E_p = strand elastic modulus (196 GPa (28,500 ksi))

α_s = coefficient of thermal expansion for steel (6.5 με/°C (11.7 με/°F))

T_{out} = temperature outside blanket

T_j = temperature at time of jacking

T_{strand} = temperature of strand under the blanket

L_{out} = length of strand in bed not covered by blanket

L_{in} = length of strand in bed covered by blanket

L_{bed} = length of casting bed (assumed unchanged by temperature change)

The strands for girder 2B were stressed approximately at 1:00 P.M. on March 9, 1997. At this time the air temperature was 4.67 °C (40.4 °F). The length of the casting bed was 61 m (200 ft). The length of the casting bed covered by the blanket during curing was 46 m (150 ft), and 15 m (50 ft) was left uncovered. To estimate the strand temperature, the temperature of the average bottom gauges (BL and BR) at mid-span, which were placed near the prestressing strand centroid, were assumed to be at the same temperature as the strands under the blanket. The outside air temperature was used for the strand temperature outside of the blanket. Based on these assumptions, Figure 8.4 shows the jacking (T_j), outside (T_{out}), and strand temperatures (T_{strand}).

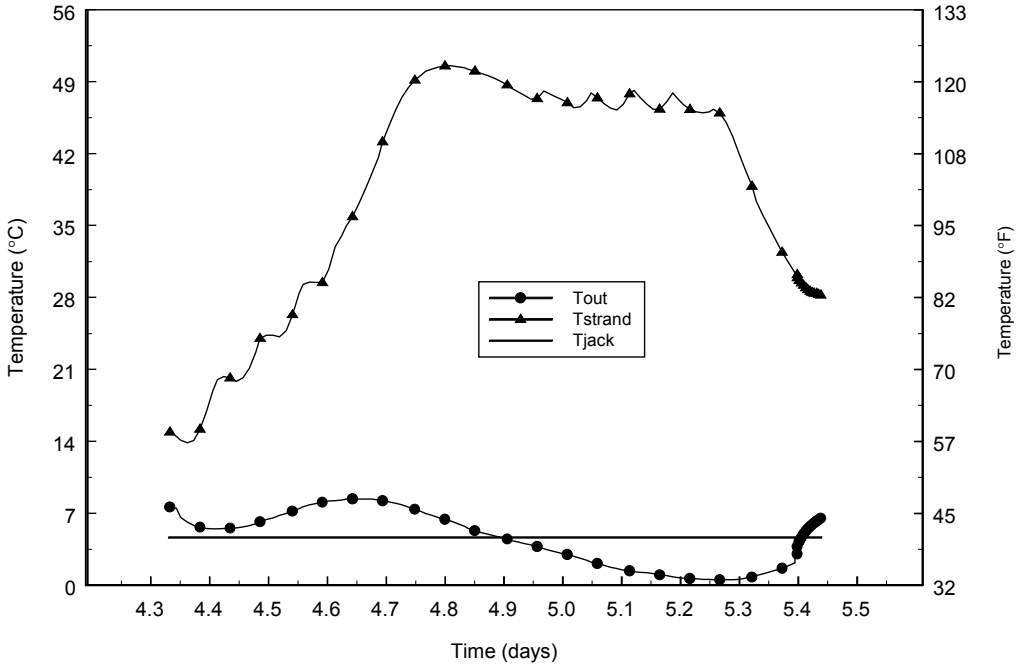

Figure 6.5. Strand Temperatures During Curing of Girder 2B

Day 4.3 in Figure 6.5 corresponds to 7:15 A.M. on March 10, 1997, which was when the concrete was placed. The ripples in the strand temperature correspond to the activation of the steam curing. During the first few hours (4.3 to 4.7) after the steam curing was shut off, the temperature in the strand actually decreased. This phenomenon is a result of the cold outside temperature and the admixtures in the mix delaying the start of hydration. At day 4.6, the strand temperature begins to climb because of hydration. The outside temperature (T_{out}) shows a cyclical pattern of getting hotter during the day and colder at night. The jacking temperature is plotted as a straight line throughout curing to give a reference for the outside and strand temperatures.

Figure 6.6 shows a plot of the prestress loss calculated using Equation 8.4 and the temperatures in Figure 6.5. At some point during curing, the concrete bonded to the

prestressing strand, and any further change in length of the strand due to a change in temperature would be inhibited. It is reasonable to assume that this did not take place before hydration started (day 4.5 from maturity data), therefore the bonding occurred between days 4.5 and 5.4. As a result, the stress loss due to temperature changes during curing was between 48 and 83 MPa (7 and 12 ksi) (3.5 percent and 6 percent of jacking stress). This loss is usually not considered in design but is significantly larger than the relaxation loss of 14 MPa (2.0 ksi).

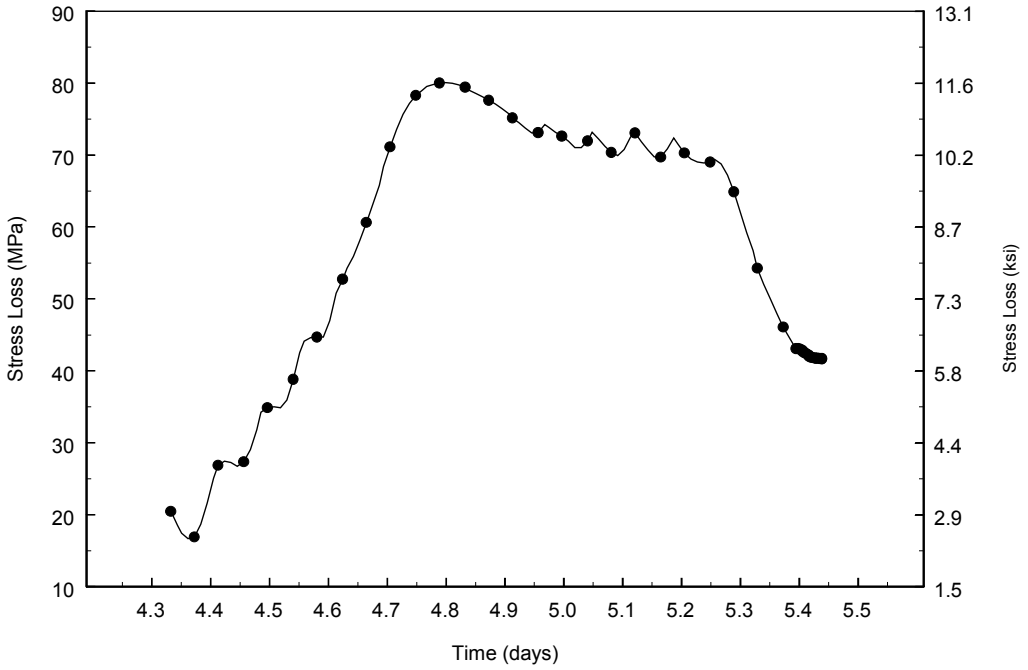

Figure 6.6. Calculated Prestress Loss Due to Temperature Variations

6.6 SUMMARY OF OBSERVED PRESTRESS LOSSES

Figure 6.7 provides a summary of the prestress losses estimated in the previous sections.

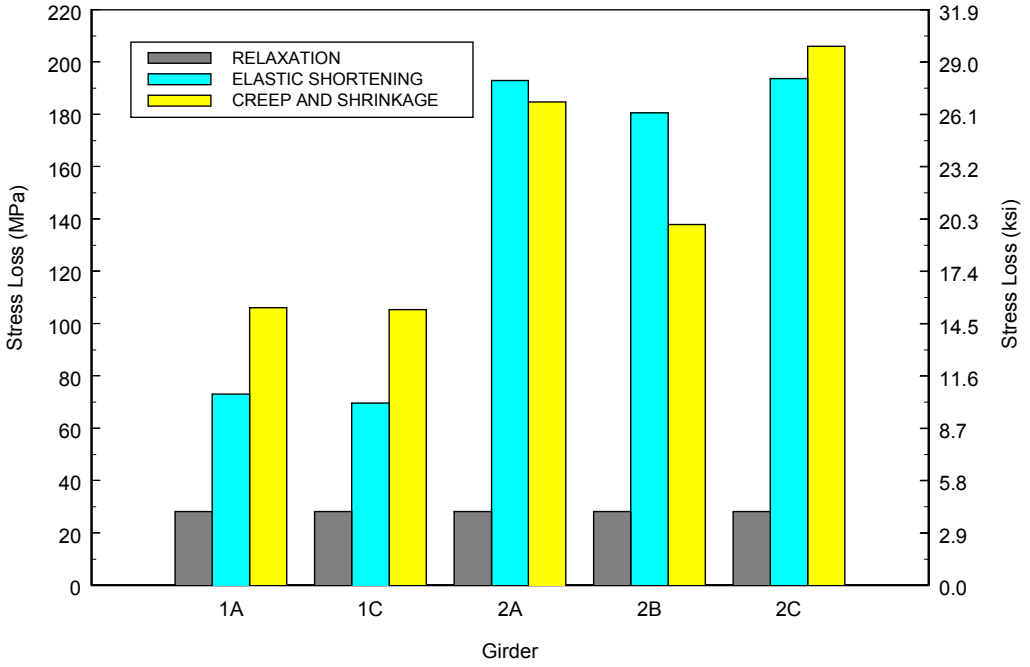

Figure 6.7. Summary of Observed Prestress Losses

The relaxation losses are the smallest of all the losses in spans 1 and 2. For the girders in span 1, the losses due to elastic shortening are smaller than those due to shrinkage and creep. The losses due to relaxation, elastic shortening, and shrinkage and creep are very similar in the two girders in span 1 (girders 1A and 1B). This is expected since they were cast, cured, and destressed together. The elastic shortening losses for girders 2A and 2B were larger than the shrinkage and creep losses. This is the opposite of what occurred in girder 2C.

Table 6.5 lists, at day 200, the total prestress losses for the instrumented girders and the corresponding percentage of jacking force.

Table 6.5. Total Observed Prestress Losses at Day 200

Span	1			2			
Girder	1A	1C	Average	2A	2B	2C	Average
Total Loss (MPa)	207	203	205	406	347	428	394
Percent Jacking Stress	14.9	14.6	14.7	29.1	24.8	30.7	28.2

CHAPTER 7

COMPARISON OF CALCULATED AND OBSERVED PERFORMANCES

In this chapter, the observed values of prestress loss (Chapter 6) and camber (Section 5.2.3) are compared with calculated values using the recommended PCI (PCI, 1975) and AASHTO (AASHTO, 1994) methods. All material properties used in these two methods were calculated based on design equations, rather than measured values of these properties. The PCI general method is a time-stepping algorithm, in which the incremental loss of prestress in each time interval is calculated using the stress at the start of the interval. All stresses are updated before performing calculations of loss in the next interval. In the AASHTO method, the total prestress loss at the end of the service life is calculated in a single step. The AASHTO method was modified into a time-step method in this chapter by multiplying the ultimate prestress loss predicted by the AASHTO method, by creep and shrinkage coefficients provided in the AASHTO code.

7.1 RELAXATION

The PCI method recommends Equation 7.1 for the loss of prestress in low-relaxation strand due to relaxation.

$$\Delta f_{p,REL} = fpi\left(\frac{\log(tn)-\log(tr)}{45}\right)\left(\frac{fpi}{fpy}-0.55\right) \quad (7.1)$$

where

$\Delta f_{p,REL}$ = change in stress due to relaxation during time interval

f_{pi} = stress at start of time interval

t_n = end of time interval (h)

t_r = start of time interval (h)

f_{py} = effective yield stress of prestressing strand

$(f_{pj} / f_{py} - 0.55) \geq 0.05$

To implement this method, the stress at the start of the time interval must be known. This stress is calculated by subtracting all losses up to that time from the initial jacking stress. To avoid numerical problems, jacking is treated as occurring at $t = t_1 = 1$ h.

The AASHTO-LRFD method considers the loss in stress due to relaxation to occur in two stages. The first stage is the loss in stress at transfer. Equation 7.2 shows the recommended equation for calculating the loss in stress at transfer for low-relaxation strands stressed in excess of 0.5 times the ultimate strand stress.

$$\Delta frel = \log(t) / 40.0 * \left[fpj / fpy - 0.55 \right] * fpj \quad (7.2)$$

where

Δf_{rel} = change in stress due to relaxation at transfer

t = time in hours from stressing to transfer

f_{pj} = jacking stress

f_{py} = effective yield stress of prestressing strand

The second stage is the loss in stress after transfer. During this stage, consideration is given to the continual reduction of the strand stress as a result of creep and shrinkage. To reflect this continual change in strand stress, the AASHTO-LRFD method recommends Equation 7.3 as the means to calculate the relaxation loss after transfer in low-relaxation strands.

$$\Delta f_{p,\,REL} = 0.30 * \left[138 - 0.4 * \Delta f_{p,\,ES} - 0.2 * \left(\Delta f_{p,\,SH} + \Delta f_{p,\,CR}\right)\right] \qquad (7.3)$$

where

$\Delta f_{p,REL}$ = change in stress in the strand due to relaxation throughout time

$\Delta f_{p,ES}$ = change in stress in the strand due to elastic shortening (Section 7.2)

$\Delta f_{p,SH}$ = change in stress in the strand due to shrinkage (Section 7.3)

$\Delta f_{p,CR}$ = change in stress in the strand due to creep (Section 7.3)

Prestress losses due to relaxation could not be measured, so estimates of the loss are shown in Figures 7.1 and 7.2 for the girders in span 2 and span 1, respectively. Equation 7.1 was used for the PCI method, Equations 7.2 and 7.3 were used for the AASHTO LRFD method, and the estimate based on the manufacturer's test data was obtained from Equation 6.1, with f_{pj} = 1396 MPa (202.5 ksi).

In both cases the PCI method predicts a loss that varies with time in a manner similar to that based on the test data. The PCI value is slightly lower, largely because it is based on f_{pi} rather than f_{pj}.

The AASHTO-LRFD method suggests a loss that, after transfer, decreases with time. This prediction is counterintuitive, and arises from the fact that the method is really intended for calculation of prestress loss only at one time (e.g., the end of service life) rather than continually over time. However, its use as a time-dependent function has been suggested by Lwin and Khaleghi (1996). Figures 7.1 and 7.2 show that it unsuitable for that purpose.

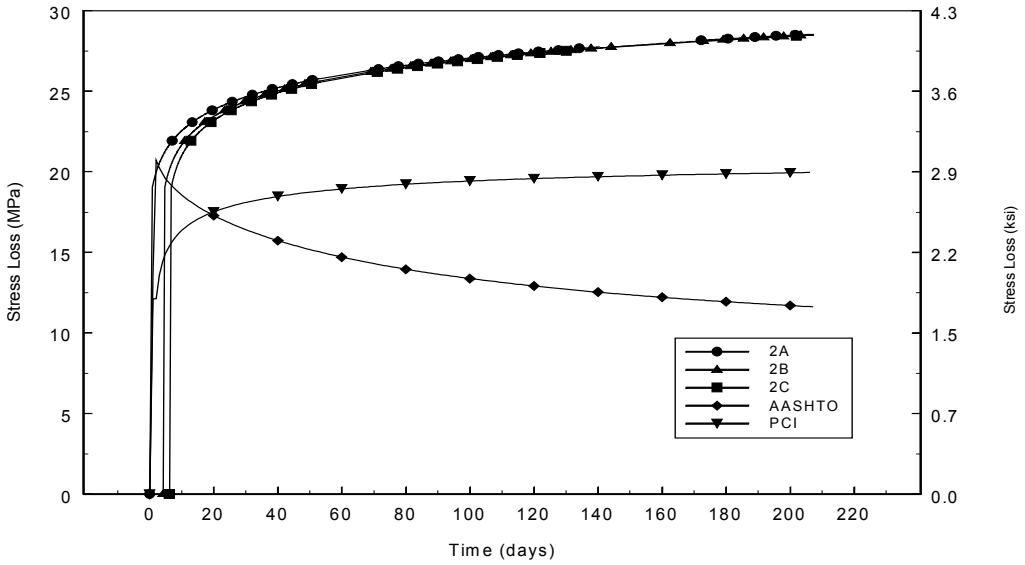

Figure 7.1. Predicted Relaxation Losses in Span 2 Girders

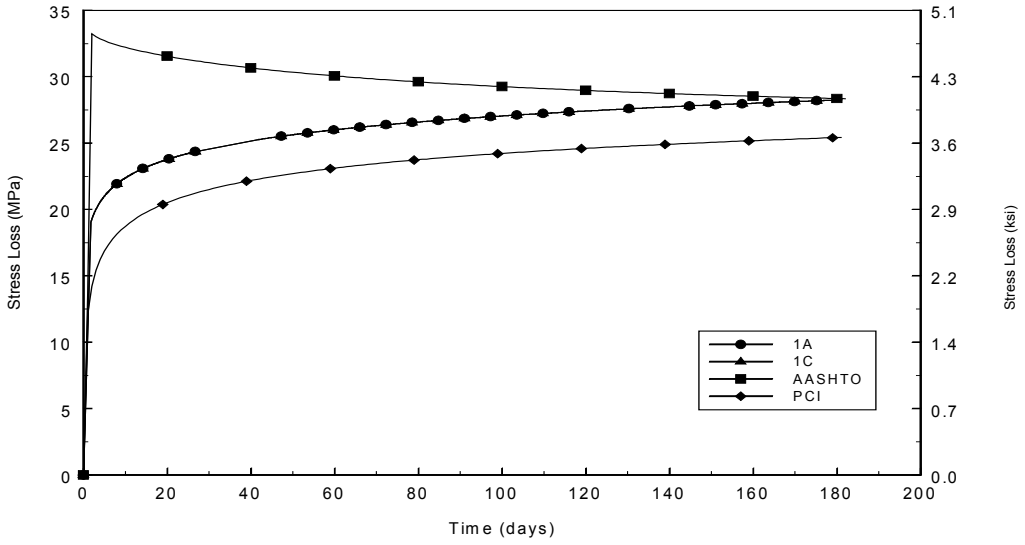

Figure 7.2. Observed and Predicted Relaxation losses in Span 1 Girders

Table 7.1 lists the values for the prestress losses for the two methods at day 207 as a percentage of the jacking stress.

Table 7.1. Predicted Relaxation Loss as a Percentage of Jacking Stress at Day 207

	Manufacturer's	PCI	AASHTO
Span 1	2.0	1.8	2.0
Span 2	2.0	1.4	0.08

7.2 ELASTIC SHORTENING

Both the PCI and AASHTO methods rely on the following iterative procedure for calculating the elastic shortening losses:

Step 1: Calculate relaxation loss ($\Delta f_{p,REL}$) at time of destress (MPa).

Step 2: Calculate the moment due to dead load at mid-span.

$$M_{dl} = \left(\frac{w * l^2}{8} \right) \tag{7.4}$$

where

M_{dl} = moment due to dead load of girder (kN-m)

w = self-weight of girder (kN/m)

l = girder span (m)

Step 3: Calculate the concrete stress at mid-span due to dead load.

$$f_{cdl} = \frac{(M_{dl} * e)}{I} \tag{7.5}$$

where

f_{cdl} = concrete stress at prestress centroid due to dead load (MPa)

e = distance from neutral axis of girder to centroid of prestress (m)

Step 4: Guess an elastic shortening loss ES_{guess} (MPa) in the steel.

Step 5: Calculate prestress force using $\Delta f_{p,REL}$ and $ES_{guess.}$

$$P = \left(f_{pj} - \Delta f_{rel} - ES_{guess}\right) * n * A_p \tag{7.6}$$

where

P = prestressing force after transfer (MN)

f_{pj} = jacking stress (MPa) directly before transfer

n = number of strands

A_p = area of one strand (mm^2)

Step 6: Calculate concrete stress at center of gravity of prestressing steel.

$$f_{cgp} = \frac{P}{Ag} + \frac{P * e^2}{I} + fcdl \tag{7.7}$$

where

f_{cgp} = concrete stress at center of gravity of steel after destressing (MPa)

A_g = cross-sectional area of girder (mm^2)

Step 7: Calculate elastic shortening loss in steel.

$$ES_{calc} = f_{cs} * \left(\frac{E_p}{E_{ci}}\right) \tag{7.8}$$

where

ES_{calc} = calculated elastic shortening loss (MPa)

E_p = modulus of elasticity of prestressing strand (MPa)

E_{ci} = modulus of elasticity of concrete at transfer (MPa)

Step 8: Compare guessed and calculated elastic shortening loss. If $ES_{guess} = ES_{calc}$, then that is the elastic shortening loss of the girder, otherwise repeat steps 4 to 7 until $ES_{guess} = ES_{calc.}$

The elastic shortening loss was measured in three girders in span 2 (Section 6.2). To calculate the elastic shortening loss, a value for E_c is needed. The value given in Section 8.5.1 of ACI 318-95 is known to be too high for most high-strength concretes, so an alternative, derived especially for high strength concrete by Nawy (1996), was used. The equation for the elastic modulus was a function of the concrete compressive strength; therefore, an equation for the strength concrete with type III cement was also needed. Equations 7.9 and 7.10 (Nawy, 1996) are the equations used to calculate the concrete compressive strength and elastic modulus that was used in the PCI and AASHTO methods.

$$f'_c(t) = \frac{t}{\alpha + \beta t} f'_c \tag{7.9}$$

where

$f'_c(t)$ = concrete compressive strength

f'_c = 28-day compressive strength

t = time in days

α = factor depending on type of cement and curing conditions

= 0.70 for steam-cured type III cement

β = factor depending on the same parameters as α

= 0.98 for steam-cured type III cement

$$Ec = \left(3.32\sqrt{f'c} + 6895\right)\left(\frac{wc}{2320}\right)^{1.5} \qquad (7.10)$$

where

E_c = modulus of elasticity (MPa)

f'_c = concrete compressive strength (MPa)

w_c = unit weight of hardened concrete in kg/m^3

= 2480 kg/m^3 for girder concrete

The elastic shortening losses predicted by the PCI and AASHTO methods were calculated for span 2. Figure 7.3 compares the measured and predicted elastic shortening loss for span 2. The PCI and AASHTO methods predict similar losses and both underestimate the observed elastic shortening losses for the girders in span 2. The values for the elastic shortening losses for the PCI and AASHTO method are similar. A small difference exists between the methods, even though they use the same procedure, because of the difference between the two methods in predicting the relaxation loss at transfer.

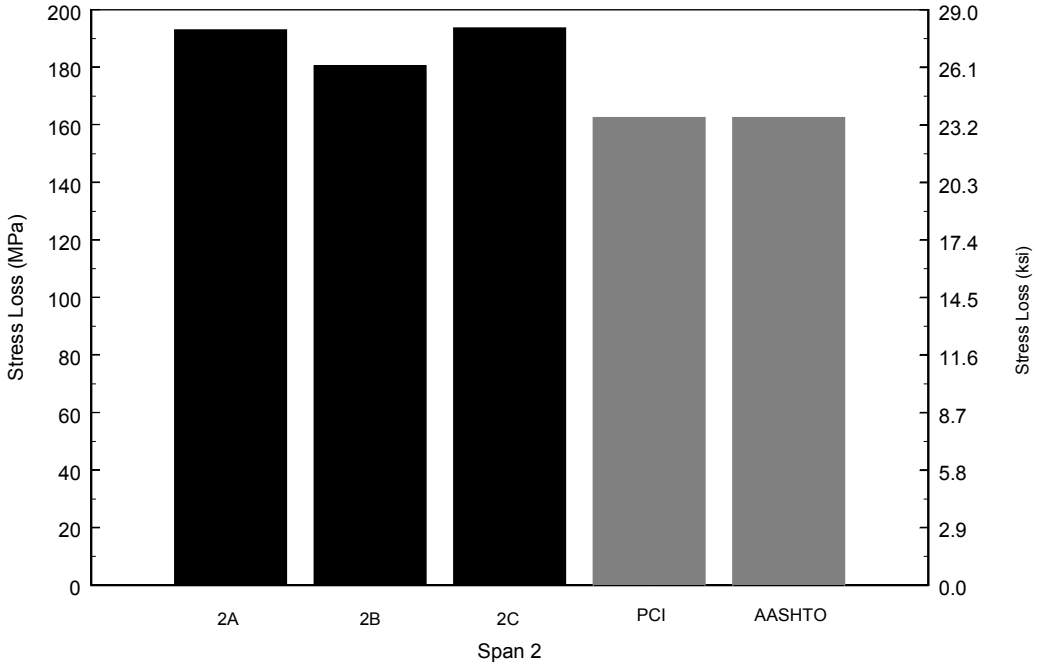

Figure 7.3. Observed and Computed Elastic Shortening Losses for Span 2 Girders

The elastic shortening losses were also calculated for the span 1 girders using the PCI and AASHTO methods. The losses are smaller than those in span 2 because there were fewer prestressing strands. The PCI and AASHTO methods also underestimated the observed elastic shortening losses in span 1. Figure 7.4 shows the elastic shortening losses for span 1. Table 7.1 lists the average observed and predicted elastic shortening losses for each span.

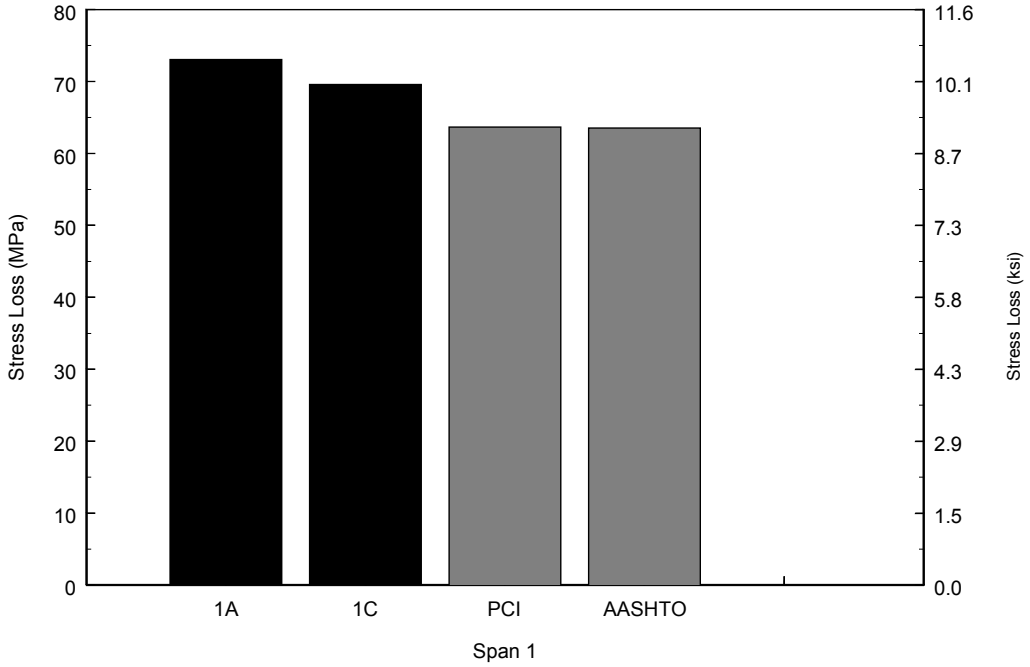

Figure 7.4. Observed and Predicted Elastic Shortening Losses for Span 1 Girders

Table 7.2. Elastic Shortening Loss as a Percentage of Jacking Stress

	Average Girder	PCI	AASHTO
Span 1	5.1	4.6	4.6
Span 2	13.5	11.6	11.6

7.3 SHRINKAGE

The PCI method calculates the loss of prestress due to shrinkage over a particular time period as the product of: (1) the ultimate stress loss for a concrete with a particular modulus of elasticity (USH), (2) a shape factor (SSF), and (3) a percentage of the ultimate shrinkage (PSH). This relationship is given by Equation 7.11.

$$\Delta f_{p,SH} = (USH)(SSF)(PSH) \tag{7.11}$$

where

$\Delta f_{p,SH}$ = is the change is stress due to shrinkage for a particular time interval

USH = ultimate loss of shrinkage of concrete for accelerated cure

= 186-20.7*$E_c/10^3$>87.6 psi

E_c = concrete modulus of elasticity at 28 days (Equations 7.9 and 7.10)

SSF = shrinkage factor for a volume to surface ratio (0.86 for W74G)

PSH = amount of shrinkage during each time step

=$(AUS)_t$ - $(AUS)_{t1}$

t = end of time step (days after curing)

t_1 = beginning of time step (days after curing)

The values for AUS are provided in Table 7.3. An equation fit to this data was attained (Fekete, 1997) and is shown in Equation 7.12.

Table 7.3. Values of *AUS*

Time after end of curing (days)	Portion of ultimate shrinkage (*AUS*)
1	0.08
3	0.15
5	0.20
7	0.22
10	0.27
20	0.36
30	0.42
60	0.55
90	0.62
180	0.68
365	0.86
End of service life	1.0

$$AUS = \frac{t^{0.65}}{12 + t^{0.65}} \tag{7.12}$$

The refined estimate of prestress loss due to shrinkage in the AASHTO method can be made time-dependent by multiplying the ultimate stress loss due to shrinkage by the ratio of shrinkage strain at any point in time divided by the ultimate shrinkage strain. The expression for shrinkage strain in the AASHTO method is given by Equation 7.13.

$$\varepsilon_{sh} = -k_s * k_h * \left(\frac{t}{55.0 + t}\right) * 0.56x10^{-3} \tag{7.13}$$

where

ε_{sh}= strain due to shrinkage of concrete

k_s = size factor

$$= \left[\frac{\frac{t}{26 * e^{0.36*(v/s)} + t}}{\frac{t}{45 + t}}\right]\left[\frac{1064 - 94*(v/s)}{923}\right]$$

$$= \left[\frac{45 + t}{26 * e^{(0.3V/S)} + t}\right]\left(1.153 + 0.102V/S\right)$$

t = time in days

v/s = volume to surface ratio of girder (for W74G)

k_h = humidity factor (0.80 for Western Washington)

The ultimate time for shrinkage calculations was taken as 1800 days. The expression for stress loss at any time interval was computed using Equation 7.14.

$$\Delta f_{sh} = (117.0 - 1.035 * H)\left(\frac{\varepsilon_{sh}(t = ti)}{\varepsilon_{sh}(t = 1800)}\right) \tag{7.14}$$

where

H = average annual ambient relative humidity (%) (80 % for Western Washington)

The loss of stress due to shrinkage was not obtained in the instrumented girders because of the difficulties of separating shrinkage and creep. Figure 7.5 compares the prestress losses due to shrinkage for the girders in span 1 and span 2 calculated with the AASHTO and PCI methods. Note that the short girders were cast approximately 27 days after the long ones.

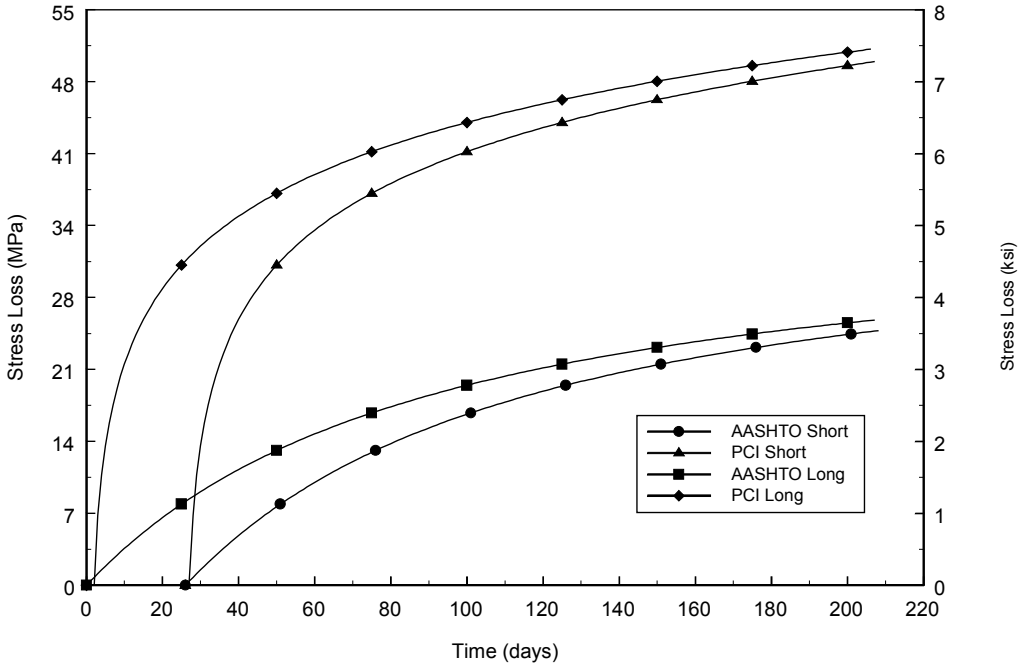

Figure 7.5. AASHTO and PCI Shrinkage Loss Predictions

Figure 7.5 shows a large difference in the predictions for the prestress loss due to shrinkage. The PCI method predicts an ultimate shrinkage loss of 51 MPa (7.4 ksi) at 1800 days, while the AASHTO method predicts an ultimate loss of 24 MPa (3.5 ksi). The refined estimate used in the AASHTO method is the simplest method, and the ultimate loss is only a function of the humidity, while the PCI method is a function of the elastic modulus, volume-to-surface ratio, and time since curing. Each method predicts the same stress loss due to shrinkage for the two different spans. This is expected since shrinkage depends only on properties that are the same for both girders.

7.4 CREEP

The PCI method calculates the prestress loss over each time interval as a percentage of the ultimate creep (UCR) multiplied by factors that take into account the volume-to-surface ratio (SCF), the rate at which creep occurs throughout time (PCR), and the stress in the concrete at the prestressing centroid (f_c). Equation 7.15 predicts the prestress loss for a particular time interval for concrete with an accelerated cure.

$$\Delta f_{pcr} = (UCR)(SCF)(PCR)\left(f_c\right) \tag{7.15}$$

where

Δf_{pcr} = change in prestressing force during a particular time interval

UCR = ultimate creep loss

$= 63 - 138 * Ec / 1.0^3 \geq 11$

E_c = concrete modulus of elasticity at 28 days (Equations 9.9 and 9.10)

SCF = volume to surface factor (0.87 for W74G girder)

PCR = portion of ultimate creep over the time interval t_1 to t

$= (AUC)_t - (AUC)_{t1}$

t = end of time step (days after curing)

t_1 = beginning of time step (days after curing)

f_c = net compressive stress at the center of gravity of the prestressing force at time t_1, taking into account the loss of prestress force occurring over the preceding time interval

The values for AUC are listed in Table 7.4. An equation fit to this data was attained (Fekete, 1997) and is shown in Equation 7.16.

Table 7.4. Values of *AUC*

Time after prestress transfer (days)	Portion of ultimate creep (*AUC*)
1	0.08
2	0.15
5	0.18
7	0.23
10	0.24
20	0.30
30	0.35
60	0.45
90	0.51
180	0.61
365	0.74
End of service life	1.0

$$AUC = \frac{t^{0.70}}{20 + t^{0.70}} \tag{7.16}$$

The AASHTO Refined Estimate method for calculating prestress losses due to creep of the concrete may be time rated upon the maximum ultimate creep coefficient. This method takes into account the initial concrete stress due to the prestressing force, and the dead load of the girder plus the weight of the slab and diaphragm. Equation 7.17 predicts the ultimate prestress loss due to creep of the concrete.

$$\Delta f_{p,CR} = 12.0 * fcgp - 7.0 * \Delta fcdp \tag{7.17}$$

where

$\Delta f_{p,CR}$ = ultimate prestress loss due to creep

f_{cgp} = stress at centroid of prestressing strand after destressing (Equation 9.7)

Δf_{cdp} = change in prestress due to dead weight of diaphragm and slab

$$= \frac{M_{sd} * e}{I}$$

M_{sd} = moment due to superimposed dead weight of diaphragm and slab

e = distance from centroid of girder to prestressing centroid

I = moment of inertia of girder

Equation 7.18 is made time dependent by multiplying it by the ratio of the creep coefficient at the current time step divided by the creep coefficient at the end of service life. Equation 7.18 predicts the variation with time of prestress loss due to creep.

$$\Delta f_{pcr(t)} = \Delta f_{pcr} * \left(\frac{\Psi_{(t)}}{\Psi_{(t\ =\ end)}} \right) \tag{7.18}$$

where

$\Delta f_{pcr(t)}$ = prestress loss due to creep at a particular time

$\Psi_{(t)}$ = creep coefficient

$$= 3.5 * k_c * k_f * \left(1.58 - \frac{H}{120} \right) t_i^{-0.118} \left(\frac{(t - t_i)^{0.6}}{\left(10.0 + (t - t_i)^{0.6} \right)} \right)$$

k_c = factor for volume-to-surface ratio

$$= \left[\frac{\frac{t}{26 * e^{0.36(v/s)} + t}}{\frac{t}{45 + t}} \right] \left[\frac{1.80 + 1.77 * e^{-0.54(v/s)}}{2.587} \right]$$

$$= \left[\frac{45 + t}{26 * e^{(0.36V/S) + t}} \right] \left[0.696 + 0684 * e^{(-0.54V/S)} \right]$$

k_f = factor for the effect of concrete strength

$$= \frac{1}{0.67 + \left(\frac{f'c(t)}{62} \right)}$$

f'_c = Equation 7.9 (MPa)

H = relative humidity in % (80 for Western Washington)

t_i = age of concrete when load is initially applied (days)

t = age of concrete of time interval (days)

The prestress losses due to creep in the concrete were calculated for both the PCI and AASHTO methods. Figure 7.6 shows the prestress losses due to creep for the girders in spans 1 and 2.

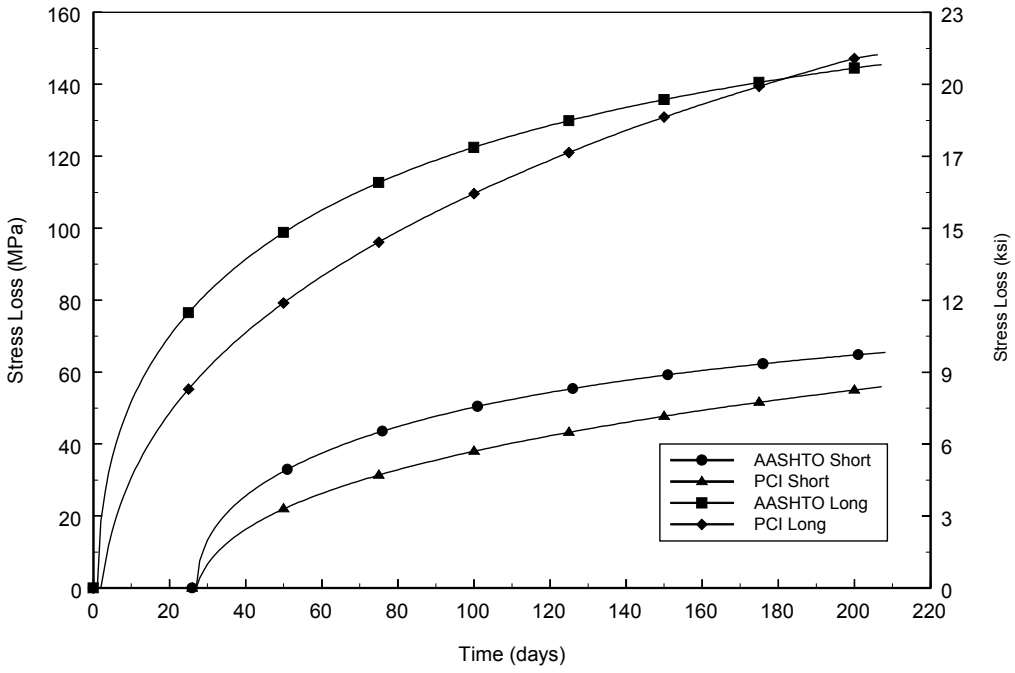

Figure 7.6. Computed Prestress Losses Due to Creep in the Concrete

The creep losses calculated with the two methods are similar. For the girders in span 1 the AASHTO method predicts slightly higher losses than does the PCI method. For the girders in span 2 the AASHTO method initially predicts higher losses in span 2, but after day 180, the PCI method predicts a higher prestress loss.

7.5 COMBINED CREEP AND SHRINKAGE

The combination of the creep and shrinkage was measured in the instrumented girders. The calculated creep and shrinkage prestress losses for the two methods were added together for the respective spans. Figure 7.7 shows the observed and predicted creep and shrinkage losses for the girders in span 2.

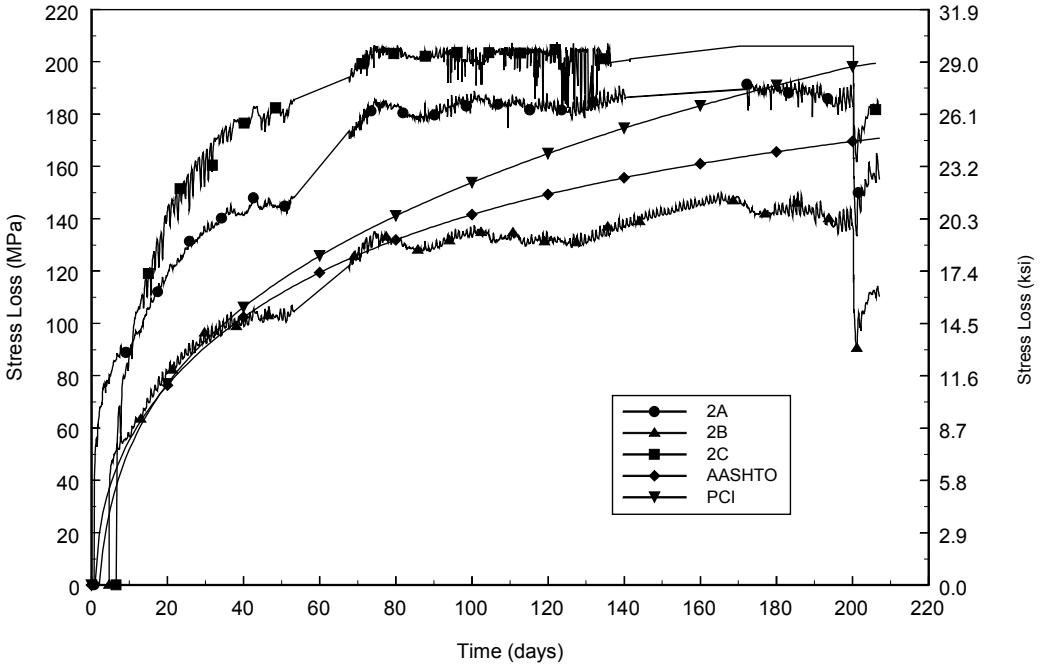

Figure 7.7. Comparison of Observed and Predicted Creep and Shrinkage Losses

The predicted creep and shrinkage losses from the AASHTO and PCI methods fall within the range of observed losses. The calculated values are lower than the average observed values for the first 200 days. The PCI method predicts losses higher than the AASHTO method, but the difference is small compared with the variation among the girders. Girder 2C has the largest observed creep and shrinkage losses, followed by

girder 2A and then 2B. While the observed losses in girders 2C and 2A are reasonably close to each other, the observed losses in girder 2B are noticeably smaller. The methods both predict higher losses than what was observed in girder 2B.

The combination of creep and shrinkage losses was also computed from strain measurements for both of the instrumented girders in span 1. Figure 7.8 shows the observed and predicted creep and shrinkage losses for the girders in span 1.

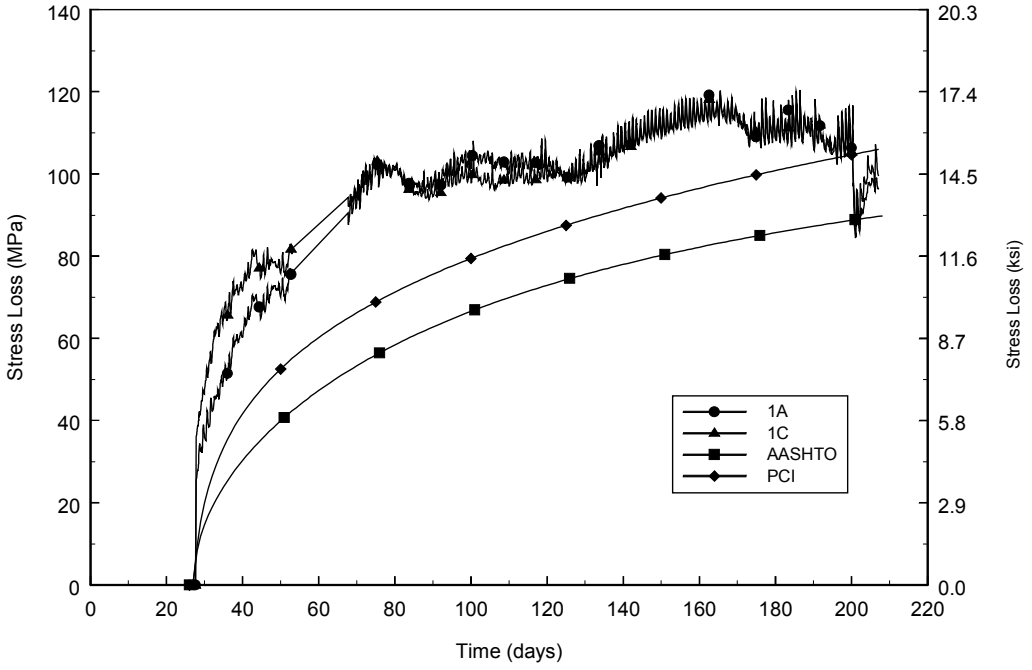

Figure 7.8. Observed and Predicted Creep and Shrinkage Losses for Span 1 Girders

The predicted values for creep and shrinkage also closely match the observed values at day 207. However, the predicted values are lower than the observed values for the first 200 days of the girder. The PCI method predicts a higher creep and shrinkage loss than does the AASHTO method. This difference is consistent with the trend in the

span 2 girders. Table 7.5 lists the numerical values for creep and shrinkage as a percentage of the initial jacking force at day 200.

Table 7.5. Creep and Shrinkage Losses as Percent of the Jacking Stress at Day 200

Girder	Observed	AASHTO	PCI
1A	7.6	6.4	7.6
1C	7.5	6.4	7.6
2A	13.2	12.2	14.3
2B	9.8	12.2	14.3
2C	14.7	12.2	14.3

7.6 TOTAL PRESTRESS LOSSES

The total calculated prestress losses due to relaxation of the prestressing strand, elastic shortening, shrinkage, and creep were added to obtain the total prestress losses. Figure 7.9 shows the total prestress losses for what were observed and predicted for the girders in span 2.

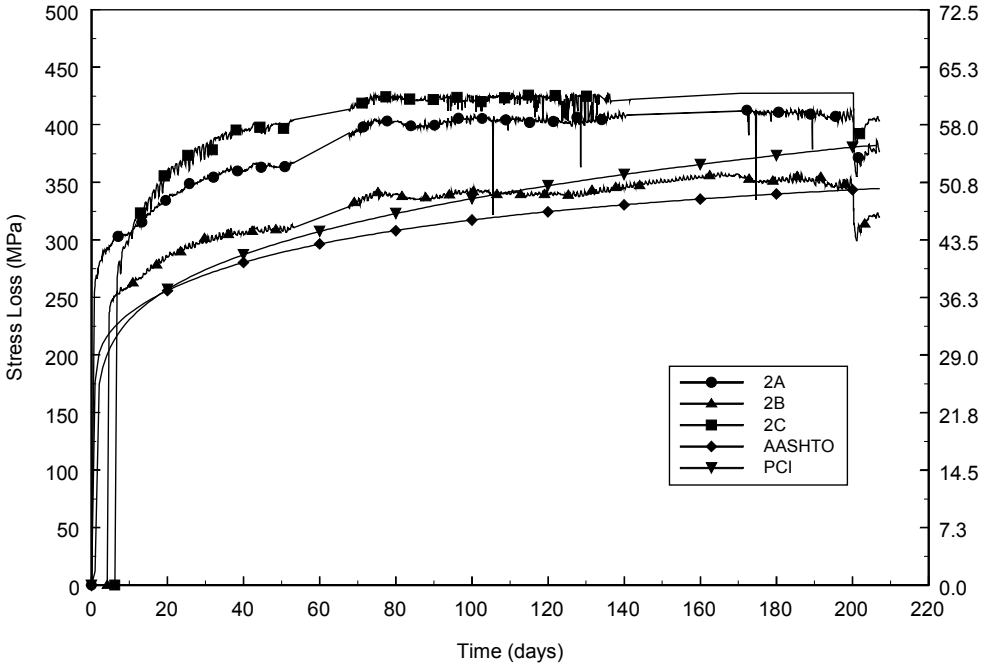

Figure 7.9. Total Prestress Losses for Span 2 Girders

Figure 7.9 shows that the observed prestress losses for span 2 girders nearly all exceed the predicted losses. The only exception is that the PCI method predicts a higher prestress loss than was observed in girder 2B after 170 days. The difference between the observed prestress loss values is larger at first and reduces with time. The PCI method predicts a higher prestress loss than the AASHTO method. After the slab is cast at day 200, the difference between the observed prestress losses and calculated prestress losses is smaller.

Figure 7.10 shows the total observed and predicted prestress losses for the girders in span 1.

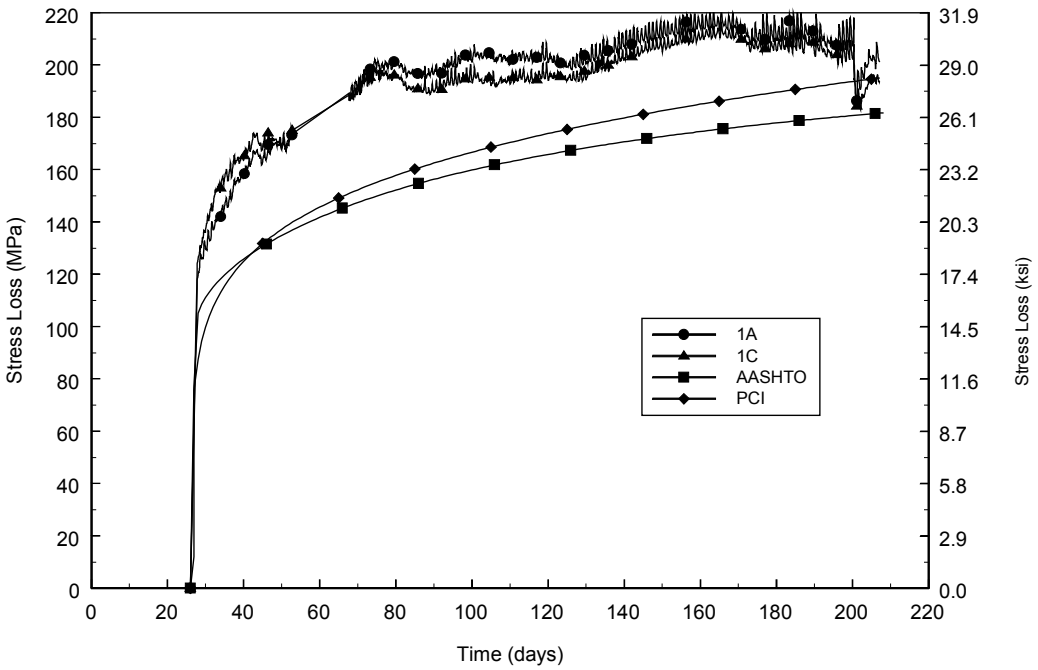

Figure 7.10. Total Prestress Losses for Span 1 Girders

The total observed prestress losses for the girders in span 1 are higher than the predicted losses for both the PCI and AASHTO methods. The difference between the observed and predicted values is larger at first and diminishes with time. The PCI method predicts a total prestress loss that is slightly higher than the AASHTO method. Table 7.6 lists the total prestress losses at day 200 as a percentage of the initial jacking stress.

Table 7.6. Total Prestress Losses at Day 200 as Percentage of Jacking Stress

Girder	Observed	AASHTO	PCI
1A	14.4	13.0	13.9
1C	13.9	13.0	13.9
2A	29.1	24.7	27.4
2B	24.8	24.7	27.4
2C	30.6	24.7	27.4

7.7 CAMBER

The PCI method uses long-term deflection multipliers (applied to the immediate elastic shortening) to calculate the long-term camber. The upward and downward components of the immediate elastic deflection are separated, because the upward component due to prestressing will be influenced by both creep and prestress loss, whereas the downward component will be influenced by creep alone. Equation 7.19 calculates the initial downward deflection at mid-span due to the dead load of the girder in span 2.

$$\Delta_{dl} = \frac{5 * w * L^4}{384 * E_{ci} * I} \tag{7.19}$$

where

Δ_{dl} = downward deflection due to dead load of the girder

w = weight of girder (0.012 KN/mm for ρ=2480 kg/m^3 (0.0670 kips/in for ρ=155 lbs/ft^3))

L = girder span (40.1 m (1580 in) span 2 only)

E_{ci} = modulus of elasticity at transfer (34 GPa (4900 ksi) using Equation 6.10, f'c=51 MPa (7,400 psi))

I = moment of inertia (228x10^9 mm^4 (547,000 in^4))

The initial calculated downward deflection is 51 mm (2.0 in) for span 2. The initial upward camber is due to the prestressing force after transfer. Equation 7.20 predicts the upward mid-span camber after transfer.

$$\Delta ps = \frac{P * L^2}{8 * Eci * I}\left[ec + (ee - ec)\frac{4}{3}\frac{a^2}{L^2}\right] \tag{7.20}$$

where

Δ_{ps} = camber due to prestressing force

P = prestressing force in tendons after transfer (6760 KN (1520 kips))

e_c = eccentricity of prestressing strand at midspan (871 mm (34.3 in))

e_e = eccentricity of prestressing strand at end (511 mm (20.1 in))

a = distance from end of girder to harping point (16100 mm (632 in))

By using Equation 7.20, the initial camber due to the prestressing force is 135 mm (5.3 in) upwards. The total initial camber at transfer is the sum of the deflection due to the dead load [51 mm (2.0 in) downward] plus the deflection due to the prestressing force [140 mm (5.5 in) upward], resulting in a deflection of 89 mm (3.5 in) upward. This is expressed in Equation 7.21.

$$\Delta_{total} = \Delta_{ps} + \Delta_{dl} \tag{7.21}$$

$$\Delta_{total} = -135mm + 51mm = -84mm$$

The deflection before slab casting can be found by using the PCI multipliers of 1.80 for the upward elastic deflection and 1.85 for the downward elastic deflection (PCI, 1992). Using these multipliers and the values for the upward and downward deflection

that are already calculated, the total calculated deflection before slab casting is 146 mm (5.85 in) upwards.

The deflection after slab casting is the deflection before slab casting plus the downward deflection due to the casting of the deck. The equation of the downward deflection due to the casting of the deck is the same as Equation 7.21, except instead of the weight of the girder, the weight of the slab [0.014 KN/mm (0.082 kips/in)] is used, and also the modulus of elasticity of the girder at deck casting (38.3 GPa (5560 ksi)) is used. The downward deflection due to the deck casting is 55 mm (2.2 in). Therefore, the predicted deflection after casting is 93 mm (3.7 in) upward. This is expressed in Equation 7.22.

$$\Delta total = 1.8 * \Delta_{ps} + 1.85 * \Delta_{dl} + \Delta_{slab} \qquad (7.22)$$

$$\Delta_{total} = -1.8 * 135mm + 1.85 * 51mm + 55mm = -93mm$$

The camber predicted using the PCI multipliers was calculated at transfer, before the slab was cast, and after the slab was cast. The values are shown with the measured deflections using the surveyor's level in Figure 7.11.

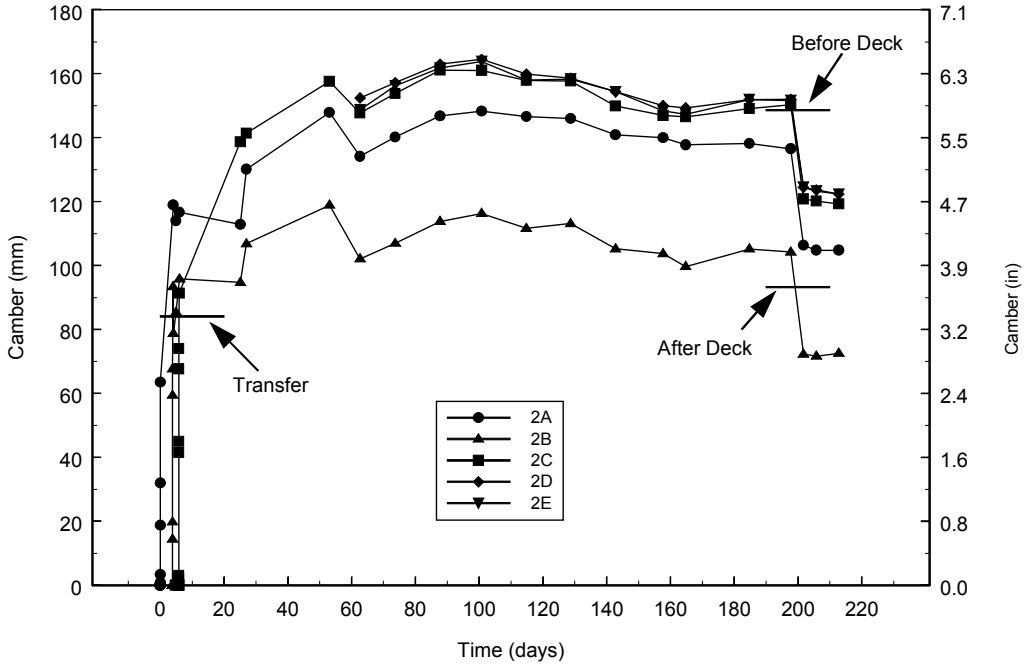

Figure 7.11. Comparison of PCI Multipliers and Measured Camber

The PCI method for calculating deflections overestimated the deflection at transfer. The measured transfer deflection was about 61 mm (2.4 in) for each girder in span 2, whereas the predicted camber of 84 mm (3.3 in) is 37.5 percent higher. This finding indicates that the elastic modulus was higher at release or the prestressing force was smaller than predicted. This is in contrast to the findings of the elastic shortening loss, which would indicate that the elastic modulus was lower than predicted.

The PCI multipliers did predict the camber prior to deck casting accurately for girders 2C, 2D, and 2E. In Girders 2A and 2B the measured camber was lower than predicted. In all girders except 2B, the predicted camber after deck casting was lower than was measured. This finding suggests that either the methods underpredicted E_c, or

the lower sections of the pier diaphragms, which were in place at the time, offered some continuity in the girder.

7.8 SUMMARY OF EVALUATION

This chapter compares the observed prestress loss and camber values in the five instrumented girders to the values calculated by the PCI and AASHTO methods. The main findings are:

- Both the PCI and AASHTO methods predicted a lower relaxation loss than was tested by the manufacturer for girders in both spans.
- The elastic shortening losses predicted from both methods were lower than those observed in the instrumented girders for both spans.
- The combination of creep and shrinkage was over-predicted for girder 2B; however, they were under-predicted for girders 2A and 2C at day 200. Stress losses in girders 1A and 1C were higher than the predicted results for the first 200 days and then corresponded well.
- The total prestressing losses were under-predicted for girders 1A, 1C, 2A, and 2C. The predicted total loss for the AASHTO method was within 0.7 MPa (0.1 ksi) for girder 2B and the PCI method over-predicted the total losses.
- The PCI method over-predicted the initial camber after destressing for the girders in span 2. The predicted camber before the deck was cast was close to the measured camber values for girders 2C, 2D, and 2E, while girders 2B and 2A had lower camber values than predicted. The predicted camber values after the deck was cast were high for all girders in span 2, except girder 2B.

CHAPTER 8

PRELIMINARY CONCLUSIONS

This research project focused on evaluating the effectiveness of using high performance concrete (HPC) in precast, prestressed concrete girders. This HPC was used in the fabrication of 15 W74G girders for a bridge located in Washington State (SR18/516 Undercrossing). One test girder and five bridge girders were instrumented and monitored for 207 days. The observed behavior of the instrumented bridge girders was compared with that calculated with current design methods. This chapter provides preliminary conclusions that can be drawn from the information available at this time.

8.1 DESIGN

- The use of HPC permitted WSDOT engineers to reduce the number of girder lines from seven to five.
- To reduce strand congestion, 15.2-mm (0.6-in), instead of normal 12.7-mm (0.5-in), diameter prestressing strands were used at a standard spacing of 50mm (2 in).
- In many girders, the concrete mix design is likely to be dominated by the concrete strength required at release, because the critical stress occurs then.
- Requiring a high concrete strength at release may force the fabricator to implement a 2-day curing cycle. The economic impacts of this choice should be considered during design.
- Prestress losses may be higher in HPC girders than in those made with conventional concrete. The elastic shortening and creep components dominate the losses. The elastic shortening component will almost certainly be higher because the applied stress will likely increase in direct proportion to the release strength, whereas the Young's modulus (E_{ci}) is usually treated as increasing only with the square root, or even some lower power, of concrete strength. Whether the creep component is larger depends on E_{ci}/C_c, where C_c is the creep coefficient. If the

creep coefficient increases with concrete strength, the prestress loss due to creep will fall, and vice versa.

- In this bridge, LRFD and LFD designs for HS-25 live loading yielded similar results.

8.2 FABRICATION

During curing, the internal concrete temperatures varied approximately 25 C° (50 F°) over the depth of the girder. The lowest temperatures were recorded at the bottom of the girder. Because the strength of concrete usually increases as curing temperature increases, the bottom of the girder would be expected to have the weakest concrete.

The fabricator used a thermocouple in the girder that was connected to a sure-cure system to monitor concrete strength prior to strand release. The thermocouple was placed at mid-height for all of the girders (except 2B, in which it was placed 457 mm (18 in) from the bottom of the girder). Consequently, the concrete in the cylinders connected to the sure-cure system was stronger than that at the bottom of the girder. This finding is significant, because it means that the weakest concrete is located at the bottom flange of the girder where the compressive stress is highest.

Twenty-four strands were instrumented to measure end slip. For 19 of these strands, the computed transfer length exceeded the 914 mm (36 in) predicted by the AASHTO prediction method (AASHTO, 1994).

8.3 OBSERVED PRESTRESS LOSSES

Table 8.1 lists the observed and calculated prestress losses for the five instrumented girders on day 200, just prior to casting of the deck. Losses are calculated by the PCI and AASHTO methods (PCI 1979, AASHTO 1994).

Table 8.1. Observed and Calculated Prestress Losses at Day 200 (MPa)

Prestress Losses	Girder Length (m)	1A (23.2)	1C (23.2)	2A (40.5)	2B (40.5)	2C (40.5)
Total	Observed	208	203	406	346	427
	PCI	195	195	381	381	381
	AASHTO	182	182	343	343	343
Relaxation	Manufacturer	28.3	28.3	28.3	28.3	28.3
	PCI	28.4	28.4	19.3	19.3	19.3
	AASHTO	28.3	28.3	11.0	11.0	11.0
Elastic Shortening	Observed	73.1	69.6	193	181	194
	PCI and AASHTO	64.1	64.1	162	162	162
Creep and Shrinkage	Observed	107	105	184	137	205
	PCI	106	106	200	200	200
	AASHTO	89.6	89.6	170	170	170

- The total observed prestress losses at day 200 for the 3 monitored long-span girders (2A, 2B, and 2C) constitute 25 to 30 percent of the total jacking stress of 1396 MPa (202.5 ksi). For the short-span girders (1A and 1C), the total losses constitute approximately 15 percent of the total jacking stress.
- The observed elastic shortening losses for the long-span girders 2A, 2B, and 2C constitute approximately 13.5 percent of the total jacking stress. For girders 1A and 1C, the elastic shortening loss constitute approximately 5 percent of the total jacking stress.
- The total observed creep and shrinkage losses at day 200 for girders 2A, 2B, and 2C constitute 10 to 15 percent of the total jacking stress. For girders 1A and 1C, the total

creep and shrinkage losses constitute approximately 7.5 percent of the total jacking stress.

8.4 COMPARISON WITH CALCULATED PRESTRESS LOSSES

- The total observed prestress losses ranged from 12 percent lower to 9 percent higher than the total prestress loss calculated with the PCI method. The observed prestress losses were between 1 and 18 percent higher than the total calculated prestress losses with the AASHTO method.
- The observed elastic shortening losses are 8 to 16 percent higher than the elastic shortening losses calculated with the PCI and AASHTO methods for all the girders.
- The observed losses for creep and shrinkage were between 0 and 32 percent higher than the losses calculated with the PCI method. The observed losses for creep and shrinkage ranged from 21 percent lower to 19 percent higher than the losses calculated with the AASHTO method.
- Between 9 to 16 percent of the creep and shrinkage losses occurred during destressing. The magnitude of the contribution depended on the time it took to destress.
- Additional prestress losses could occur due to temperature variations between the time the strands were stressed and the time the concrete bonds to the strand. For girder 2B the magnitude of this loss was estimated as ranging between 48.2 and 82.7 MPa (7 and 12 ksi).

8.5 CAMBER

Camber was monitored with a stretched-wire system and, intermittently, with a surveyor's level. At day 200, the cambers for girders 2C, 2D, and 2E were approximately 150 mm (5.9 in), while the cambers for girders 2A and 2B were 13 and 46 mm (0.5 and 1.8 in) lower. On day 200, the camber for girders 1A and 1B was 23 mm (0.9 in), while the camber in girder 1C was approximately 6.4 mm (0.25 in).

On a typical day, the camber varied by approximately 20 mm (0.8 in) for the long girders. The variation is attributed to thermal effects. On the same day the thermal camber for the short girders ranged from 5.1 to 8.1 mm (0.2 to 0.32 in). The maximum and minimum camber readings occurred at 3:00 P.M. and 6:00 A.M., respectively. The maximum and minimum temperature readings for the same day occurred at 4:30 P.M. and 6:15 A.M. The difference is attributed to the fact that the thermal camber depends on temperature gradient rather than on absolute temperature.

8.6 RESEARCH RECOMMENDATIONS

A designer needs to be able to predict the prestress losses and cambers for various concrete mixes. These predictions are ideally done with instrumentation programs, but it is not economical to perform an instrumentation program for every mix. A more economical approach would be to perform materials testing that could be used to calibrate a prestress loss model. Research is needed to provide the link between creep and shrinkage observed in the laboratory and creep and shrinkage to be expected in the field.

This study identified the critical need to improve the means of predicting girder creep and shrinkage based on the measured behavior of cylinders. To achieve this goal, it is necessary to closely simulate in the laboratory specimens the curing conditions and time of loading of the girders. Greater consistency between the cylinder and girder strains could be achieved by conducting a laboratory testing program in which the mix proportions, curing conditions, and time of loading were more carefully controlled than was possible in this study. The measured strains appear to be very sensitive to the curing history, age at loading, and environmental conditions. Such a study would also permit investigation of the use of maturity as a measure of the intrinsic age of the concrete.

This project was one of many similar projects being performed in several States. The prestress losses and camber values from girders from various States need to be compared. After comparing the prestress losses and cambers of all the girders from the other States, one needs to develop a model that better predicts the observed prestress losses and camber for HPC girders.

Service I - 1.0 DC + 1.0 (LL+IM)

Compression in prestressed components is investigated using this load combination.

Service III - 1.0 DC + 0.8 (LL+IM)

Load combination relating only to tension in prestressed concrete structures with the objective of crack control.

Vehicular Live Load

Design live load, HL-93, shall be taken as:

(Design truck (HS20) or tandem) (1 + IM) + Lane

Dynamic load allowance, IM = 33%

The distribution factor can be shown to be D.F. = 0.63.

Table 1 - Section Properties

	Girder	Composite
Depth, mm	1 865	2 045
Area, mm^2	485 300	765 100
I, mm^4	227.5 x 10^9	400.4 x 10^9
y_b, mm	970	1 330
S_b, mm^3	234.4 x 10^6	301.0 x 10^6
y_t girder, mm	895	535
S_t girder, mm^3	254.3 x 10^6	748.8 x 10^6
y_t slab, mm	-	715
S_t slab, mm^3	-	560.2 x 10^6

Note: 1 mm = 0.0394 in.

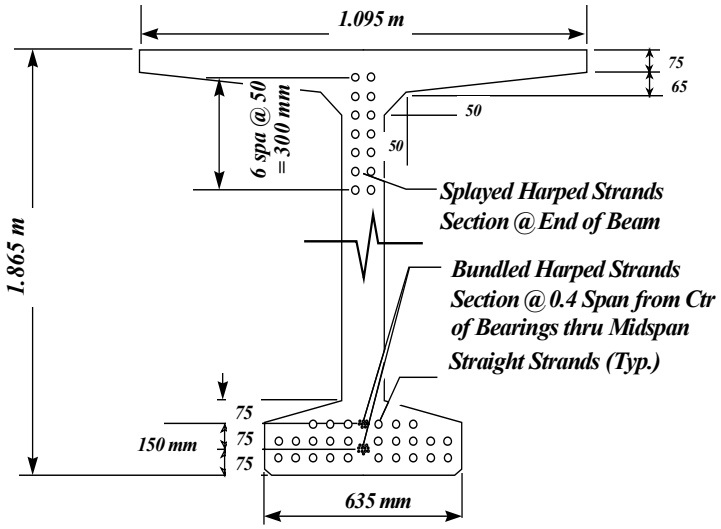

Figure 2 - Typical W74MG Prestressed Girder and Strand Pattern

Allowable Concrete Stresses at Service Limit State

Current WSDOT design practice does not allow any tension at the bottom of prestressed girder at Service III limit state. The zero tension criteria practiced by WSDOT provides some reserve to mitigate construction, operational, and fatigue related problems. It is usually achieved by adding one or two strands to the total number of strands per girder. The other allowable concrete stresses follow the LRFD Specifications.

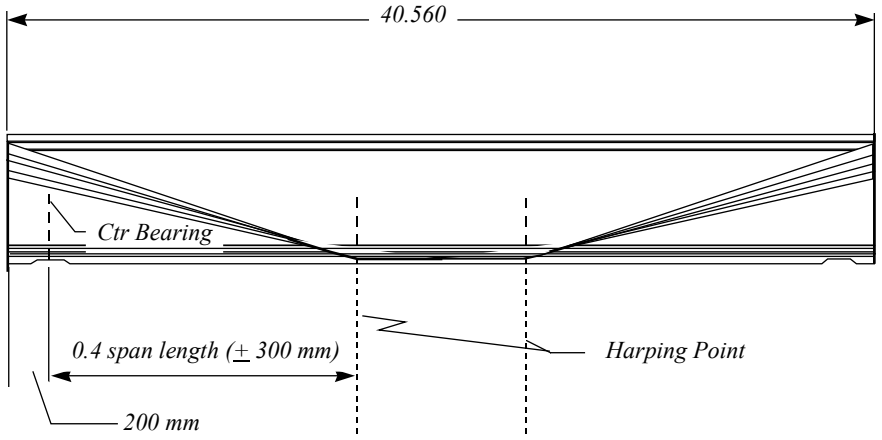

Figure 3 - Prestressed Girder Elevation

Determination of Prestressing Forces

A trial and error method was used to determine the proper number of prestressing strands. The jacking stress at transfer, 0.75 f_{pu}, is used as allowed in the LRFD code.

Table 2 - Summary of Stresses at Service

	At mid-span			At harping point		
Stress (MPa)	f_b	f_t(girder)	f_t(slab)	f_b	f_t(girder)	f_t(slab)
Girder	10.15	-9.35	-	9.74	-8.98	-
Slab + haunch	12.26	-11.30	-	11.77	-10.85	-
Diaphragm	1.41	-1.30	-	1.27	-1.17	-
Traffic barrier	1.85	-0.74	-0.99	1.77	-0.71	-0.95
ΣDL	25.67	-22.69	-0.99	24.55	-21.71	-0.95
LL - Service I	-	-4.73	-6.33	-	-4.58	-6.12
LL - Service III	9.42	-	-	9.11	-	-
Prestressing	-35.98	8.66	-	-35.98	8.66	-
Stresses under permanent load	-	-14.03	-0.99	-	-13.04	-0.95
Allowables	-	-31.05	-12.60	-	-31.05	-12.60

Stresses under all loads	-0.89	-18.76	-7.32	-2.32	-17.62	-7.07
Allowables	0.00	-41.40	-16.80	0.00	-41.40	-16.80

Note: Tension (+); 1 MPa = 0.145 ksi

For the final design, 14 harped and 26 straight strands are used, as shown in Figures 2 and 3. The total prestress loss at service is calculated to be 283.5 MPa (42 ksi) using the Modified Rate of Creep method (see next section). The final stresses at service at the mid-span and the harping point are summarized in Table 2. It can also be shown that concrete stresses at transfer satisfy the code requirement.

PRESTRESS LOSSES IN PRESTRESSED GIRDERS

Despite wide use of prestressing, there is no simple, practical method for predicting accurately the time-dependent losses of prestressed concrete structures. This is partly because of the difficulty in predicting the time-dependent properties of concrete and prestressing steel, and the uncertain environmental conditions to which the structure will be subjected after prestressing.[4] For HPC, the difficulty also comes from the limited experience and data available.

TIME-DEPENDENT PRESTRESS LOSSES

Prestress Loss Due to Creep

Creep loss due to permanent loads occurs immediately after initial prestressing. The stress in the concrete at the level of prestressing steel at transfer is the elastic response, while the creep effect will occur over a long period of time under a sustained load. For composite girders, part of initial compressive strain induced in the concrete immediately after transfer is reduced by the tensile stress resulting from superimposed permanent loads. Loss of prestress due to creep is proportional to the net compressive stress in the concrete. In accordance with the AASHTO LRFD Specifications, the creep loss is given by:

$$\Delta f_{PCR} = 12.0\, f_{cgp} - 7.0\, \Delta f_{cdp} \quad > 0.0 \qquad (1)$$

where

f_{cgp} = sum of the concrete stresses due to prestressing and weight of the girder at the center of gravity of prestressing strands at mid-span

Δf_{cdp} = change in concrete stress at the level of prestressing strands due to applied dead loads of concrete deck slab and diaphragms.

The term $7.0\, \Delta f_{cdp}$ in the above equation is the approximate estimate of prestress gain due to dead load of slab and diaphragm.

In the Modified Rate of Creep method, prestress loss due to creep may be considered in two stages: Stage 1 is the creep loss between time of transfer and slab casting, which may be expressed as:

$$\Delta f_{PCR1} = n\, f_{cgp}\, \Psi_{t,tisc}\, (1-\Delta F_{SC}/2F_o) \qquad (2)$$

Stage 2 is the creep loss for any time after slab casting, which may be expressed as:

$$\Delta f_{PCR2} = n\, f_{cgp}\, (\Psi_{t,ti}-\Psi_{t,tisc})\, (1-(\Delta F_{SC}+\Delta F_t)/2F_o)\, I_g/I_c \qquad (3)$$

where

$\Psi_{t,ti}$ = creep coefficient of girder at any time
$\Psi_{t,tisc}$ = creep coefficient of girder at the time of slab casting
ΔF_{SC} = total loss at the time of slab casting minus initial elastic shortening loss
F_o = prestressing force at transfer after elastic losses
ΔF_t = total prestressing loss at any time minus initial elastic shortening loss
I_g/I_c = ratio of moment of inertia of prestressed girder to composite girder

In the above equations, the terms $\Psi_{t,tisc}(1-\Delta F_{SC}/2F_o)$ and $(\Psi_{t,ti}-\Psi_{t,tisc})(1-(\Delta F_{SC}+\Delta F_t)/2F_o)$ represent the effect of variable stress history from the time of transfer to the time of slab casting and from slab casting to final conditions, respectively. The term I_g/I_c represents the effect of composite section properties after slab casting.

Prestress Loss Due to Shrinkage

Shrinkage of concrete can vary over a wide range depending on the material properties and surface drying conditions. Prestress loss due to shrinkage of concrete for prestressed members according to AASHTO LRFD Specifications is given by:

$$\Delta f_{PSR} = (117.0 - 1.035\, H) \qquad (4)$$

where

H = relative humidity
Δf_{PSR} = shrinkage loss in MPa

Prestress Loss Due to Relaxation of Prestressing Strands

Relaxation of prestressing strands depends upon the stress level in the strands. However, because of the other prestressing losses, there is a continued reduction of the strand stress, thus causing a reduction in prestress. The reduction in strand stress due to elastic shortening of concrete occurs instantaneously. On the other hand, the reduction in strand stress due to creep and shrinkage takes place for a long period of time.

The loss due to relaxation of prestressing strands given by AASHTO LRFD Specifications is considered in two stages: relaxation loss at transfer and relaxation loss

after transfer of prestress force. In a prestressed member, with low-relaxation strands, the relaxation loss in prestressing steel, initially stressed in excess of $0.5f_{pu}$, is given by:

$$\Delta f_{PR1} = \log(24t)/40.0\ [f_{pj}/f_{py}-0.55]f_{pj} \qquad \text{at transfer} \qquad (5)$$

$$\Delta f_{PR2} = 0.30\ [\ 138 -0.4\ \Delta f_{PES} - 0.2(\Delta f_{PSR} + \Delta f_{PCR})] \qquad \text{after transfer} \qquad (6)$$

In prestressed members, the part of the loss due to relaxation that occurs before transfer may be deducted from the total relaxation loss by an adjustment in initial prestress force.

Prestress Gain Due to Slab Casting

The AASHTO LRFD Specifications recognizes the prestress gain by the term $7.0\ \Delta f_{cdp}$ in the creep equation. In the Modified Rate of Creep method, the creep effect of slab and diaphragm dead load may be considered as a prestress gain. Part of the initial compressive strain induced in the concrete immediately after transfer is reduced by the tensile strain resulting from permanent loads. The prestress gain due to slab dead load consists of two parts. The first part is due to instantaneous elastic prestress gain. The second part is time-dependent creep effect. Prestress gain due to elastic and creep effect of slab casting is given as[6]:

$$\Delta f_{EG} = n_{SC}\ f_{S+D} \qquad \text{elastic prestress gain} \qquad (7)$$

$$\Delta f_{CRG} = n_{SC}\ f_{S+D}\ (\Psi_{t,ti} - \Psi_{t,tisc})\ I_g/I_c \qquad \text{creep effect prestress gain} \qquad (8)$$

where

n_{SC} = modular ratio at the time of slab casting
f_{S+D} = stress in concrete at the level of prestressing strands due to dead load of slab and diaphragms

Prestress Gain Due to Differential Shrinkage

In composite prestressed girder bridges, the concrete in the girder is steam-cured while the concrete in slab is usually cast-in-place and moist-cured. Slab concrete is also cast at a later time when girders are in place. Due to the difference in the quality of concrete, curing process, and time of casting, a prestress gain due to differential shrinkage may be considered as:[5]

$$\Delta f_{DS} = n_{SC}\ f_{CD} \qquad (9)$$

where

$f_{CD} = [\Delta\varepsilon_{S\text{-}G}\ A_S\ E_S / (1 + \Psi_{t,ti})]\ (y_{CS}\ e_c / I_c)$ = concrete stress at the level of prestressing strands

$\Delta\varepsilon_{S\text{-}G}$ = differential shrinkage strain
A_S = area of concrete deck slab

E_S = modulus of elasticity of slab
y_{CS} = distance between the c.g. of composite section to the c.g. of slab
e_c = eccentricity of prestressing strands in composite section
I_c = moment of inertia of composite section

The denominator $(1 + \Psi_{t,ti})$ approximates the long-term creep effect.

METHODS OF DETERMINATION OF TIME-DEPENDENT LOSSES

Approximate Lump Sum Estimate of Time-Dependent Prestress Losses

According to AASHTO LRFD Specifications, the approximate time-dependent prestress losses, for I-shaped girders, prestressed with low-relaxation strands, and ultimate strength of 1860 MPa (270 ksi), without partial prestressing and strength of concrete above 41 MPa (6 ksi), is given by:

$$\Delta f_{PT} = 230 \, [1 - 0.15 \, (f'_c - 41) / 41] \qquad (10)$$

For specified concrete strength above 35 MPa (5 ksi), methods such as AASHTO LRFD Specifications, the Time Step method, and Modified Rate of Creep method may be used.

Refined Estimates of Time-Dependent Losses

The refined estimate of time-dependent prestress losses, according to AASHTO LRFD Specifications, is given as the summation of losses due to shrinkage and creep of concrete and relaxation of prestressing strands.

$$\Delta f_{PT} = \Delta f_{PSH} + \Delta f_{PCR} + \Delta f_{PR} \qquad (11)$$

Time Step Method

The Time Step Method is a numerical step-by-step procedure based on having constant values over short time intervals. During each time interval, all the factors having an influence on the long-term deformations and prestress losses are taken into account.

Prestress force in a prestressed concrete member continuously decreases and at any time may be estimated based on the effective prestressing force in the prestressing strands. Effective prestressing force at any time is considered as the initial applied force at the time of transfer minus the total estimated loss at that time. Several cycles of loss calculation are needed in order to converge to an acceptable range of variation.[1]

Modified Rate of Creep Method

The Modified Rate of Creep method takes into account the instantaneous and time-dependent effect of slab casting, and the transition from non-composite to composite section properties.

Prestress losses due to each time-dependent source may be evaluated in detail by considering the effect of creep and shrinkage on different construction stages. Casting of deck slab in composite girders affects prestressing force in the member by the influence on the creep coefficient, shrinkage strain of concrete, and steel relaxation. When an added load is applied, sometimes after initial prestressing, and sustained on the structure up to time t_i, its contribution to the prestress force may be considered by including the elastic and creep effect gain due to dead load of slab, using appropriate creep factors before and after slab casting. The effect of differential shrinkage between concrete deck slab and prestressed girder on prestress losses shall be included in time-dependent losses. In detailed evaluation of prestress losses due to each time-dependent parameter, the appropriate section properties of the stage under consideration shall be used. Time-dependent prestress losses using the Modified Rate of Creep may be given as:

$$\Delta f_{PT} = \Delta f_{PSH} + \Delta f_{PCR1} + \Delta f_{PCR2} + \Delta f_{PR} - \Delta f_{EG} - \Delta f_{CRG} - \Delta f_{DSH} \quad (12)$$

For non-composite girders, the time-dependent prestress losses may be taken as:

$$\Delta f_{PT} = \Delta f_{PSH} + \Delta f_{PCR1} + \Delta f_{PR} \quad (13)$$

Comparison of Prestress Losses

Table 3 summarizes time-dependent prestress losses obtained from different methods discussed in this paper. Losses from the Time Step method are lower than the ones obtained from the AASHTO LRFD refined estimate analysis, because the Time Step method is based on effective prestress force rather than the initial force at transfer. Prestress losses computed from the Modified Rate of Creep method are lower than the ones obtained from other methods, because this method performs an in-depth analysis of the effects of slab casting. It includes, as mentioned previously, the elastic and creep effect of slab casting as well as the prestress gain obtained from differential shrinkage, using appropriate creep coefficient and shrinkage strain of concrete before and after slab casting.

Table 3 - Comparison of Prestress Losses in MPa

	AASHTO-LRFD Approx. Method	AASHTO-LRFD Refined Method	Time Step Analysis	Modified Rate of Creep Method
Transfer	159.2	159.2	159.2	159.2
Before Slab Cast.	-	238.5	227.3	197.3
After Slab Cast.	-	232.5	214.2	175.8
Final	348.2	376.1	327.5	283.5

1 MPa = 0.145 ksi

DEFLECTION OF PRESTRESSED GIRDER

Prestressed girder deflection may be evaluated in detail by considering the effect of creep and shrinkage of concrete on different construction stages. Prestress force produces moment and axial force in the girder that tends to bow the girder upward. Girder dead load resists this upward deflection, but is overpowered by the deflection due to prestressing and the girder continues to deflect upward due to creep effect. The result for a non-composite girder prior to slab casting is a net upward deflection. Casting of slab results in a downward deflection; it is also accompanied by continuing downward deflection due to creep and differential shrinkage between precast girder and slab, which are cast in different times and cured in different processes. The long-term downward deflections after slab casting, for the most part, are compensated for by the long-term upward deflection due to prestressing. Many measurements of actual structure deflections have shown that once slab is cast, the girder tends to act as it is locked in position. The final deflection of a prestressed girder according to the Modified Rate of Creep method may be given as:[6]

$$\Delta t = \Delta_{DLg}+\Delta_{DLgbsCR}+\Delta_{P/S}+\Delta_{P/SbsCR}+\Delta_{P/SasCR}+\Delta_{DLs}+\Delta_{DLgasCR}+\Delta_{DLsCR}+\Delta_{SH} \quad (14)$$

where

Δ_{DLg} is the deflection due to girder dead load and may be taken as:

$$\Delta_{DLg} = 5w_gL^4/384E_gI_g \quad (15)$$

$\Delta_{DLgbsCR}$ is the deflection due to creep effect of girder dead load and may be taken as:

$$\Delta_{DLgbsCR} = \Psi_{t,ti}\ \Delta_{DLg} \quad (16)$$

$\Delta_{DLgasCR}$ is the creep effect deflection of composite girder due to slab load after slab casting and may be taken as:

$$\Delta_{DlgasCR} = \Delta_{DLg}\ (\Psi_{t,ti}-\Psi_{t,tisc})\ I_g/I_c \quad (17)$$

Δ_{DLs} is the deflection due to slab plus diaphragm dead and may be taken as:

$$\Delta_{DLs} = 5w_sL^4/384E_gI_g + 19PL^3/384E_gI_g \quad (18)$$

Δ_{DLsCR} is the creep effect deflection of composite girder after slab casting and may be taken as:

$$\Delta_{DLsCR} = \Psi_{t,ti}\ \Delta_{DLs}\ I_g/I_c \quad (19)$$

$\Delta_{P/S}$ is the deflection due to straight and harped prestressing strands and may be taken as:

$$\Delta_{P/S} = P_s\, e_s\, L^2/(8E_gI_g) + P_h\, /E_gI_g\, (L^2/8 - a^2/6)\, (e_s - e_h) \qquad (20)$$

$\Delta_{P/SbsCR}$ is the creep effect deflection of prestressing before slab casting and may be taken as:

$$\Delta_{P/SbsCR} = [(1-\Delta F_{SC}/2F_o)\, \Psi_{t,ti} - \Delta F_{SC}/F_o]\, \Delta_{P/S} \qquad (21)$$

$\Delta_{P/SasCR}$ is the creep effect deflection of prestressing of composite girder after slab casting and may be taken as:

$$\Delta_{P/SasCR} = [(1-(\Delta F_{SC}+\Delta F_t)/2F_o)\, (\Psi_{t,ti} - \Psi_{t,tisc}) - (\Delta F_t - \Delta F_{SC})/F_o]\, \Delta_{P/S}\, I_g/I_c \qquad (22)$$

Δ_{SH} is the deflection due to differential shrinkage and may be taken as:

$$\Delta_{SH} = [\Delta\varepsilon_{S\text{-}G}\, A_S\, E_S / (1 + \Psi_{t,ti})]\, (y_{CS}\, L^2 / 8E_gI_c) \qquad (23)$$

where

w_g = unit weight of girder
E_g = modulus of elasticity of girder
w_s = unit weight of slab and pad
P = weight of diaphragm
P_s = prestressing force in straight strands
P_h = prestressing force in harped strands
a = distance from the centerline of bearing to the harping point
e_s = eccentricity of straight strands from neutral axis
e_h = eccentricity of harped strands from neutral axis

The denominator $(1 + \Psi_{t,ti})$ approximates the long-term creep effect.

In the above equations, the terms $\Psi_{t,ti}(1-\Delta F_{SC}/2F_o)$ and $(\Psi_{t,ti}-\Psi_{t,tisc})(1-(\Delta F_{SC}+\Delta F_t)/2F_o)$ represent the effect of variable stress history from the time of transfer to the time of slab casting and from slab casting to final conditions, respectively. The term I_g/I_c represents the effect of composite section properties after slab casting.

Prestressed girder deflection according to the Modified Rate of Creep method is presented in Table 4.

Table 4 - Prestressed Girder Deflection

	Total Deflection in mm
At Transfer	-80

Before Slab Casting	-107
After Slab Casting	-56
Final	-44

Note: Upward deflection (-); 1 mm = 0.0394 in.

LESSONS LEARNED

1. Design of concrete strength should be based upon the required concrete strength at release. The final live and dead loads will usually not induce stresses in girders more than that which the girders experience at prestress release. Instead of a 56-day concrete compressive strength, a 28-day strength, equal to release strength plus 7 MPa (1 ksi), can be specified.

2. Some concern was expressed about going to an initial prestress strength of 52 to 55 MPa (7.5 to 8.0 ksi). The concern was that this would require the girder manufacturer to go to a 2-day cycle for girder fabrication and consequently increase the cost. Consequently, we would limit the release strength to 52 MPa (7.5 ksi) or less.

3. Using HPC reduces seven lines of girders to five.

4. If necessary, 15.24-mm (0.6-in.), instead of normal 12.7-mm (0.5-in.), diameter prestressing strands can be used for the standard WSDOT girders. The standard 50-mm (2-in.) strand spacing need not be increased.

5. The LRFD design yields similar results as an LFD design using HS-25 live loading.

6. Near the end of the beams, the confinement reinforcement of the standard girders in the bottom flange needs to be increased per LRFD 5.10.10.2.

7. To a small extent, using pretension temporary strands can reduce the concrete strength at release and increase stability during lifting and shipping.

8. The enhanced strength parameters of high performance concrete results in lower creep and shrinkage values and reduces prestress losses and girder deflection. The Modified Rate of Creep method provides a reasonable method for predicting more accurate prestress losses. In computation of prestress losses and girder deflection, the modulus of elasticity of concrete is taken in accordance with the current AASHTO LRFD Specifications, as a direct function of strength of concrete. Higher strength concrete results in a higher modulus of elasticity and therefore reduced prestress losses and girder deflection. According to the researchers at UW, more performance tests are needed to redefine the equation of the modulus of elasticity as a function of strength of concrete. More accurate creep coefficient and shrinkage strain of high

performance concrete mix specific to this project may also have a direct effect on the prestress losses and girder deflection.

REFERENCES

1. *AASHTO LRFD Bridge Design Specifications*, First Edition, 1994 and Interim Specifications through 1996.

2. *Bridge Design Manual*, Publication No. M23-50, Washington State Department of Transportation, Bridge and Structures Office, Olympia, Washington, 1997.

3. AASHTO Standard Specifications for Highway Bridges, Sixteenth Edition, 1996.

4. Hernandez, H. D. and Gamble W. L., "Time-Dependent Prestressed Losses in Pretensioned Concrete Construction," Report No. UILU - ENG - 75 - 2005, Department of Civil Engineering, University of Illinois at Urbana Champaign, Illinois, May 1975.

5. Branson, D. E. and Panarayanan K. M, "Loss of Prestress of Non-composite and Composite Prestressed Concrete Structures," *PCI Journal*, September-October 1971.

REFERENCES

American Association of State Highway and Transportation Officials. *Standard Specifications for Highway Bridges.* 1st Edition LRFD. Washington, D.C., 1994.

American Concrete Institute (ACI). *Building Code Requirements for Structural Concrete.* Farmington Hills, Michigan, 1995.

Barr, Paul. "Behavior of High Performance Prestressed Concrete Girders" Master's Thesis. University of Washington. 1997.

Burns, N. H., and Russell, B. W. "Measured Transfer Lengths of 0.5 and 0.6 inch Strands in Pretensioned Concrete Girders." *Prestressed Concrete Institute Journal.* Volume 41, No.5, September/October 1996, pp.44-63.

Fekete, E., Barr, P., Stanton, J., Eberhard, M., Janssen, D. "High Performance Concrete in Washington State SR 15/ SR 516 Overcrossing." Washington State Department of Transportation Bridge and Structures Office. Olympia, Washington, 1991.

Fekete, Elizabeth. "Prestress Losses in High Performance Concrete Girders". Master's Thesis. University of Washington, 1997.

Goodspeed, C. H., Vanikar, S., and Cook, R. A. "High-Performance Concrete Definition for Highway Structures". *Concrete International*. Volume 18, No.2, February 1996, pp.62-67.

Lew, H. S., and Reichard, T. W. "Prediction of Strength of Concrete from Maturity." *Accelerated Strength Testing.* ACI Publication SP-56, American Concrete Institute, 1978, pp.229-248.

Logan, D. "Acceptance Criteria for Bond Quality of Strand for Pretensioned Prestressed Concrete Applications." *Prestressed Concrete Institute Journal.* Volume 42, No.4, March/April 1997, pp.52-90.

Lwin, M. Myint, and Bijan Khaleghi. "Time-Dependent Prestress Losses in Prestress Concrete Girders Built of High Performance Concrete (Preprint)." Transportation Research Board. 76th Annual Meeting. January 1997.

FHWA, The National Bridge Inventory. US Department of Transportation, Federal Highway Administration, Washington, D.C., July 1997.

Nawy, E. G. *Prestressed Concrete: A Fundamental Approach.* Prentice-Hall, New Jersey, 1989.

Nawy, E. G. *Fundamentals of High Strength High Performance Concrete.* Longman Group Limited, London, 1996.

Nilson, Arthur H. *Design of Prestressed Concrete*. Second Edition. John Wiley & Sons, New York, 1987.

PCI Committee on Prestress Losses. "Recommendations for Estimating Prestress Losses." *Prestressed Concrete Institute Journal.* July/August 1975, pp.44-75.

PCI Industry Handbook Committee. *PCI Design Handbook.* Fourth Edition. Precast/Prestressed Concrete Institute. Chicago, 1992.

Russell, Bruce W., and Dallas R. Rose. "Investigation of Standardized Tests to Measure the Bond Performance of Prestressing Strand." *Prestressed Concrete Institute Journal.* July/August 1997.

APPENDIX A
PRESTRESSED I-GIRDER DESIGN USING HPC AND THE LRFD[1] SPECIFICATIONS

This design procedure illustrates the design of an interior girder of the middle span.

Design Conditions
Span length of 40.56 m (133.1 ft) with 11.58-m (38-ft) roadway width and a 40.37^o skew angle.
HL-93 live load - 3 lanes.
Use WSDOT's W74MG[2] girders at 2.44-m (8-ft) spacing.
Consider composite construction with 190-mm (7.5-in.) deck slab, which includes a 10-mm (0.4-in.) integral wearing surface. The typical section of the bridge is shown in Figure 1.

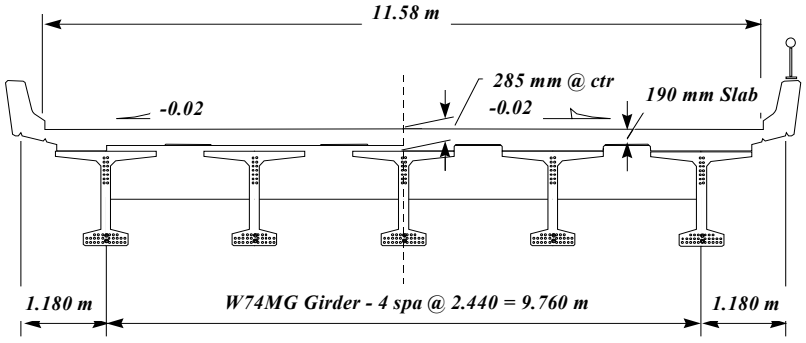

Figure 1 - Bridge Typical Section

Materials
Precast concrete: normal weight, 56 day's f'_c = 69 MPa (10 ksi), f'_{ci} = 51 MPa (7.4 ksi)
Slab concrete: normal weight, 28 day's f'_c = 28 MPa (4 ksi).
Density of concrete: for computing E_c, y_c = 2480 kg/m^3; for weight, y_c = 2560 kg/m^3.
Prestressing steel: AASHTO M-203M, uncoated 15 mm (0.6 in.) diameter, 7 wire, 1860 MPa (270 ksi) low-relaxation strands. Strand area = 140 mm^2 (0.217 in.^{2}). E_p = 197000 MPa (28500 ksi).
Reinforcing Steel: AASHTO M-31M, Grade 400 (60 ksi), E_s = 200000 MPa (29000 ksi).

Section Properties
Use modular ratio, $n = \sqrt{f'_c}(\text{girder}) / \sqrt{f'_c}(\text{slab}) = 1.57$; section properties are shown in Table 1.

Limit States

Service I - 1.0 DC + 1.0 (LL+IM)

Compression in prestressed components is investigated using this load combination.

Service III - 1.0 DC + 0.8 (LL+IM)

Load combination relating only to tension in prestressed concrete structures with the objective of crack control.

Vehicular Live Load

Design live load, HL-93, shall be taken as:

(Design truck (HS20) or tandem) (1 + IM) + Lane

Dynamic load allowance, IM = 33%

The distribution factor can be shown to be D.F. = 0.63.

Table 1 - Section Properties

	Girder	Composite
Depth, mm	1 865	2 045
Area, mm^2	485 300	765 100
I, mm^4	227.5 x 10^9	400.4 x 10^9
y_b, mm	970	1 330
S_b, mm^3	234.4 x 10^6	301.0 x 10^6
y_t girder, mm	895	535
S_t girder, mm^3	254.3 x 10^6	748.8 x 10^6
y_t slab, mm	-	715
S_t slab, mm^3	-	560.2 x 10^6

Note: 1 mm = 0.0394 in.

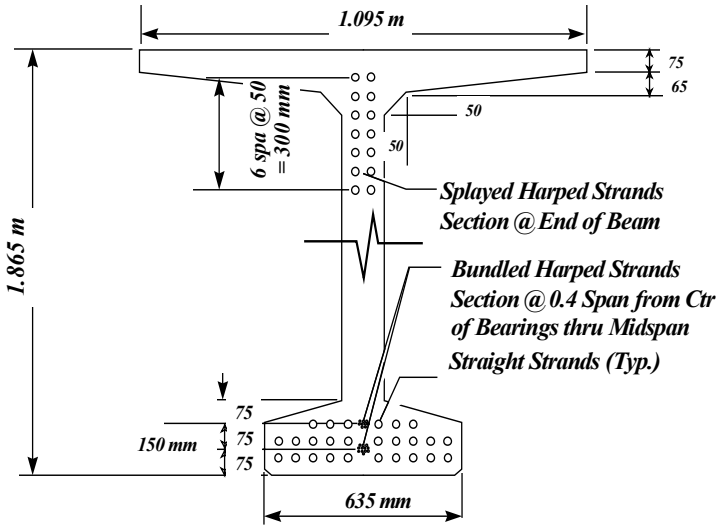

Figure 2 - Typical W74MG Prestressed Girder and Strand Pattern

Allowable Concrete Stresses at Service Limit State

Current WSDOT design practice does not allow any tension at the bottom of prestressed girder at Service III limit state. The zero tension criteria practiced by WSDOT provides some reserve to mitigate construction, operational, and fatigue related problems. It is usually achieved by adding one or two strands to the total number of strands per girder. The other allowable concrete stresses follow the LRFD Specifications.

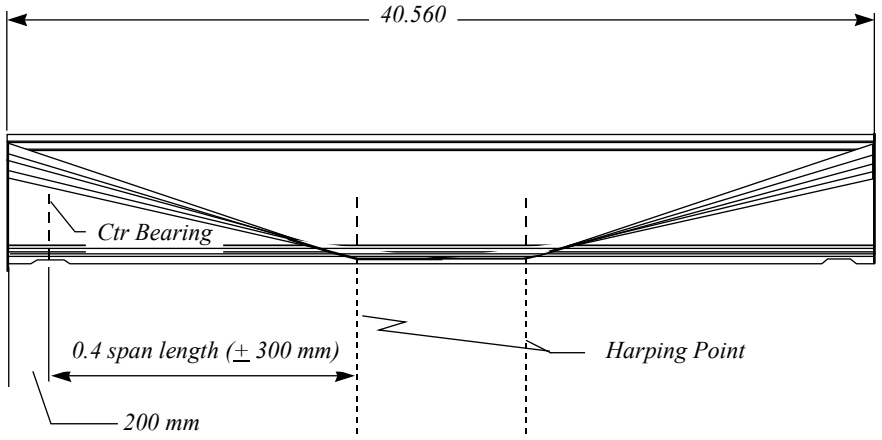

Figure 3 - Prestressed Girder Elevation

Determination of Prestressing Forces

A trial and error method was used to determine the proper number of prestressing strands. The jacking stress at transfer, 0.75 f_{pu}, is used as allowed in the LRFD code.

Table 2 - Summary of Stresses at Service

	At mid-span			At harping point		
Stress (MPa)	f_b	f_t(girder)	f_t(slab)	f_b	f_t(girder)	f_t(slab)
Girder	10.15	-9.35	-	9.74	-8.98	-
Slab + haunch	12.26	-11.30	-	11.77	-10.85	-
Diaphragm	1.41	-1.30	-	1.27	-1.17	-
Traffic barrier	1.85	-0.74	-0.99	1.77	-0.71	-0.95
ΣDL	25.67	-22.69	-0.99	24.55	-21.71	-0.95
LL - Service I	-	-4.73	-6.33	-	-4.58	-6.12
LL - Service III	9.42	-	-	9.11	-	-
Prestressing	-35.98	8.66	-	-35.98	8.66	-
Stresses under permanent load	-	-14.03	-0.99	-	-13.04	-0.95
Allowables	-	-31.05	-12.60	-	-31.05	-12.60

Stresses under all loads	-0.89	-18.76	-7.32	-2.32	-17.62	-7.07
Allowables	0.00	-41.40	-16.80	0.00	-41.40	-16.80

Note: Tension (+); 1 MPa = 0.145 ksi

For the final design, 14 harped and 26 straight strands are used, as shown in Figures 2 and 3. The total prestress loss at service is calculated to be 283.5 MPa (42 ksi) using the Modified Rate of Creep method (see next section). The final stresses at service at the mid-span and the harping point are summarized in Table 2. It can also be shown that concrete stresses at transfer satisfy the code requirement.

PRESTRESS LOSSES IN PRESTRESSED GIRDERS

Despite wide use of prestressing, there is no simple, practical method for predicting accurately the time-dependent losses of prestressed concrete structures. This is partly because of the difficulty in predicting the time-dependent properties of concrete and prestressing steel, and the uncertain environmental conditions to which the structure will be subjected after prestressing.[4] For HPC, the difficulty also comes from the limited experience and data available.

TIME-DEPENDENT PRESTRESS LOSSES

Prestress Loss Due to Creep

Creep loss due to permanent loads occurs immediately after initial prestressing. The stress in the concrete at the level of prestressing steel at transfer is the elastic response, while the creep effect will occur over a long period of time under a sustained load. For composite girders, part of initial compressive strain induced in the concrete immediately after transfer is reduced by the tensile stress resulting from superimposed permanent loads. Loss of prestress due to creep is proportional to the net compressive stress in the concrete. In accordance with the AASHTO LRFD Specifications, the creep loss is given by:

$$\Delta f_{PCR} = 12.0\, f_{cgp} - 7.0\, \Delta f_{cdp} \quad > 0.0 \qquad (1)$$

where

f_{cgp} = sum of the concrete stresses due to prestressing and weight of the girder at the center of gravity of prestressing strands at mid-span

Δf_{cdp} = change in concrete stress at the level of prestressing strands due to applied dead loads of concrete deck slab and diaphragms.

The term $7.0\, \Delta f_{cdp}$ in the above equation is the approximate estimate of prestress gain due to dead load of slab and diaphragm.

In the Modified Rate of Creep method, prestress loss due to creep may be considered in two stages: Stage 1 is the creep loss between time of transfer and slab casting, which may be expressed as:

$$\Delta f_{PCR1} = n\, f_{cgp}\, \Psi_{t,tisc}\, (1-\Delta F_{SC}/2F_o) \qquad (2)$$

Stage 2 is the creep loss for any time after slab casting, which may be expressed as:

$$\Delta f_{PCR2} = n\, f_{cgp}\, (\Psi_{t,ti}-\Psi_{t,tisc})\, (1-(\Delta F_{SC}+\Delta F_t)/2F_o)\, I_g/I_c \qquad (3)$$

where

$\Psi_{t,ti}$ = creep coefficient of girder at any time
$\Psi_{t,tisc}$ = creep coefficient of girder at the time of slab casting
ΔF_{SC} = total loss at the time of slab casting minus initial elastic shortening loss
F_o = prestressing force at transfer after elastic losses
ΔF_t = total prestressing loss at any time minus initial elastic shortening loss
I_g/I_c = ratio of moment of inertia of prestressed girder to composite girder

In the above equations, the terms $\Psi_{t,tisc}(1-\Delta F_{SC}/2F_o)$ and $(\Psi_{t,ti}-\Psi_{t,tisc})(1-(\Delta F_{SC}+\Delta F_t)/2F_o)$ represent the effect of variable stress history from the time of transfer to the time of slab casting and from slab casting to final conditions, respectively. The term I_g/I_c represents the effect of composite section properties after slab casting.

Prestress Loss Due to Shrinkage

Shrinkage of concrete can vary over a wide range depending on the material properties and surface drying conditions. Prestress loss due to shrinkage of concrete for prestressed members according to AASHTO LRFD Specifications is given by:

$$\Delta f_{PSR} = (117.0 - 1.035\, H) \qquad (4)$$

where

H = relative humidity
Δf_{PSR} = shrinkage loss in MPa

Prestress Loss Due to Relaxation of Prestressing Strands

Relaxation of prestressing strands depends upon the stress level in the strands. However, because of the other prestressing losses, there is a continued reduction of the strand stress, thus causing a reduction in prestress. The reduction in strand stress due to elastic shortening of concrete occurs instantaneously. On the other hand, the reduction in strand stress due to creep and shrinkage takes place for a long period of time.

The loss due to relaxation of prestressing strands given by AASHTO LRFD Specifications is considered in two stages: relaxation loss at transfer and relaxation loss

after transfer of prestress force. In a prestressed member, with low-relaxation strands, the relaxation loss in prestressing steel, initially stressed in excess of $0.5f_{pu}$, is given by:

$$\Delta f_{PR1} = \log(24t)/40.0\ [f_{pj}/f_{py}-0.55]f_{pj} \qquad \text{at transfer} \qquad (5)$$

$$\Delta f_{PR2} = 0.30\ [\ 138 -0.4\ \Delta f_{PES} - 0.2(\Delta f_{PSR} + \Delta f_{PCR})] \qquad \text{after transfer} \qquad (6)$$

In prestressed members, the part of the loss due to relaxation that occurs before transfer may be deducted from the total relaxation loss by an adjustment in initial prestress force.

Prestress Gain Due to Slab Casting

The AASHTO LRFD Specifications recognizes the prestress gain by the term $7.0\ \Delta f_{cdp}$ in the creep equation. In the Modified Rate of Creep method, the creep effect of slab and diaphragm dead load may be considered as a prestress gain. Part of the initial compressive strain induced in the concrete immediately after transfer is reduced by the tensile strain resulting from permanent loads. The prestress gain due to slab dead load consists of two parts. The first part is due to instantaneous elastic prestress gain. The second part is time-dependent creep effect. Prestress gain due to elastic and creep effect of slab casting is given as[6]:

$$\Delta f_{EG} = n_{SC}\ f_{S+D} \qquad \text{elastic prestress gain} \qquad (7)$$

$$\Delta f_{CRG} = n_{SC}\ f_{S+D}\ (\Psi_{t,ti} - \Psi_{t,tisc})\ I_g/I_c \qquad \text{creep effect prestress gain} \qquad (8)$$

where

n_{SC} = modular ratio at the time of slab casting
f_{S+D} = stress in concrete at the level of prestressing strands due to dead load of slab and diaphragms

Prestress Gain Due to Differential Shrinkage

In composite prestressed girder bridges, the concrete in the girder is steam-cured while the concrete in slab is usually cast-in-place and moist-cured. Slab concrete is also cast at a later time when girders are in place. Due to the difference in the quality of concrete, curing process, and time of casting, a prestress gain due to differential shrinkage may be considered as:[5]

$$\Delta f_{DS} = n_{SC}\ f_{CD} \qquad (9)$$

where

$f_{CD} = [\Delta\varepsilon_{S\text{-}G}\ A_S\ E_S / (1 + \Psi_{t,ti})]\ (y_{CS}\ e_c / I_c)$ = concrete stress at the level of prestressing strands

$\Delta\varepsilon_{S\text{-}G}$ = differential shrinkage strain
A_S = area of concrete deck slab

E_S = modulus of elasticity of slab
y_{CS} = distance between the c.g. of composite section to the c.g. of slab
e_c = eccentricity of prestressing strands in composite section
I_c = moment of inertia of composite section

The denominator $(1 + \Psi_{t,ti})$ approximates the long-term creep effect.

METHODS OF DETERMINATION OF TIME-DEPENDENT LOSSES

Approximate Lump Sum Estimate of Time-Dependent Prestress Losses

According to AASHTO LRFD Specifications, the approximate time-dependent prestress losses, for I-shaped girders, prestressed with low-relaxation strands, and ultimate strength of 1860 MPa (270 ksi), without partial prestressing and strength of concrete above 41 MPa (6 ksi), is given by:

$$\Delta f_{PT} = 230 \, [1 - 0.15 \, (f'_c - 41) / 41] \qquad (10)$$

For specified concrete strength above 35 MPa (5 ksi), methods such as AASHTO LRFD Specifications, the Time Step method, and Modified Rate of Creep method may be used.

Refined Estimates of Time-Dependent Losses

The refined estimate of time-dependent prestress losses, according to AASHTO LRFD Specifications, is given as the summation of losses due to shrinkage and creep of concrete and relaxation of prestressing strands.

$$\Delta f_{PT} = \Delta f_{PSH} + \Delta f_{PCR} + \Delta f_{PR} \qquad (11)$$

Time Step Method

The Time Step Method is a numerical step-by-step procedure based on having constant values over short time intervals. During each time interval, all the factors having an influence on the long-term deformations and prestress losses are taken into account.

Prestress force in a prestressed concrete member continuously decreases and at any time may be estimated based on the effective prestressing force in the prestressing strands. Effective prestressing force at any time is considered as the initial applied force at the time of transfer minus the total estimated loss at that time. Several cycles of loss calculation are needed in order to converge to an acceptable range of variation.[1]

Modified Rate of Creep Method

The Modified Rate of Creep method takes into account the instantaneous and time-dependent effect of slab casting, and the transition from non-composite to composite section properties.

Prestress losses due to each time-dependent source may be evaluated in detail by considering the effect of creep and shrinkage on different construction stages. Casting of deck slab in composite girders affects prestressing force in the member by the influence on the creep coefficient, shrinkage strain of concrete, and steel relaxation. When an added load is applied, sometimes after initial prestressing, and sustained on the structure up to time t_i, its contribution to the prestress force may be considered by including the elastic and creep effect gain due to dead load of slab, using appropriate creep factors before and after slab casting. The effect of differential shrinkage between concrete deck slab and prestressed girder on prestress losses shall be included in time-dependent losses. In detailed evaluation of prestress losses due to each time-dependent parameter, the appropriate section properties of the stage under consideration shall be used. Time-dependent prestress losses using the Modified Rate of Creep may be given as:

$$\Delta f_{PT} = \Delta f_{PSH} + \Delta f_{PCR1} + \Delta f_{PCR2} + \Delta f_{PR} - \Delta f_{EG} - \Delta f_{CRG} - \Delta f_{DSH} \quad (12)$$

For non-composite girders, the time-dependent prestress losses may be taken as:

$$\Delta f_{PT} = \Delta f_{PSH} + \Delta f_{PCR1} + \Delta f_{PR} \quad (13)$$

Comparison of Prestress Losses

Table 3 summarizes time-dependent prestress losses obtained from different methods discussed in this paper. Losses from the Time Step method are lower than the ones obtained from the AASHTO LRFD refined estimate analysis, because the Time Step method is based on effective prestress force rather than the initial force at transfer. Prestress losses computed from the Modified Rate of Creep method are lower than the ones obtained from other methods, because this method performs an in-depth analysis of the effects of slab casting. It includes, as mentioned previously, the elastic and creep effect of slab casting as well as the prestress gain obtained from differential shrinkage, using appropriate creep coefficient and shrinkage strain of concrete before and after slab casting.

Table 3 - Comparison of Prestress Losses in MPa

	AASHTO-LRFD Approx. Method	AASHTO-LRFD Refined Method	Time Step Analysis	Modified Rate of Creep Method
Transfer	159.2	159.2	159.2	159.2
Before Slab Cast.	-	238.5	227.3	197.3
After Slab Cast.	-	232.5	214.2	175.8
Final	348.2	376.1	327.5	283.5

1 MPa = 0.145 ksi

DEFLECTION OF PRESTRESSED GIRDER

Prestressed girder deflection may be evaluated in detail by considering the effect of creep and shrinkage of concrete on different construction stages. Prestress force produces moment and axial force in the girder that tends to bow the girder upward. Girder dead load resists this upward deflection, but is overpowered by the deflection due to prestressing and the girder continues to deflect upward due to creep effect. The result for a non-composite girder prior to slab casting is a net upward deflection. Casting of slab results in a downward deflection; it is also accompanied by continuing downward deflection due to creep and differential shrinkage between precast girder and slab, which are cast in different times and cured in different processes. The long-term downward deflections after slab casting, for the most part, are compensated for by the long-term upward deflection due to prestressing. Many measurements of actual structure deflections have shown that once slab is cast, the girder tends to act as it is locked in position. The final deflection of a prestressed girder according to the Modified Rate of Creep method may be given as:[6]

$$\Delta t = \Delta_{DLg}+\Delta_{DLgbsCR}+\Delta_{P/S}+\Delta_{P/SbsCR}+\Delta_{P/SasCR}+\Delta_{DLs}+\Delta_{DLgasCR}+\Delta_{DLsCR}+\Delta_{SH} \quad (14)$$

where

Δ_{DLg} is the deflection due to girder dead load and may be taken as:

$$\Delta_{DLg} = 5w_gL^4/384E_gI_g \quad (15)$$

$\Delta_{DLgbsCR}$ is the deflection due to creep effect of girder dead load and may be taken as:

$$\Delta_{DLgbsCR} = \Psi_{t,ti}\ \Delta_{DLg} \quad (16)$$

$\Delta_{DLgasCR}$ is the creep effect deflection of composite girder due to slab load after slab casting and may be taken as:

$$\Delta_{DlgasCR} = \Delta_{DLg}\ (\Psi_{t,ti}-\Psi_{t,tisc})\ I_g/I_c \quad (17)$$

Δ_{DLs} is the deflection due to slab plus diaphragm dead and may be taken as:

$$\Delta_{DLs} = 5w_sL^4/384E_gI_g + 19PL^3/384E_gI_g \quad (18)$$

Δ_{DLsCR} is the creep effect deflection of composite girder after slab casting and may be taken as:

$$\Delta_{DLsCR} = \Psi_{t,ti}\ \Delta_{DLs}\ I_g/I_c \quad (19)$$

$\Delta_{P/S}$ is the deflection due to straight and harped prestressing strands and may be taken as:

$$\Delta_{P/S} = P_s\, e_s\, L^2/(8E_gI_g) + P_h\, /E_gI_g\, (L^2/8 - a^2/6)\, (e_s - e_h) \qquad (20)$$

$\Delta_{P/SbsCR}$ is the creep effect deflection of prestressing before slab casting and may be taken as:

$$\Delta_{P/SbsCR} = [(1-\Delta F_{SC}/2F_o)\, \Psi_{t,ti} - \Delta F_{SC}/F_o]\, \Delta_{P/S} \qquad (21)$$

$\Delta_{P/SasCR}$ is the creep effect deflection of prestressing of composite girder after slab casting and may be taken as:

$$\Delta_{P/SasCR} = [(1-(\Delta F_{SC}+\Delta F_t)/2F_o)\, (\Psi_{t,ti} - \Psi_{t,tisc}) - (\Delta F_t - \Delta F_{SC})/F_o]\, \Delta_{P/S}\, I_g/I_c \qquad (22)$$

Δ_{SH} is the deflection due to differential shrinkage and may be taken as:

$$\Delta_{SH} = [\Delta\varepsilon_{S\text{-}G}\, A_S\, E_S / (1 + \Psi_{t,ti})]\, (y_{CS}\, L^2 / 8E_gI_c) \qquad (23)$$

where

w_g = unit weight of girder
E_g = modulus of elasticity of girder
w_s = unit weight of slab and pad
P = weight of diaphragm
P_s = prestressing force in straight strands
P_h = prestressing force in harped strands
a = distance from the centerline of bearing to the harping point
e_s = eccentricity of straight strands from neutral axis
e_h = eccentricity of harped strands from neutral axis

The denominator $(1 + \Psi_{t,ti})$ approximates the long-term creep effect.

In the above equations, the terms $\Psi_{t,ti}(1-\Delta F_{SC}/2F_o)$ and $(\Psi_{t,ti}-\Psi_{t,tisc})(1-(\Delta F_{SC}+\Delta F_t)/2F_o)$ represent the effect of variable stress history from the time of transfer to the time of slab casting and from slab casting to final conditions, respectively. The term I_g/I_c represents the effect of composite section properties after slab casting.

Prestressed girder deflection according to the Modified Rate of Creep method is presented in Table 4.

Table 4 - Prestressed Girder Deflection

	Total Deflection in mm
At Transfer	-80

Before Slab Casting	-107
After Slab Casting	-56
Final	-44

Note: Upward deflection (-); 1 mm = 0.0394 in.

LESSONS LEARNED

1. Design of concrete strength should be based upon the required concrete strength at release. The final live and dead loads will usually not induce stresses in girders more than that which the girders experience at prestress release. Instead of a 56-day concrete compressive strength, a 28-day strength, equal to release strength plus 7 MPa (1 ksi), can be specified.

2. Some concern was expressed about going to an initial prestress strength of 52 to 55 MPa (7.5 to 8.0 ksi). The concern was that this would require the girder manufacturer to go to a 2-day cycle for girder fabrication and consequently increase the cost. Consequently, we would limit the release strength to 52 MPa (7.5 ksi) or less.

3. Using HPC reduces seven lines of girders to five.

4. If necessary, 15.24-mm (0.6-in.), instead of normal 12.7-mm (0.5-in.), diameter prestressing strands can be used for the standard WSDOT girders. The standard 50-mm (2-in.) strand spacing need not be increased.

5. The LRFD design yields similar results as an LFD design using HS-25 live loading.

6. Near the end of the beams, the confinement reinforcement of the standard girders in the bottom flange needs to be increased per LRFD 5.10.10.2.

7. To a small extent, using pretension temporary strands can reduce the concrete strength at release and increase stability during lifting and shipping.

8. The enhanced strength parameters of high performance concrete results in lower creep and shrinkage values and reduces prestress losses and girder deflection. The Modified Rate of Creep method provides a reasonable method for predicting more accurate prestress losses. In computation of prestress losses and girder deflection, the modulus of elasticity of concrete is taken in accordance with the current AASHTO LRFD Specifications, as a direct function of strength of concrete. Higher strength concrete results in a higher modulus of elasticity and therefore reduced prestress losses and girder deflection. According to the researchers at UW, more performance tests are needed to redefine the equation of the modulus of elasticity as a function of strength of concrete. More accurate creep coefficient and shrinkage strain of high

performance concrete mix specific to this project may also have a direct effect on the prestress losses and girder deflection.

REFERENCES

1. *AASHTO LRFD Bridge Design Specifications*, First Edition, 1994 and Interim Specifications through 1996.

2. *Bridge Design Manual*, Publication No. M23-50, Washington State Department of Transportation, Bridge and Structures Office, Olympia, Washington, 1997.

3. AASHTO Standard Specifications for Highway Bridges, Sixteenth Edition, 1996.

4. Hernandez, H. D. and Gamble W. L., "Time-Dependent Prestressed Losses in Pretensioned Concrete Construction," Report No. UILU - ENG - 75 - 2005, Department of Civil Engineering, University of Illinois at Urbana Champaign, Illinois, May 1975.

5. Branson, D. E. and Panarayanan K. M, "Loss of Prestress of Non-composite and Composite Prestressed Concrete Structures," *PCI Journal*, September-October 1971.